



OIL SEEDS AS NATURAL RESOURCES OF SELENIUM

Xénia Vágó^{[a]*}, Kinga Nagy^[a], Zita Burján^[a], Dávid András^[a], Béla Kovács^[a]

Paper was presented at the 4th International Symposium on Trace Elements in the Food Chain, Friends or Foes, 15-17 November, 2012, Visegrád, Hungary

Keywords: Selenium, Brazil nut, Trace element, ICP-MS, ICP-OES

Selenium is an essential trace element that has beneficial health effects in adequate concentration i.e. about 60 µg/day – in humans. Besides its antioxidant function selenium incorporated in seleno-aminoacids, selenomethionine and selenocysteine, as these aminoacids support anti-cancer and anti-aging effects. However ensuring the sufficient intake of this element may be limited in some countries, such as Hungary, because of the soil, which is deficient of selenium. In some literature it has been reported that oil seeds contain higher concentration of selenium, therefore they are potential selenium sources. The main aim of our work is to study and survey the role of these seeds in selenium intake into a human body. It has been pointed out that consuming these food products can minimize but not eliminate inadequate selenium intake, except that of brazil nut (*Bertholletia excelsa*) with its high (20 µg g⁻¹) selenium-content.

* Corresponding Authors

Fax: +36.52.417.572

E-Mail: xenia.vago@agr.unideb.hu

Institute of Food Science, Quality Assurance and Microbiology, Centre for Agricultural and Applied Economic Sciences, University of Debrecen, 138. Böszörményi Str. Debrecen, H-4032, Hungary

Introduction

Selenium is an essential trace element. It is very important for the healthy function of the human body. It has importance in the antioxidant defense and also active center of the deiodinase enzyme which requires for the peripheral thyroid hormone metabolism⁹.

Selenium is essential for metabolism, energy releasing processes and - promotes normal functioning of the immune system.⁹ The adequate amount of selenium is also required for the brain and thyroid function. It is a key nutrient for the protection against variety of environmental toxicants, viruses, and it helps in the delaying of the premature aging of cells, keeps the tissues young, and resiliency. Selenium strengthens the defense mechanisms against cancer, as well as the heart - protective mechanisms against cardiovascular diseases. Plays a role for improving fertility and has a positive effect on the antibody production, stimulates the immune system and also has an anti-inflammatory property.¹¹

Selenium gets through the plants and animals into the food chain from the soil. So the selenium concentration of soils has an enormous influence on selenium concentration of food. Hungary is not sufficient in selenium diet that may lead to the incomplete intake of Hungarian population.¹

The best selenium sources are oil seeds, nuts, among these one important seed is Brazilian nut – each piece contains up to 100 µg, which is about 182 % of the daily needs^{10,11}. Peanuts, hazelnuts, almonds, walnuts, cashews, sunflower or pumpkin seeds and peanuts also can help to ensure the daily amount of selenium. On the basis of the information given in the literature these seeds' selenium concentration can

change in wide range, so one part of our study was to determine whether the packaged seeds selenium concentration is high, and the influence of Hungarian soil's poor selenium concentration on the plants grown here.

By these results and discussion one can make an inference that for the balanced, systematic, conscious nutrition oil seeds and nuts are have important role to meet the adequate daily need for selenium.

Methods

Experimental

Brazil nut (*Bertholletia excelsa*) is derived from a soil that has a high selenium concentration. It is grown in the Amazonian basin that is native plant of the Brazilian tropical forest. Its proteins have are rich in methionine. Because the SeMet-Met ratio is regulated by the selenium/sulphur value that occurs in the soil, so the balance moves to the direction of the Met-aminoacid. In case of lack of selenium this raises the possibility of the use of an additional food source.²

A 12-week randomized controlled experiment was conducted by Thomson and colleagues, in the year 2007, New Zealand, in which it was found that daily consumption of two grains of Brazil nuts are effectively increases the levels of selenium concentration in blood and glutathione peroxidase activity, than 100 µg of synthetic selenomethionin.

The Brazil nuts are the richest known selenium source. Its selenium concentration varies between 8 to 83 µg g⁻¹.³ Selenium concentration of Brazil nuts which was grown in the middle and eastern part of the Amazonas basin, is up to 512 µg g⁻¹, while in the western part it is just 0.03 - 31.7 µg g⁻¹.⁴ only.

We mostly eat it raw, in a sock or other combinations of seed mixture, but we also use it in chopped or ground form for sweets, cakes, and salads.

In Hungary in general, Brazil nuts are sold without a nutshell. In Western Europe it is used, as a dessert since the British Government told public that Brazil nut is a good, natural selenium source, therefore, by eating it, the blood's selenium concentration can be reinstated.⁵

According to the USDA database, 100 g Brazil nut consist of 1917 µg selenium, sunflower seed 79.3 µg, cashew nut 20.3 µg, almond 2.9 µg, walnut 4.9 µg, pine nut 0.7 µg and peanut 7.5 µg selenium⁶ respectively.

Oil seeds have low glycemic index, they are rich in fiber, vitamins and minerals and those are good vegetable protein sources. The high fat content of oil seeds can lead to obesity that is the causing of several modern diseases, but Rajaram and Sabate⁷ found that the consumption of Brazil nuts is not causing body weight gain, because they make a full diet.⁷

Instrumentation

The oil seeds, we used in our experiment, were bought in from several stores in Debrecen: Brazil nuts, cashews, walnuts, peanuts, hazelnuts, almonds, sunflower seeds, pumpkin seeds and pine nuts. Preparation and measurement of the samples were made at the University of Debrecen, Centre for Agricultural and Applied Economic Sciences, Faculty of Agricultural and Food Sciences and Environmental Management, Institute of Food Processing, Quality Assurance and Microbiology.

50 g of the samples were measured in teflon vessels with electronic analytical balance. 8 cm³ of cc. HNO₃ (65% w/w, Scharlau Chemie, Spain) has been added, and then allow to stand for overnight in a fume hood. Then the samples were digested for 20 minutes in 200 °C in a Milestone Start D microwave digestion apparatus.¹²

Selenium determination

For the trace element analysis an inductively coupled plasma emission spectrometer with mass spectrometer (ICP-MS), Type X7, made by Thermo Elemental was used. For measuring elements in relatively high concentration a Thermo Scientific iCAP6300 Duo inductively coupled plasma optical emission spectrometer (ICP-OES) was used.

Results

The selenium concentrations of different samples are shown in Table 1., compared with the average, given in the literature.⁸ Selenium concentration of sunflower seeds that was grown in Hungary was much less, than the literature data. It is because Hungarian soils are lacking in selenium.

Overall, in the oil seeds the selenium concentration was meager than the expected, except in the Brazil nut. In view of the selenium content only, in some cases we should eat more than 1 kg nut or seed per day to ensure the needed amount of Selenium for covering the daily intake demand to save our health. Such a huge dose would be harmful, in the view of other components.

Table 1. Measured selenium concentration of the samples (µg g⁻¹)

	Se concentration (µg g ⁻¹)		Quantity (g) required for 60 µg Se intake
	Literature average	Own measurements	
brazil nut	1-50	20.52 ± 0.13	2.9
pumpkin seed	0.06	0.226 ± 0.000	266
sunflower seed	0.6	0.083 ± 0.034	722
nut	0.12	0.051 ± 0.001	1173
peanut	0.01	0.052 ± 0.002	1148
cashew	0.12	0.052 ± 0.002	1163
peanut	0.05	0.173 ± 0.001	346
almond	0.03	0.106 ± 0.000	564
hazelnut	0.02	0.081 ± 0.001	745

The selenium concentration measured in Brazil nut was found to be 20.5 µg g⁻¹. Because one piece of Brazil nut is 3.5 g in average, so each one has at least 71.8 µg selenium. Ordinary a 150g package of Brazil nut has 42 pieces, which cost 810 HUF. Therefore we had to pay 20 HUF per Brazil nut, so 71.8 µg Se costs that price. When it is compared to the Se pills, sold in the market, we can see that it's much worth eating one piece of Brazil nut a day, because the Se food supplements costs 53.3 Ft/80 µg Se. Brazil nut consists beside selenium some other useful nutrients including minerals as well. It has a very high concentration of zinc (40.4 µg g⁻¹ phosphorus (7.24 mg g⁻¹), copper (18.7 µg g⁻¹), and magnesium (3.18 mg⁻¹).

Table 2. The amount of oil seeds for the daily mineral intake (g)

Oil seed	Zn	Co	Mn	Cu	Fe	Ca	Cr	K	Mg	P
brazil nut	513	66	562	96	560	746	768	775	126	138
pumpkin seed	286	4160	74	177	185	2451	412	451	66	47
sunflower seed	345	429	76	82	242	1002	610	526	98	98
nut	952	5283	106	189	481	1515	708	1162	275	299
peanut	313	6667	33	106	227	5386	437	674	164	164
cashew	465	3232	120	91	231	2126	142	793	158	223
peanut	513	80206	246	317	754	2297	866	783	245	256
almond	781	508	180	194	348	374	571	694	155	213
hazelnut	741	3642	60	107	406	726	11	791	233	299

Table 3. Element content of Brazil nut (mg kg⁻¹)

	Element concentration (mg kg ⁻¹)	
	literature average	own measurements
K	6 300	5 350
P	6 900	6 962
Mg	4 100	3 183
Ca	1 700	1 415
Na	30	47.0
Fe	27	27.6
Zn	42	48.4
Cu	18	20.9
Mn	13	7.1
Cr	0.02-8	0.18
Ni	7	5.06
Mo	0.02	0.14

Table 2 shows the daily needed amount of oil seeds to reach the minimal intake of other important mineral substances.

For the calculation we used the following values: 20 mg of zinc, 140 µg of cobalt, 4 mg of manganese, 2 mg of copper, 15 mg of iron, 1000 mg of calcium, 140 µg of chromium, 3800 mg of potassium, 400 mg of magnesium and 1000 mg of phosphorus. We also measured the other element concentration in Brazil nut. The results are shown in the Table 3.

Discussion

Nuts and oil seeds are one of the oldest food for the mankind. It had a major role in the hunter-gatherer way people's life. Oil seeds are a part of the healthy and balanced diet. So it is worth eating natural, unsalted seeds. It is a good delicacy for everyone, because it contains a lot of vitamins and antioxidants. To live a healthy life our body requires enough trace elements.

Selenium concentration of the soil determines the concentration of the product, therefore if the plant grown on a selenium poor soil, the product would also be low in Se. So it is hard to assure the selenium intake with only the different kind of food.

Brazil nut contains the maximum amount of selenium, each of them has 72 µg, which corresponds to the dietary supplement pills' concentration. We can cover with it our daily need. The Brazil nuts are not only cheaper, but also having good flavor also, which is very useful for the human. In addition, other valuable nutrition, some other good elements are also found in it.

Acknowledgements

The publication is supported by the TÁMOP-4.2.2/B-10/1-2010-0024 and TÁMOP-4.2.1./B-09/1/KONV-2010-0007 projects. The projects are co-financed by the European Union and the European Social Fund.

References

- ¹Rayman, M. P. *The Lancet*, **2000**, 233-241.
- ²Stefánka Zs. *Nagyhatékonyágú mintabevételi technikák alkalmazási lehetőségei nyomelemek speciációs analízisének*. Doktori disszertáció, Szent István Egyetem, **2003**.
- ³Thomson, C. D., Chisholm, A., McLachlan, S. K., Campbell, J. *M. Am. J. Clin. Nutr.*, **2007**, 87(2), 379-384.
- ⁴Lemire, M., Fillion, M., Barbosa, F. Jr., Guimarães, J. R., Mergler, D. *Sci. Total Environ.* **2010**, 408, 4076-4084.
- ⁵Dernovics M. *Mintaelőkészítési módszerek kidolgozása és referenci anyagok előállítása módszeranalitikai célokra*. Doktori disszertáció, Szent István Egyetem, **2003**.
- ⁶www.usda.com
- ⁷Rajaram, S., Sabate, J. *Brit. J. Nutr.*, **2006**, 96, S79-86.
- ⁸Preedy, V. R., Watson, R. R., Patel, V. B. *Nuts and seeds in health and disease prevention*. Elsevier Inc., **2011**.
- ⁹Tamás, L. *A szelén betegség-megelőző szerepe*. Komplementer Medicina. Budapest, TDC Alapítvány, Naturamed Kft., **2000**, 4.4, 16-20. p.
- ¹⁰Thomson, C. D., *Eur. J. Clin. Nutr.*, **2004**, 58, 391-402
- ¹¹Yang, G. Q., Xia, Y. M., *Biomed. Environ. Sci.*, **1995**, 8, 187-201.
- ¹²Pál, K. *Szelén a környezetben*. Budapest, BME OMIKK, **2002**, 48 p.
- ¹³Kovács, B., Győri, Z., Prokisch, J., Loch, J., Dániel, P., *Commun. Soil Sci. Plant Anal.*, **1996**, 27, 1177-1198.

Received: 15.10.2012.

Accepted: 11.11.2012.



SALINE IRRIGATION WATER AFFECTS ELEMENT UPTAKE BY BEAN PLANT (*VICIA FABEA* L.)

Lana Matijević^{[a]*}, Davor Romić^[a], Nada Maurović^[a], Marija Romić^[a]

Paper was presented at the 4th International Symposium on Trace Elements in the Food Chain, Friends or Foes, 15-17 November, 2012, Visegrád, Hungary

Keywords: saline irrigation, element uptake, faba bean

Use of saline water for agricultural irrigation is leading towards salt accumulation in the root zone and consequent damage to crop production and soil fertility. Furthermore, it is known that increased root zone salinity can potentially increase plant trace element uptake. In this context, crop salt tolerance and growth response assessment is useful tool in managing salinity stress. A greenhouse pot experiment was set up to study the effects of irrigation water salinity on growth and element uptake of faba bean (*Vicia faba* L.). Three weeks old faba bean seedlings were transplanted into pots and automatically fertigated with a modified Hoagland nutrient solution. Two weeks after transplanting, treatment with four NaCl salinity concentrations in nutrient solution was applied as follows: NaCl₀ – control (basic nutrient solution without added NaCl), NaCl₃₅ (control + 35 mM NaCl), NaCl₅₀ (control + 50 mM NaCl), NaCl₆₅ (control + 65 mM NaCl). Increasing root zone salinity significantly enhanced Na and Cl accumulation in faba bean leaves. A decrease in Mo and K leaf content occurred most significantly at NaCl₅₀ treatment, as well as an increase in Mn leaf content. NaCl treatments reduced P leaf content in regard to control but without significant difference amongst treatments. Results have shown that increased root zone salinity can affect certain faba bean leaf element accumulation, although trace element leaf content was not significantly altered. Hence, faba bean could be considered as rather salt tolerant horticultural crop.

* Corresponding Author
Fax: +38512394099
E-Mail: lmatic@agr.hr

^[a] University of Zagreb Faculty of Agriculture, Department of Amelioration, Svetosimunska 25, 10000 Zagreb, Croatia

Introduction

An attempt to meet world food demands accompanied with decline in availability in fresh water has resulted in using water of poor quality for crop irrigation. It is known that horticultural production is dependent on soil and water quality. Use of saline water may alter soil's physical and chemical properties, which consequently may lead to decrease in crop yield.¹ Considering the need for increasing the crop yield, as well as the decline of good quality irrigation water, crop salt tolerance assessment can be a useful tool. It may provide information needed for deciding either to expose plants to moderate salt stress or to moderate water stress.² Furthermore, increased root zone salinity can affect plant element uptake. In the context of nutrient uptake, it reflects on fertilizers application. In addition, possible toxic element food chain intrusion is already recognized in a saline environment³. A site – specific approach that includes the specific crop salt stress response could be a potential solution in merging opposite agricultural demands. It will determine the economic threshold for growing horticultural crops in salt affected areas, as well as whether and when to irrigate crops with saline water.²

Using saline water for agricultural irrigation is prevalent in the Croatian Mediterranean coastal region, where seawater intrudes through porous media and salinizes both ground and surface waters. In addition, climatic conditions

are increasing the demand for irrigation water, forcing farmers to utilize water of poor quality.⁴

Plant responses to salinity differ but main salinity effects on plant are osmotic and ionic stress. Ionic stress generates nutrient imbalances and affects their bioavailability, competitive uptake, transport or partitioning within the plant⁴. Common indicators of plant salt stress are increased tissue concentrations of sodium and chloride, accompanied with decreased potassium concentration.³ Although, legume chickpea (*Cicer arietinum* L.) revealed no difference in shoot potassium content, during vegetative stage of development, under saline conditions.⁵ Legumes are either sensitive or moderately tolerant to salinity but variability in salinity tolerance among legumes has also been reported. *Vicia faba* (L.) is moderately sensitive to salinity, registering 50% growth reduction at 6.7 dS m⁻¹ salinity.⁶

Faba bean is one of the major cool season grain legume crops produced worldwide. It is mainly grown for its high protein content for food and feed. Faba bean popularity has increased recently as its high yield makes it attractive to producers while its high protein content makes it attractive to consumers.⁷ Effect of salt stress on faba bean growth (plant height, number of leaves, leaf area, etc.) and yield has been studied.^{8,9,10,11} Abdelhamid *et al.*⁶ reported that salinity significantly decreased nitrogen, phosphorus, calcium, magnesium and potassium in faba bean leaves while significantly increasing sodium and chloride. Thus, investigations on faba bean element uptake in a saline environment have been limited.

The aim of this study was to elucidate *Vicia faba* (L.) salt stress response after exposing faba bean to rising irrigation water salinity.

Experimental

Growing conditions

The study was carried out during autumn (9 September – 14 November 2011) in a polyethylene greenhouse at experimental station of the Faculty of Agriculture, University of Zagreb, Croatia. Faba bean (*Vicia faba* L. cv. Aguadulce) seeds were sown into polystyrene cups containing a peat soil (Klasmann, Potground P). Three weeks old uniform faba bean seedlings were transplanted into pots (3 litres) containing agricultural soil that was added to commercial substrate (1:1) to increase soil organic matter content. During the first two weeks after transplanting, the seedlings were irrigated daily, using automatic drip irrigation system with water-soluble NPK fertilizer (Poly-Feed Drip 20–20–20 with micronutrients: B, Cu, Fe, Mn, Mo and Zn; c = 2 g/l). In order to ensure soil/substrate mixture aeration and prevent waterlogging, good drainage conditions were ensured. The fertigation rate and frequency was the same for all treatments and was adjusted to the plant phenology and to the climatic conditions in the greenhouse.

Treatments applied and experimental design

Two weeks after transplanting (one plant per pot), treatment with four NaCl salinity concentrations in nutrient solution was applied as follows: NaCl₀ – control (basic nutrient solution without added NaCl), NaCl₃₅ (control + 35 mM NaCl), NaCl₅₀ (control + 50 mM NaCl), NaCl₆₅ (control + 65 mM NaCl).

The experimental design used was randomized block design with four replicates, including five plants per replicate, total of twenty plants per treatment.

Data collecting and sampling

Leaf samples were collected four weeks after salinity treatment started. One sample consisted of fully developed mature leaves from plants subjected to the same salinity treatment. Soil/substrate mixture samples from the pots were also collected at the same time. Soil/substrate mixture from pots subjected to the same salinity treatment was merged, mixed thoroughly and representative samples of each treatment were taken.

Plant and soil/substrate mixture analysis

Leaf samples were dried (24h at 60°C) and ground using an inox grinder (Zepter). Dried plant material was dissolved by multiwave-assisted digestion in concentrated HNO₃ : H₂O₂ (10:1, v/v) mixture. P, Fe, Mo, Mn, Cu and Zn concentrations were determined using inductively coupled plasma-optical emission spectrometry (ICP-OES Vista MPX, Varian). Na and K concentrations were measured by atomic emission spectrometry (Atomic Absorption Spectrometer 3110, Perkin-Elmer). Chloride content was measured in a plant water extract colorimetrically (470 nm) using continuous flow auto-analyzer (San++ Continuous Flow Analyzer, Skalar). Certified plant reference material (WEPAL) and blanks were included in digestion and mineral detection.

Soil/substrate mixture samples were air-dried and passed through a 2 mm mesh. All analyses were conducted in a saturated soil/substrate water extract. pH and electrical conductivity was measured. Na and K content was determined by atomic emission spectrometry (Atomic Absorption Spectrometer 3110, Perkin-Elmer). Cl was measured using continuous flow auto-analyzer (San++ Continuous Flow Analyzer, Skalar). Ca and Mg were determined titrimetrically.

Statistical analysis

Data on leaf and soil/substrate mixture element accumulation were subjected to the analysis of variance (ANOVA) using the SAS statistical software package (SAS Institute, 2007). The significance of differences between means was determined with Tukey's HSD test at P ≤ 0.05.

Results

Soil/substrate mixture element content

Irrigation with saline water (NaCl₃₅, NaCl₅₀, NaCl₆₅) affected the ionic composition of saturated soil/substrate water extract (Table 1). The salinity treatments did not influence the pH of saturated soil/substrate water extracts. Electrical conductivity (dS m⁻¹) increased significantly, proportionally to the treatments, as well as the contents of sodium and chloride (Table 1). Salinity treatments significantly increased calcium, magnesium and potassium content in saturated soil/substrate water extract (Table 1).

Table 1. Effect of different irrigation water salinity levels on electrical conductivity (dS m⁻¹), sodium, chloride, potassium, magnesium and calcium content (mg L⁻¹) in a saturated soil/substrate mixture water extract.

		NaCl ₀	NaCl ₃₅	NaCl ₅₀	NaCl ₆₅
dS m ⁻¹	pH	7.7	7.7	7.7	7.8
	E.C.	2.6 D	4.7 C	7.5 B	8.6 A
mg/l	Na ⁺	54.1 D	335.8 C	646.3 B	841 A
	Cl ⁻	160.1 D	1193.9 C	2185.3 B	2735.3 A
	K ⁺	31.1 BC	30.7 C	41 BA	43.3 A
	Mg ²⁺	95.3 B	126.4 B	166.7 A	179.9 A
	Ca ²⁺	396.8 B	510.6 B	747.1 A	799.2 A

Means with different superscripts in the same row are significantly different at P ≤ 0.05.

Leaf damage symptoms

During the experiment, plants exposed to increased NaCl salinity developed salt burning symptoms at the leaf edges, causing marginal chlorosis on the basal, actually the oldest leaves. With time, chlorosis spread over the complete basal leaf area and gradually progressed to necrosis (data not shown).

Leaf tissue element content

Increased root zone salinity significantly increased sodium and chloride content (g kg^{-1}) in faba bean leaves (Figure 1).

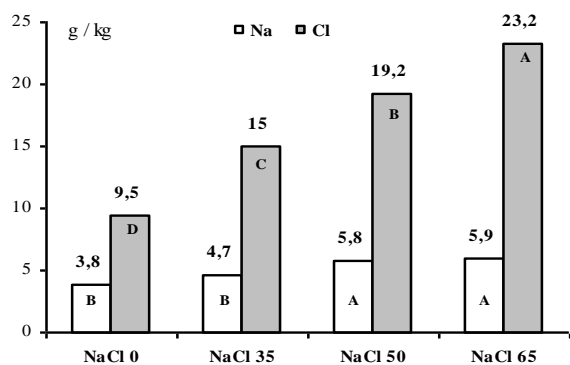


Figure 1. Effect of different irrigation water salinity levels on sodium and chloride content (g/kg) in faba bean. Means with different superscripts are significantly different at $P \leq 0.05$.

Irrigation water salinity significantly affected phosphorus and potassium content (g/kg) in faba bean leaves (Table 2). Phosphorus leaf content of all treated plants decreased regarding to control, but without significant difference amongst salinity treatments. Potassium leaf content most significantly decreased at NaCl_{50} treatment regarding to control plants.

Table 2. Effect of different irrigation water salinity levels on potassium (g/kg), phosphorus (g/kg), molybdenum (mg/kg), manganese (mg/kg), iron (mg/kg), copper (mg/kg) and zinc (mg/kg) content in faba bean leaf tissue.

		NaCl 0	NaCl 35	NaCl 50	NaCl 65
g/kg	K	19.4 A	18.8 BA	15.4 B	17.7 BA
	P	4.4 A	3.4 B	3.2 B	3.5 B
mg/kg	Mo	8.9 A	7.6 BA	4.5 B	7.3 BA
	Mn	90 B	104.3 BA	113.2 A	95.3 BA
	Fe	99.2 A	122.1 A	122.7 A	106 A
	Cu	3.2 A	3.8 A	3.3 A	3.4 A
	Zn	27.1 A	31.6 A	26.8 A	25.2 A

Means with different superscripts in the same row are significantly different at $P \leq 0.05$.

Differences between control plants and salinity treated plants were determined for molybdenum and manganese leaf content (Table 2). At NaCl_{50} treatment, molybdenum leaf content significantly decreased and manganese leaf content significantly increased, compared to control.

Compared to control plants, iron, copper and zinc faba bean leaf content was not significantly altered with the use of saline water.

Discussion

Salinity treatments significantly increased sodium, chloride, calcium, magnesium and potassium content in saturated soil/substrate water extract (Table 1). Increased potassium, magnesium and calcium content indicate that the process of ion exchange took place in the soil/substrate mixture¹². If a soil contained equal amounts of the Na, K, Mg and Ca, their distribution would be $\text{Ca} > \text{Mg} > \text{K} > \text{Na}$ on the soil adsorption complex¹³. Results suggest that excessive Na content added by saline irrigation water, induced release of K, Mg and Ca ions from soil/substrate adsorption complex into soil/substrate solution.

Increasing root zone salinity significantly increased Na and Cl accumulation in faba bean leaves. High sodium concentration in the rhizosphere may disrupt the integrity and selectivity of root membranes. As a result, imbalance in the availability of different ions may occur, affecting mineral uptake by roots^{14,15}. In addition, high soil Na content may interfere with K uptake by the roots. K in plants plays an important role in metabolic processes, in regulation of ion transport and osmotic adjustment. Under salt stress, elevated tissue K levels are required for shoot growth and for the maintenance of full photosynthetic capacity¹⁵. Results shown in Table 2 suggest that irrigation water salinity caused a decrease in K faba bean leaf content, although not being linear in relation to treatments. Significant decrease in K leaf content occurred at NaCl_{50} treatment, in reference to control plants. Results indicate that decreased K^+ activity in soil and/or competitive mechanisms with Na^+ at the root surface, took place under certain salinity levels. In the review given by Grattan and Grieve,¹⁵ the decline in K concentration in plant tissue occurred with increased Na-salinity of the root media. However, some of the studies show K level increase in bean leaves caused by increasing salinity^{16,17}. In our experiment, the critical level of salinity was NaCl_{50} , at which the decrease of K uptake was detected (Table 2). However, it seems that in further higher levels of salinity the plant of faba bean activates the salt stress tolerance mechanisms.

The effect of salinity on phosphorus (P) content of plant tissue depends on the level of salinity, plant available P content, plant species (cultivar) and developmental stage of plant.¹⁵ Salt stress caused decrease in P concentration of the plant tissue¹⁸, which is consistent with the results obtained in present study (Table 2). Use of saline irrigation water caused a decrease in phosphorus leaf content, but without significant difference amongst different salinity levels. The ionic strength effects that reduce the activity of phosphate, sorption processes that control phosphate concentrations in soil solution and low solubility of Ca-P minerals are the usual explanations for salinity-induced reduction in P availability.¹⁵

Studies on Mo uptake by crops in a saline environment are generally scarce. Grattan and Grieve¹⁵ suggest that type of growing media (soil or solution) used in experiment plays role in molybdenum behavior in physiological processes. In a maize study carried out on soil, authors found that salinity increased Mo content¹⁹. Thus, other authors found salinity had no effect on plant Mo uptake from solution²⁰. Results of this study (Table 2) show a slight decrease in Mo accumulation under saline conditions. Decrease was

significant at NaCl₅₀ treatment, comparing to control plants. Mo plant availability depends on soil pH²¹. During this experiment, salinity treatments did not affect pH of saturated soil water extracts, thus indicating that the application of saline irrigation water could interfere with plant Mo uptake.

The majority of studies with crops grown under saline conditions, indicate that salinity decreases Mn shoot content^{19,20}. Salt stress induced Mn deficiency in shoot has been reported for barley²². Authors have confirmed their hypothesis that increase in leaf Mn content, alleviate salt stress symptoms (increase in relative growth rate, net assimilation rate and net photosynthetic rate of salt stressed plants). In this experiment, treatments with saline irrigation water resulted with slight increase in Mn faba bean leaf content (Table 2). In reference to control plants, increase in Mn leaf content was significant at NaCl₅₀ treatment. Considering analyzed plant tissue, salinity composition and growing conditions have been constant for all the treatments during the experiment, variation in results of Mn leaf content can be assigned to different irrigation water salinity levels. In addition, Mn uptake is metabolically mediated²¹ and faba bean leaves accumulate Mn from the soil solution²³. Mn in soil solution participates in cation competition and magnesium particularly depresses Mn uptake²¹. Results at NaCl₅₀ treatment also show a significant increase in Mg content of a saturated soil/substrate water extract. Nevertheless, faba bean was able to increase Mn uptake from a soil/substrate mixture with high Mg content. Thus, salinity induced increase in Mn leaf content suggests presence of faba bean salt stress adaptation mechanism.

Mn in plants functions as an active center of superoxide dismutase (Mn-SOD) and participates in plant antioxidant defense. Such stress is produced by high levels of activated forms of oxygen and free radicals (ROS – reactive oxygen species), which are deleterious to plants. Mn-SOD is considered to play an important role in the adaptive plant responses and tolerance improvement under salt stress²⁴. Transgenic *Arabidopsis* plants over-expressed Mn-SOD, which played a major role in preventing accumulation of ROS caused by salt stress, thus enhancing their salt stress tolerance²⁵. Transgenic tomato plants also have improved NaCl-stress tolerance by Mn-SOD overexpression²⁶. Thus, increased Mn level in plant tissue under salt stress suggests possibility that Mn is used for SOD activation, as an adaptive response to increased salinity.

At NaCl₅₀ treatment (7,5 dS/m), the most significant differences in faba bean leaf occurred in element accumulation under saline conditions (K and Mo most significantly decreased, Mn most significantly increased), as compared to control plants. Results of NaCl₆₅ treatment, actually the highest one, are also consistent with a general trend in salinity effect on element accumulation, in reference to control plants, but slightly diminishing that difference. These results suggest that at electrical conductivity of the root zone >7,5 dS/m, faba bean activates certain salt stress adaptation mechanism, which may be a subject of further studies.

Conclusions

Results of this study show that the use of saline irrigation water increases root zone salinity and affects certain faba bean leaf element accumulation. However, trace element leaf content was significantly altered only for Mo and Mn at certain salinity level. In addition, this research implies existence of Mn-associated faba bean salt stress adaptation and tolerance improvement mechanism. If so, this mechanism occurred as a natural faba bean salt stress response. Results provide foundation for further research to identify faba bean mechanisms of adaptive responses under salt stress. It can also be used as a basis for determination of salt tolerance traits in horticultural crops.

References

- ¹Romic D., Ondrasek G., Romic M., Borosic J., Vranjes M., Petosic D., *Irrig. Drain.*, 2008, 57, 463.
- ²Maggio A., De Pascale S., Fagnano M., Barbieri G., *Ital. J. Agron.*, 2011, 6:e7, 36.
- ³Ondrasek G., Romic D., Rengel Z., Romic M., Zovko M., *Sci. Total Environ.*, 2009, 407, 2175.
- ⁴Ondrasek G., Romic D., Romic M., Duralija B., Mustač I., *Agric. Conspec. Sci.*, 2006, 4, 155.
- ⁵Samineni S., Siddique K. H. M., Gaur P. M., Colmer T. D., *Environ. Exp. Bot.*, 2011, 71, 260.
- ⁶Abdelhamid M. T., Shokr M. M. B., Bekheta M. A., *Commun. Soil Sci. Plant Anal.*, 2010, 41, 2713.
- ⁷Daur I., Sepetoglu H., Marwat K. B., Geverek M. N., *Pak. J. Bot.*, 2010, 42(5), 3477.
- ⁸Al-Tahir O. A., Al-Abdulsalam M. A., *Agric. Water Manage.* 1997, 34, 161.
- ⁹Katerji N., Van Hoorn J. W., Hamdy A., Mastrotrilli M., Oweis T., *Agric. Water Manage.*, 2005, 72, 177.
- ¹⁰Qados A. M. S., *J. Saudi Soc. Agric. Sci.*, 2011, 10, 7.
- ¹¹Katerji N., Mastrotrilli M., Lahmer F. Z., Maalouf F., Oweis T., *Eur. J. Agron.*, 2011, 35, 2.
- ¹²Romic D., Romic M., *Proc. Int. Conf. Water Manage. Salinity Pollut. Control Sustainable Irrig. Mediterr. Reg.*, 1997 (4), 275.
- ¹³Bohn H. L., McNeal B. L., O'Connor G. A., *Soil chemistry, 3rd Edition, John Wiley & Sons*, 2001.
- ¹⁴Manchanda G., Garg N., *Acta Physiol. Plant.*, 2008, 30, 595.
- ¹⁵Grattan S.R., Grieve C.M., *Sci. Hortic.*, 1999, 78, 127.
- ¹⁶Meiri, A., Kamburoff, J., Poljakoff-Mayber, A., 1971, *Ann. Bot.*, 35, 837.
- ¹⁷Cachorro, P., Ortiz, A., Cerda, A., *Plant Sci.*, 1993, 95, 23.
- ¹⁸Sharpley, A.N., Meisinger, J.J., Power, J.F., Suarez, D.L., *Adv. Soil Sci*, 1992, 19, 151.
- ¹⁹Rahman, S., Vance, G.F., Munn, L.C., *Comm. Soil Sci. Plant Anal.*, 1993, 24, 2251.
- ²⁰Izzo, R., Navari-Izzo, F., Quartacci, M.F., *J. Plant Nutr.*, 1991, 14, 687.
- ²¹Mengel K., Kirkby E. A., *Principles of plant nutrition, 2nd Edition, International Potash Institute*, 1979.
- ²²Cramer, G.R., Nowak, R.S., *Physiol. Plant.* 1992, 84, 600.
- ²³Rashed M. N., Awadallah R. M., *J. Sci. Food Agric.*, 1998, 77, 18.

²⁴Millaleo R., Reyes – Diaz M., Ivanov A. G., Mora M. L., Alberdi M., *J. Soil Sci. Plant Nutr.*, 2010, 10 (4), 476.

²⁵Wang Y., Ying Y., Chen J., Wang X., *Plant Sci.*, 2004, 167, 671.

²⁶Wang Y., Wisniewski M., Meilan R., Uratsu S. L., Cui M., Dandekar A., Fuchigami L., *J Appl. Hortic.*, 2007, 9 (1), 3.

Paper was presented at the 4th International Symposium on Trace Elements in the Food Chain, Friends or Foes, 15-17 November, 2012, Visegrád, Hungary

Received: 30.10.2012.

Accepted: 24.11.2012.



INHIBITION OF CORROSION OF CARBON STEEL IN SEA WATER BY SODIUM MOLYBDATE – Zn²⁺ SYSTEM

S. Rajendran^{[a,b]*}, K. Anuradha^[c], K. Kavipriya^[a], A. Krishnaveni^[d],
and J. Angelin Thangakani^[e]

Keywords: Carbon steel, sodium molybdate, synergistic effect, Atomic Force Microscopy (AFM), and sea water.

The inhibition efficiency of sodium molybdate (SM) - Zn²⁺ system in controlling corrosion of carbon steel in seawater has been evaluated by weight-loss method. The formulation consisting of 250 ppm of SM and 75 ppm of Zn²⁺ has 80% IE. Influence of duration of immersion on the IE of SM – Zn²⁺ has also been evaluated. The mechanistic aspects of corrosion inhibition have been investigated by polarization study and AC impedance spectra. The protective film has been analyzed by FTIR, and luminescence spectra. The surface morphology and the roughness of the metal surface have been analyzed by atomic force microscopy. The protective film consists of Fe²⁺ – molybdate complex and Zn(OH)₂. It is found to be UV - fluorescent.

Corresponding Authors

Email: srmjoany@sify.com

- [a] Corrosion Research Centre, PG and Research Department of Chemistry, GTN Arts College, Dindigul, Tamilnadu, India - 624 005.
- [b] Corrosion Research Centre, RVS School of Engineering and Technology, Dindigul, Tamilnadu, India -624 005.
- [c] Department of Chemistry, N. K. R. Government Arts College for Women, Namakkal, Tamilnadu, India - 637 001.
- [d] Department of Chemistry, Yadava College, Madurai, Tamil Nadu, India - 625 014.
- [e] C.E.O.A Matriculation Higher Secondary School, A. Kosakulam, Madurai, Tamil Nadu, India - 625 017.

INTRODUCTION

Metals like copper, aluminium and carbon steel are the dominant materials for sea water systems in many countries. The metals get corroded when they come in contact with seawater because of various corrosive ions, such as chloride present in seawater. Seawater can also be used in cooling water systems made of aluminium, copper or carbon steel. In such cases, suitable inhibitors have to be used to protect the cooling water structures. In such studies, natural seawater is used or simulated seawater or 3.5% NaCl is used as the environment. Jafar Zadeh et al.¹ have studied corrosion behaviour of AA5083-H321 aluminium alloy in 3.5% NaCl solution. Their study revealed that the pit density on the sample surface increased with increasing the rotation speed. Amadeh et al.² have used rare earth cations as corrosion inhibitors for carbon steel in aerated 3.5% NaCl solution. A maximum inhibition efficiency of 76% was achieved. John Berchmans et al.³ have used 1, 2, 4, 5 tetrazo spiro (5, 4) decane – 3 thione as a corrosion inhibitor for arsenical aluminium brass in 3.5% NaCl solution. The adsorption of this compound obeyed Temkin's adsorption isotherm. Guanidine derivative has been used by Khaled to control corrosion of copper in 3% NaCl solution. Maximum inhibition efficiency provided by this system is 99%⁴. Sherif and Su-Moon Park⁵ achieved 97% inhibition efficiency in controlling corrosion of copper in 3.0% NaCl solution, by addition of 2-Amino-5-ethyl-1, 3, 4- thiazole. Mahdavian and Naderi⁶ have controlled corrosion of mild steel in 3.5% NaCl solution by addition of some zinc complexes such as zinc gluconate and zinc acetate. Zinc gluconate formed insoluble corrosion products on the mild

steel surface, which protected the metal from corrosion. El-Sayed M. Sherif et al.⁷ have used 3-amino -1, 2, 4- triazole (ATA) to inhibit corrosion of copper in aerated synthetic sea water solution. The inhibition is due to adsorption of ATA molecules onto the copper surface. Soluble conducting poly (aniline – co-orthotoluidine) copolymer has been used to inhibit corrosion of carbon steel in 3% NaCl solution by Benchikh et al.⁸. Polyethyleneimine (PEI) has been used as corrosion inhibitor for ASTM 420 stainless steel in near-neutral saline media by Matjaz Finsgar et al.⁹. A dense layer of PEI is effective in preventing diffusion of ionic species from the film and in preventing attack by chlorine from the salt water Yazdzad et al.¹⁰ have studied the inhibition of 3003 aluminium alloy corrosion by propargyl alcohol and tartrate ion and their synergistic effects in 0.5% NaCl solution. Both the inhibitors obeyed the Langmuir isotherm and the thermodynamic calculations revealed that the adsorption of inhibitors was of physical nature.

The present work is undertaken (i) to evaluate the inhibition efficiencies of sodium molybdate SM – Zn²⁺ system in controlling corrosion of carbon steel in sea water by weight-loss method, (ii) to analyze the protective film by FTIR and luminescence spectra, (iii) to analyze the surface morphology by AFM, and (iv) to propose a suitable mechanism of corrosion inhibition based on the results from the above study.

EXPERIMENTAL

Preparation of specimens

Carbon steel specimens [0.0267 % S, 0.06 % P, 0.4 % Mn, 0.1 % C and the rest iron] of dimensions 1.0 cm x 4.0 cm x 0.2 cm were polished to a mirror finish and degreased with trichloroethylene.

Weight-loss method

Carbon steel specimens in triplicate were immersed in 100 mL of the solutions containing various concentrations of the inhibitor in the presence and absence of Zn²⁺ for one day.

The weight of the specimens before and after immersion was determined using a Shimadzu balance, model AY62. The corrosion products were cleaned with Clarke's solution¹¹. The inhibition efficiency (IE) was then calculated using the equation.

$$IE = 100 \left[1 - \frac{W_2}{W_1} \right] \% \quad (1)$$

where W_1 = corrosion rate in the absence of the inhibitor, and W_2 = corrosion rate in the presence of the inhibitor.

Polarization study

Polarization studies were carried out in an H & CH electrochemical workstation impedance analyzer, model CHI 660A.

A three-electrode cell assembly was used. The working electrode was carbon steel. A saturated calomel electrode (SCE) was used as the reference electrode and a rectangular platinum foil was used as the counter electrode.

AC impedance measurements

The instrument used for polarization study was used for AC impedance measurements too. The cell set up was the same as that was used for polarization measurements. The real part (Z') and the imaginary part (Z'') of the cell impedance were measured in ohms at various frequencies. The values of charge transfer resistance, R_t , and the double layer capacitance, C_{dl} , were calculated.

$$R_t = (R_s + R_t) - R_s \quad (2)$$

where R_s = solution resistance, and

$$C_{dl} = \frac{1}{2} \Pi R_t f_{max} \quad (3)$$

where f_{max} = maximum frequency.

Surface examination study

The carbon steel specimens were immersed in various test solutions for a period of one day. After one day, the specimens were taken out and dried. The nature of the film formed on the surface of the metal specimens was analyzed for surface analysis technique by FTIR spectra and fluorescence spectra.

FTIR spectra

The film formed on the metal surface was carefully removed and mixed thoroughly with KBr. The FTIR spectra were recorded in a Perkin Elmer 1600 spectrophotometer.

Fluorescence spectra

These spectra were recorded in a Hitachi F-4500 fluorescence spectrophotometer.

Atomic Force Microscopy

Atomic Force Microscope (AFM) is an exciting new technique that allows surface to be imaged at higher resolutions and accuracies than ever before. The microscope used for the present study was (PICOSPM 1, Molecular Imaging, USA make) polished specimens prior to the initiation of all corrosion experiments were examined through an optical microscope to find out any surface defects such as pits or noticeable irregularities like cracks, etc. only those specimens, which had a smooth pit free surface, were subjected for AFM examination. The protective films formed on the carbon steel specimens after immersion in the inhibitor systems for different time durations were examined for a scanned area of 30 x 30 μm^2 and 15 x 15 μm^2 . A two dimensional, and a three-dimensional topography of surface films gave various roughness parameters of the film.

RESULTS AND DISCUSSION

The inhibition efficiency of sodium molybdate (SM) – Zn²⁺ system in controlling corrosion of carbon steel in sea water (Table 1) has been evaluated by weight-loss method and electrochemical studies such as potentiodynamic polarization study and AC impedance spectra.

Table 1 Characteristics of sea water collected from Tiruchendur, in Thoothukudi district, Tamilnadu, India.

Parameter	Value
Total dissolved salts (mg L ⁻¹)	41,600
Electrical conductivity ($\mu\Omega^{-1} \text{cm}^{-1}$)	64,000
pH	7.4
Total Hardness (CaCO ₃ equivalent)	4000
Calcium as Ca ²⁺ (mg L ⁻¹)	600
Magnesium as Mg ²⁺ (mg L ⁻¹)	600
Sodium as Na ⁺ (mg L ⁻¹)	8900
Chloride as Cl ⁻ (mg L ⁻¹)	20,750
Fluoride as F ⁻ (mg L ⁻¹)	1.5
Free ammonia as NH ₃ (mg L ⁻¹)	0.09
Sulphate as SO ₄ ²⁻ (mg L ⁻¹)	2332

Weight loss method

Inhibition efficiencies (IE %) of SM - Zn²⁺ systems in controlling corrosion of carbon steel in sea water (immersion period = 5 days) are given in Table 2. It is observed that SM alone has good inhibition efficiency. Increasing the concentration of SM, IE also increases.¹²⁻¹⁴

In the presence of various concentration of Zn²⁺ (25, 50 and 75 ppm), the IE of SM increases. A synergistic effect exists between SM and Zn²⁺. For example, 250 ppm of SM

has only 47% IE; 75 ppm of Zn²⁺ has 39% IE. However, their combination has 80% IE. This suggests a synergistic effect existing between SM and Zn²⁺.

Table 2. Inhibition efficiency (IE %) provided by sodium molybdate (SM) - Zn²⁺ System to carbon steel in sea water, obtained by weight loss method. Duration of immersion = 5 days.

SM ppm	Zn ²⁺ , ppm			
	0	25	50	75
0	-	13	20	39
50	14	35	48	60
100	23	49	56	66
150	29	50	67	73
200	38	55	71	76
250	47	60	78	80

Influence of duration of immersion on the inhibition efficiency of the SM -Zn²⁺ system

The formulation consisting of 250 ppm SM and 75 ppm of Zn²⁺ has 80% IE (immersion period = 5 days). The influence of immersion period on the IE of this system is shown in Fig1. It is observed that the IE almost remains constant up to 5 days. Afterwards, the IE decreases. On the seventh day, the IE decreases from 80% to 78%. This is due to the fact that as the immersion period increases, the protective film formed on the metal surface, namely, Fe²⁺ - molybdate complex, is broken by the corrosive chloride ions present in sea water and hence the IE decreases. Further, a competition arises between the formation of Fe²⁺ - molybdate complex and FeCl₂/FeCl₃. As the immersion period increases, the formation of FeCl₂/ FeCl₃ is favoured to Fe²⁺ - molybdate complex at the anodic sites of the metal and hence the IE decreases¹⁵.

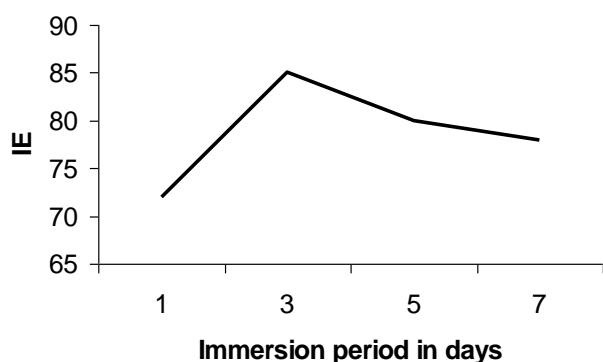


Figure 1. Influence of immersion period on the IE of the SM (250 ppm) + Zn²⁺ (75 ppm) system.

Synergism Parameters

Synergism Parameter (S_I) has been calculated to know the synergistic effect existing between two inhibitors.¹⁶⁻¹⁹ Synergism parameter is calculated using the relation.

$$S_I = \frac{1 - \theta_{1+2}}{1 - \theta'_{1+2}}$$

where, $\theta_{1+2} = (\theta_1 + \theta_2) - (\theta_1 * \theta_2)$, θ = surface coverage of inhibitor, θ_1 =surface coverage of inhibitor 1, θ_2 = surface coverage of inhibitor 2, θ'_{1+2} = combined surface coverage in presence of inhibitors 1 and 2.

$$\theta = \frac{IE \%}{100} \quad \text{and} \quad \theta'_{1,2} = \frac{\text{combined IE \%}}{100}$$

When a synergistic effect exists between two inhibitors, the synergism parameter will be greater than 1. It is observed from Table 3 the S_I values are greater than 1. This confirms the synergistic effect existing between SM and Zn²⁺. As a model, the Zn²⁺ (75 ppm)-SM (50, 100, 150, 200 and 250 ppm) system has been selected, to evaluate the synergism parameters.

Table 3. Synergism parameters (S_I) of SM (50, 100, 150, 200, 250 ppm) - Zn²⁺ (75 ppm) system

SM ppm	IE% θ_1	Zn ²⁺ ppm	IE% θ_2	Combined IE%, θ'_{1+2}	Synergism parameter, S _I
50	14	75	39	60	1.3
100	23	75	39	66	1.4
150	29	75	39	73	1.6
200	38	75	39	76	1.6
250	47	75	39	80	1.6

Potentiodynamic polarization study

Polarization study has been used to confirm the formation of protective film on the metal surface.²⁰⁻²⁴ If a protective film is formed on the metal surface, the linear polarization resistance value (LPR) increases and the corrosion current value (I_{corr}) decreases.

The polarization curves of carbon steel immersed in sea water in presence of inhibitor system are shown in Fig. 2. The corrosion parameters, namely, corrosion potential (E_{corr}), Tafel slopes (b_c = cathodic; b_a = anodic), LPR values and I_{corr} values are given in Table 4.

Table 4 Corrosion parameters of carbon steel immersed in seawater in presence of SM - Zn²⁺ system obtained from potentiodynamic polarization study

System	E_{corr} mV*	b_c mV**	b_a mV**	LPR ohm cm ²	I_{corr} A/cm ²
SW	-676	362	120	152.8	2.559x10 ⁻⁴
SW+A	-669	351	113	154.9	2,394*10 ⁻⁴

SW=sea water; SW+A=sea water + 250 ppm SM + 75 ppm Zn²⁺; *mV vs SCE; **mV in one decade

When the inhibitors, namely, SM (250 ppm) + Zn²⁺ (75 ppm) are added to the seawater, the corrosion potential of carbon steel shifts to the noble side (-676 to -669 mV vs SCE). This indicates that a film is formed on the anodic sites of the metal surface. This film controls the anodic reaction of metal dissolution ($Fe \rightarrow Fe^{2+} + 2e^-$) by forming Fe²⁺ - molybdate complex on the anodic sites of the metal surface. Formation of Fe²⁺ - molybdate complex to some extent cannot be ruled out.

The formation of protective film on the metal surface is further supported by the fact that the LPR value increases from 152.8 to 154.9 ohm cm^2 ; the corrosion current decreases from 2.559×10^{-4} to 2.394×10^{-4} A/cm^2 . Thus polarization study confirms the formation of a protective film on the metal surface.

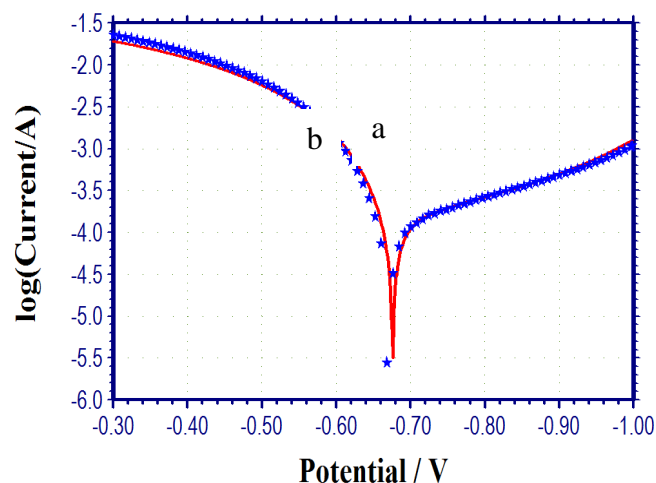


Figure 2. Polarization curves of carbon steel immersed in various test solution. a) Sea water; b) Sea water + SM 250 ppm + Zn^{2+} 75 ppm

AC impedance spectra

AC impedance spectra [Electro chemical impedance spectra] have been used to confirm the formation of protective film on the metal surface²⁵⁻²⁷. If a protective film is formed on the metal surface, the charge transfer resistance (R_t) value increases; double layer capacitance value (C_{dl}) decreases and the Impedance, $\log(z/\text{ohm})$, value increases. The AC impedance spectra of carbon steel immersed in seawater, in presence of inhibitor system (SM- Zn^{2+}) are shown in Figs 3 to 5. The Nyquist plots are shown in Fig 3. The Bode plots are shown in Figs 4 and 5. The corrosion parameters, namely, R_t , C_{dl} and Impedance, $\log(z/\text{ohm})$, values are given in Table 5.

Table 5 Corrosion parameters of carbon steel immersed in sea water in presence of SM – Zn^{2+} system obtained from AC impedance spectra.

System	Nyquist plot		Bode plot
	R_t , ohm cm^2	C_{dl} , F cm^{-2}	Impedance, $\log(Z \text{ ohm}^{-1})$
Sea water	6.88	2.849×10^{-7}	0.9291
Sea water+A	7.04	2.7825×10^{-7}	0.9830

A=SM (250 ppm) + Zn^{2+} (75 ppm)

When the inhibitors [SM (250 ppm) + Zn^{2+} (75 ppm)] are added to sea water, the R_t value increases from 6.88 to 7.04 ohm cm^2 ; the C_{dl} value decreases from 2.849×10^{-7} to 2.783×10^{-7} F/cm^2 ; The impedance value increases from 0.9291 to 0.9830.

These results lead to the conclusion that a protective film is formed on the metal surface.

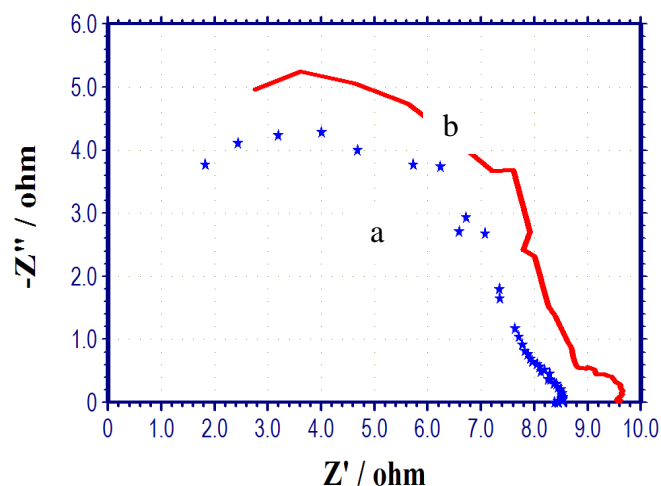


Figure 3. AC impedance spectra of carbon steel immersed in various test solution (Nyquist Plot); a) Sea water; b) Sea water + SM 250 ppm + Zn^{2+} 75 ppm

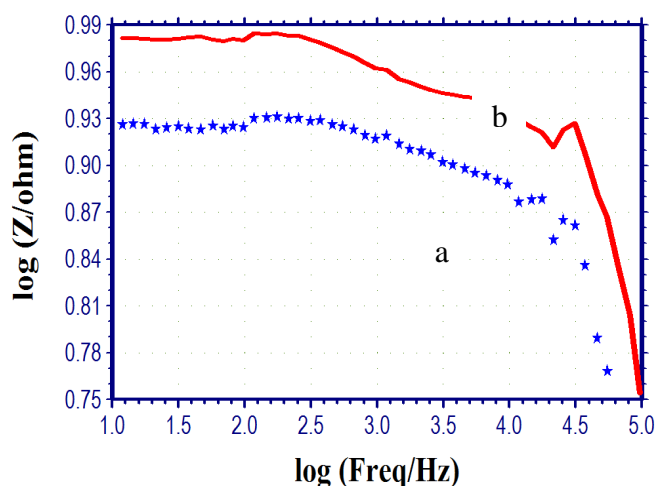


Figure 4. AC impedance spectra of carbon steel immersed in various test solution (Bode Plot); a) Sea water; b) Sea water + SM 250 ppm + Zn^{2+} 75 ppm.

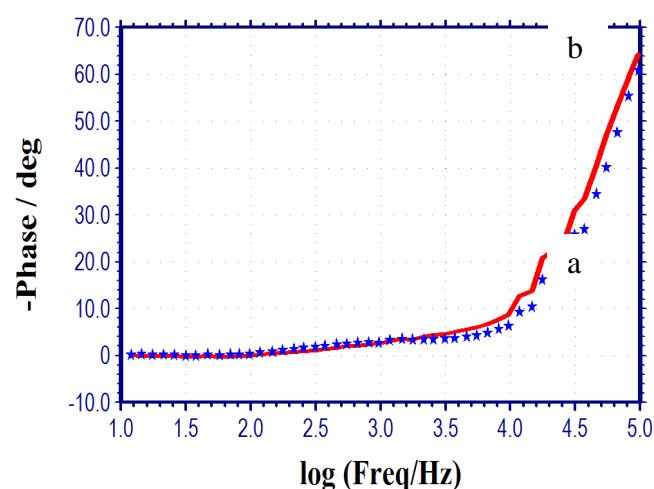


Figure 5. AC impedance spectra of carbon steel immersed in various test solution (Bode Plot); a) Sea water; b) Sea water + SM 250 ppm + Zn^{2+} 75 ppm

FTIR spectra

FTIR spectra have been used to analyze the protective film formed on the metal surface.²²⁻²⁸ The FTIR spectrum (KBr) of pure SM is shown in Fig 6a.

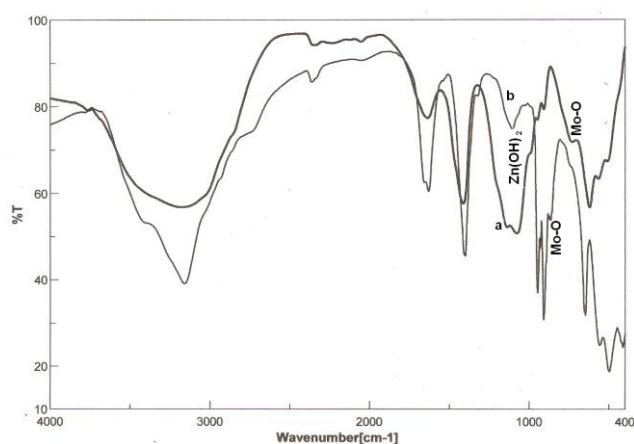


Figure 6. FT-IR Spectra; a) Pure SM; b) Film formed on the metal surface after immersion in sea water + SM (250 ppm) + Zn^{2+} (75 ppm)

The FTIR spectrum of the film formed on the metal surface after immersion in seawater containing 250 ppm of SM and 75 ppm of Zn^{2+} is shown in Fig 6b. Studies from the literature reveal that molybdates are coordinated through ring oxygen atom with metal surface and form synergistic complexes with additives like calcium and zinc cations. The band due to Zn-O stretch appears at 1107 cm^{-1} . These results confirm the presence of $\text{Zn}(\text{OH})_2$ deposited on the cathodic sites of the metal surface.²⁹

Thus FTIR spectral study leads to the conclusion that the protective film consists of Fe^{2+} – molybdate complex and $\text{Zn}(\text{OH})_2$

Luminescence Spectra

Luminescence spectra have been used to detect the presence of Fe^{2+} - inhibitor complex formed on the metal surface^{23, 29, 30}.

The luminescence spectrum ($\lambda_{\text{ex}} = 230\text{ nm}$) of the Fe^{2+} – molybdate complex solution, prepared by mixing an aqueous solution of Fe^{2+} (prepared freshly from $\text{FeSO}_4 \cdot 7\text{H}_2\text{O}$) and SM, is shown in Fig 7a. A peak appears at 690 nm.

The luminescence spectrum ($\lambda_{\text{ex}} = 230\text{ nm}$) of the film formed on metal surface after immersion in the solution containing 250 ppm of SM and 75 ppm of Zn^{2+} is shown in Fig 7b. A peak appears at 692 nm. This indicates that the film present on the metal surface consists of Fe^{2+} – molybdate complex. The slight variation in the position of the peak is due to the fact that the Fe^{2+} – molybdate complex is entrained in $\text{Zn}(\text{OH})_2$ present on the metal surface. Further, the increase in intensity of the peak is due to the fact that the metal surface, after the formation of the protective film is very bright, the film is very thin and there is enhancement in the intensity of the peak.

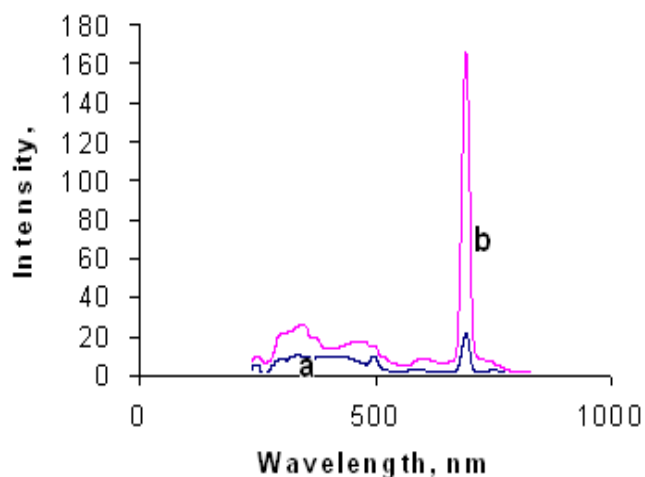


Figure 7. Luminescent spectra for carbon steel immersed in various test solutions using SM as inhibitor; a) Fe^{2+} – molybdate complex; b) Protective film formed on the surface of carbon steel after immersion in the solution containing 250 ppm SM and 75 ppm Zn^{2+}

Atomic Force Microscopy

Atomic force microscopy is a powerful technique for the gathering of roughness statistics from a variety of surfaces³¹. AFM is becoming an accepted method of roughness investigation³². All atomic force microscopy images were obtained on (PICOSPM 1, Molecular Imaging and USA make) AFM instrument operating in contact mode in air. The scan sizes of all the AFM images are $30\mu\text{m} \times 30\mu\text{m}$ areas at a scan rate of 2.4 lines per second.

The two dimensional, three dimensional AFM morphologies and the AFM cross sectional profile for polished carbon steel surface (reference sample), carbon steel surface immersed in sea water (blank sample) and carbon steel surface immersed in sea water containing 250 ppm SM and 75 ppm Zn^{2+} are shown in Fig. 8 (a,d,g), (b,e,h), (c,f,i) respectively.

Root mean square roughness, average roughness and peak to valley value:

AFM image analysis was performed to obtain the average roughness, R_a (the average deviation of all points roughness profile from a mean line over the evaluation length), root – mean – square roughness, R_q (the average of the measured height deviations taken within the evaluation length and measured from the mean line) and the maximum peak to valley (P-V) height values (largest single peak-to-valley height in five adjoining sampling heights)³³. R_q is much more sensitive than R_a to large and small height deviations from the mean³⁴.

Table 6 is a summary of the average roughness R_a , rms roughness (R_q) and maximum peak to valley height (P-V) value for carbon steel surface immersed in different environments. The values of R_q , R_a and P-V height for the polished carbon steel surface (reference sample) are 262 nm, 211 nm and 1200 nm respectively. This shows that the surface is more homogenous with some places where the

height is lower than the average depth. Fig. 8 (a, d, g) displays the non-corroded metal surface. The slight roughness observed on the polished carbon steel surface is due to atmospheric corrosion. The rms roughness, average roughness and P-V height values for the carbon steel surface immersed in sea water are 765 nm, 645 nm and 3700 nm

respectively. These values suggest that carbon steel surface immersed in sea water has a greater surface roughness than the polished metal surface, indicating that the unprotected carbon steel surface is rougher and were due to the corrosion of carbon steel in sea water environment. Fig. 8. (b, e, h) displays corroded metal surface with few pits.

Table 6. AFM data for carbon steel immersed in inhibited and uninhibited environments.

Sample	RMS (R_q) roughness, nm	Average (R_a) roughness, nm	Maximum peak to valley height, nm
Polished carbon steel, (control)	262	211	1200
Carbon steel immersed in sea water (blank)	765	645	3700
Carbon steel immersed in sea water containing 250 ppm SM and 75 ppm Zn^{2+}	665	582	2750

Fig 8 (c,f,i) shows the formulation consisting of 250 ppm SM and 75 ppm Zn^{2+} in sea water the R_q value of 665 nm and the average roughness is significantly reduced to 582 nm when compared with 645 nm for carbon steel surface immersed in sea water. The maximum peak to valley height was also reduced to 2750 nm. These parameters confirm that the surface appears smoother. The smoothness of the surface is due to the formation of a protective film of Fe^{2+} – molybdate complex and $\text{Zn}(\text{OH})_2$ on the metal surface thereby inhibiting the corrosion of carbon steel. The above parameters are also somewhat greater than the AFM data of polished metal surface which confirms the formation of film on the metal surface, which is protective in nature.

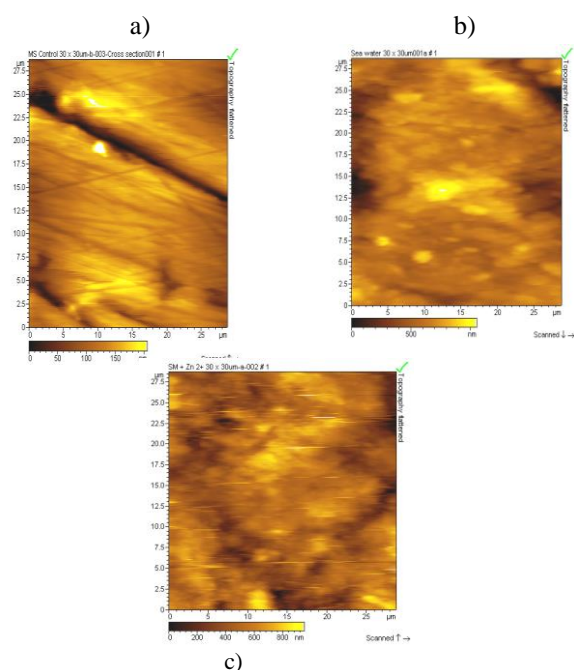


Fig 8. Two dimensional images of surface of a) polished carbon steel (control) b) carbon steel immersed in sea water (blank); c) carbon steel immersed in sea water containing 250 ppm SM and 75 ppm Zn^{2+}

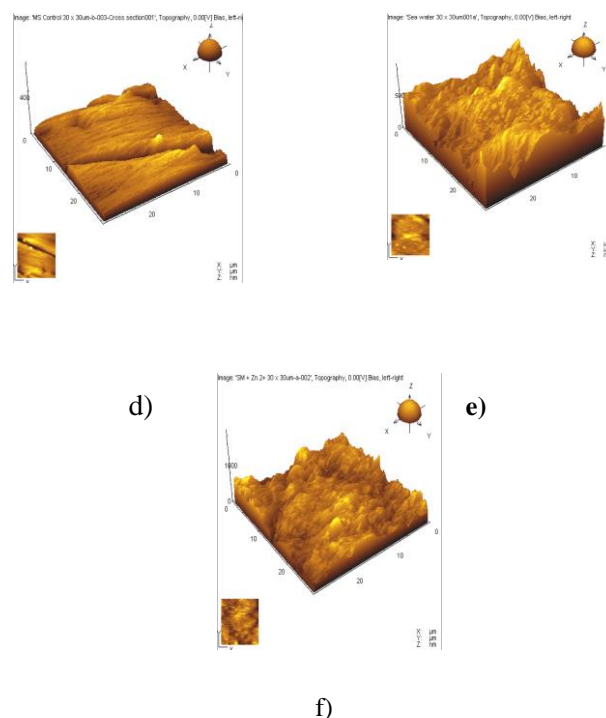


Figure 8. Three dimensional images of surface of d) polished carbon steel (control); e) carbon steel immersed in sea water (blank); f) carbon steel immersed in sea water containing 250 ppm SM and 75 ppm Zn^{2+}

MECHANISM OF CORROSION INHIBITION

Analysis of the results of weight loss method reveals that the formulation consisting of seawater, 250 ppm of SM and 75 ppm of Zn^{2+} offers an IE of 80%. Results of polarization study suggest that the formulation functions as anodic inhibitor. The AC impedance spectral studies indicate that a protective film is formed on the metal surface. FTIR spectra reveal that the protective film consists of Fe^{2+} – molybdate complex and $\text{Zn}(\text{OH})_2$.

In order to explain all these observations in a holistic way the following mechanism of corrosion inhibition is proposed.

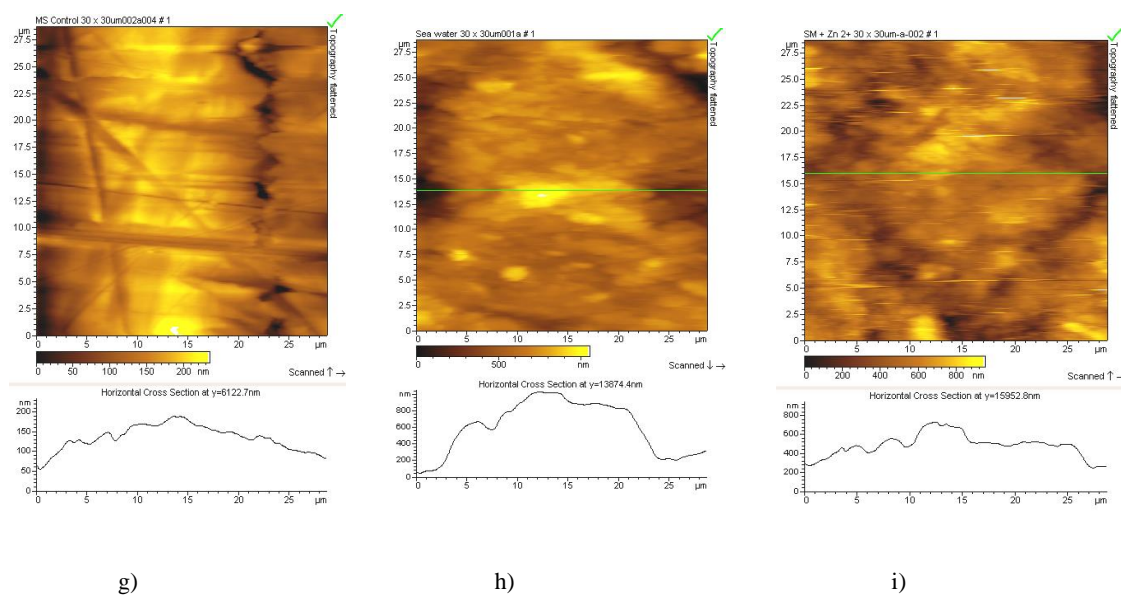


Figure 8. The cross-sectional profiles (shown as broken lines) corresponding to the AFM images of surface of g) Polished carbon steel (control); h) carbon steel immersed in sea water (blank); i) Carbon steel immersed in sea water containing 250 ppm SM and 75 ppm Zn^{2+}

- [a] When carbon steel specimen is immersed in an aqueous solution, the anodic reaction is: $\text{Fe} \rightarrow \text{Fe}^{2+} + 2\text{e}^-$ and the cathodic reaction is: $2\text{H}_2\text{O} + \text{O}_2 + 4\text{e}^- \rightarrow 4\text{OH}^-$.
- [b] When the system containing 250 ppm of SM and 75 ppm of Zn^{2+} is prepared, there is formation of Zn^{2+} – molybdate complex: $\text{Zn}^{2+} + \text{M} \rightarrow \text{Zn}^{2+} - \text{M}$.
- [c] When carbon steel is immersed in the solution, the Zn^{2+} -molybdate diffuses from the bulk of the solution to the metal surface.
- [d] The surface of metal, Zn^{2+} – molybdate complex is converted into Fe^{2+} – molybdate complex at the local anodic regions. The stability of Fe^{2+} - molybdate complex is higher than the corresponding zinc complex. $\text{Zn}^{2+} - \text{M} + \text{Fe}^{2+} \rightarrow \text{Fe}^{2+} - \text{M} + \text{Zn}^{2+}$
- [e] The released Zn^{2+} ions combine with OH^- ions to form $\text{Zn}(\text{OH})_2$ on the cathodic sites: $\text{Zn}^{2+} + 2\text{OH}^- \rightarrow \text{Zn}(\text{OH})_2$
- [e] AC impedance spectra reveal that a protective film is formed on the metal surface.
- [f] FTIR spectra show that the protective film consists of Fe^{2+} – molybdate complex and $\text{Zn}(\text{OH})_2$.
- [g] The IE of inhibitor formulation depends on the ability of the inhibitor to form complex with Zn^{2+} and ability of Fe^{2+} to react with Zn^{2+} to form iron complex.
- [h] This formulation may find applications in cooling water systems also.
- [i] AFM images and luminescent spectra confirm the formation of protective layer on the metal surface.

Thus the protective film consists of Fe^{2+} – molybdate complex and $\text{Zn}(\text{OH})_2$

CONCLUSIONS

The present study leads to following conclusions:

- [a] A synergistic effect exists between SM and Zn^{2+} in controlling corrosion of carbon steel immersed in seawater.
- [b] The formulation consisting of 250 ppm of SM and 75 ppm of Zn^{2+} provided 80% IE.
- [c] Influence of immersion period on the above inhibitor systems has also been studied.
- [d] Polarization study suggests that the combination of SM and Zn^{2+} functions as anodic inhibitor.

REFERENCES

- Jafarzadeh, K., Shahrabi, T., Hadavi, S.M.M., and Hosseini, M.G., *Anti-Corros. Met. Mater.*, **2009**, 56 (1), 35.
- Amadeh, A. Allahkaram, S.R., Hosseini, S.R., Moradi, H., and Abdolhosseini, A., *Anti-Corros. Met. Mater.*, **2008**, 55 (3), 135.
- Berchmans, J.L., Iyer, S.V.K., Sivam, V., and Quraishi, M.A., *Anti-Corros. Met. Mater.*, **2001**, 48 (6), 376.
- Khaled, K.F., *Mater. Chem. Phys.*, **2008**, 112 (1), 104.
- Sherif, E.M., and Park, S., *Corros. Sci.*, **2006**, 48 (12), 4065.
- Mahdavian, M., and Naderi, R., *Corros. Sci.*, **2011**, 53 (4), 1194.
- Sherif, E.M., Erasmus, R.M., and Comins, J.D., *J. Colloid Interface Sci.*, **2007**, 309 (2), 470.
- Benchikh, A., Aitout, R., Makholoufi, L., Benhaddad, L., and Saidani, B., *Desalination*, **2009**, 249 (2), 466.
- Finsgar, M., Fassbender, S., Nicolini, F., and Milosov, I., *Corros. Sci.*, **2009**, 51 (3), 525.
- Yazdazad, A.R., Shahrabi, T., and Hosseini, M.G., *Mater. Chem. Phys.*, **2008**, 109 (2-3), 199.

- ¹¹Wranglen, G., *Introduction to corrosion and protection of Metals*. London: Chapman & Hall, **1985**, p. 236.
- ¹²Shanthy, P., Rengan, P., Thamarai Chelvan, A., Rathika, K., and Rajendran, S., *Int. J. Chem. Tech.* **2009**, *16*.
- ¹³Rajendran, S., Apparao, B.V., and Palaniswamy, N., *J. Electrochem. Soc. India.* **1999**, *48* (1), 89.
- ¹⁴Selvi, J.A., Rajendran, S., and Jeyasundari, J., *Zastita Materijala*, **2009**, *50* (2), 91.
- ¹⁵Selvaraj, S.K., Kennedy, A.J., Amalraj, J.A., Rajendran, S., and Palaniswamy, N., *Corros.Rev.*, **2004**, *22* (3), 219.
- ¹⁶Gomma, G.K., *Mater. Chem. Phys.*, **1998**, *55* (3), 241.
- ¹⁷Aramaki, K., and Hackerman, N., *J. Electrochem. Soc.*, **1969**, *116* (15), 568.
- ¹⁸Quraishi, M.A., Rawat, J., and Ajmal, M., *Corrosion*, **1999**, *55* (10), 919.
- ¹⁹Kanimozhi, S. A., and Rajendran, S., *Int. J. Electrochem. Sci.*, **2009**, *4*, 353.
- ²⁰Roque, J.M., Pandiyan, T., Cruz, J., and Garcia-Ochoa, E., *Corros. Sci.*, **2008**, *50* (3), 616.
- ²¹Benali, O., Larabi, L., Traisnel, M., Gengembre, L., and Harek, Y., *Appl.Surf. Sci.* **2007**, *253* (14), 6130.
- ²²Amar, H., Braisaz, T., Villemin, and D., Moreau, B., *Mater. Chem. Phys.*, **2008**, *110* (1) 1.
- ²³Selvi, J.A., Rajendran, S., Ganga Sri, V., Amalraj, J.A., Narayanasamy, B., *Port. Electrochim. Acta.*, **2009**, *27* (1), 1.
- ²⁴Rajendran, S., Paulraj, J., Rengan, P., Jeyasundari, J., and Manivannan, M., *J. Dent. Oral. Hyg.* **2009**, *1* (1),1.
- ²⁵Zhang, S., Tao, Z., Li, W., and Hou, B., *Appl. Surf. Sci.*, **2009**, *255* (15), 6757.
- ²⁶El-Taib Heikal, F., Fouda, A.S., Radwan, M.S., *Mater. Chem. Phys.*, **2011**, *125* (1-2), 26.
- ²⁷Rajendran, S., Devi, K.M., Regis, P.P., A., Amalraj, J.A., Jeyasundari, J., and Manivannan, M., *Zastita materijala.*, **2009**, *50* (3), 131.
- ²⁸Sathiyabama, J., Rajendran, S., Selvi, J.A., and Jeyasundari, J., *Open Corros. J.*, **2009**, *2*, 77.
- ²⁹Kalaivani, R., Narayanaswamy, B., Selvi, J.A., Amalraj, J.A., Jeyasundari, J., and Rajendran, S., *Port. Electrochim. Acta.*, **2009**, *27* (2), 177.
- ³⁰Rajendran, S., Apparao, B.V., and Palaniswamy, N., *J. Electrochem. Soc., India* ., **1998**, *47*, 43.
- ³¹Vera, R., Schrebler, R., Cury, P., Del Rio, R., and Romero, H., *J. Appl. Electrochem*, **2007**, *37* (4), 5195.
- ³²Dumas, Ph., Butffakhreddine, B., Am, C., Vatel, O., Ands, E., Galindo, R., and Salvan, F., *Europhys. Lett.*, **1993**, *22*, 717.
- ³³Thomas, T.R., "*Rough Surfaces*", Longman, New York, **1982**.
- ³⁴Stout, K.J., Sullivan, P.J., and Mc Keown, P.A., *Annals CRIP*, **1992**, *41* (1), 621.

Received: 22.10.2012.

Accepted: 24.11.2012.



STATE-OF-CHARGE MONITORING AND ELECTROLYTE REBALANCING METHODS FOR THE VANADIUM REDOX FLOW BATTERY

Sara Corcuera^[a] and Maria Skyllas-Kazacos^{[a]*}

Keywords: vanadium redox flow battery; state-of-charge monitor; capacity loss; cell rebalancing

A major issue with all flow batteries is the control of the imbalance between the two half-cell electrolytes that arises as a result of the differential transfer of ions across the membrane and the inevitable gassing side reactions that can occur during charging. While a number of methods are available to rebalance electrolyte state of charge and restore capacity, reliable methods are needed to monitor the state-of-charge of each individual half-cell solution in order to determine the appropriate action to be taken by the battery control system. In this study different methods of state-of-charge monitoring have been considered for application in the All-Vanadium Redox Flow Battery (VRB). Half-cell potentials and electrolyte conductivities were calibrated as a function of state-of-charge and evaluated for state-of-charge monitoring of individual half-cell electrolytes for the purpose of capacity restoration and control. An empirical model based on experimental conductivity data has been shown to provide accurate predictions, with an average error of 0.77%, of the conductivity of the positive half-cell electrolyte as a potential state-of-charge detection tool. Separate monitoring of the two half-cell electrolyte potentials has also been used to determine the state-of-charge of each half-cell solution in order to detect system imbalance. This was used in small laboratory cell tests to determine necessary actions to restore capacity by either remixing the two solutions, or by using chemical rebalancing methods, depending on the cause of the solution imbalance.

Corresponding Authors

E-Mail: m.kazacos@unsw.edu.au

[a] School of Chemical Engineering,
University of New South Wales,
Sydney, New South Wales, 2052, AUSTRALIA

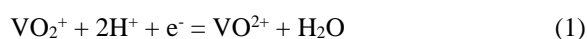
Introduction

Redox flow batteries are a form of energy storage currently receiving considerable attention owing to their favourable properties. The main benefits that make these batteries such a viable alternative are their long operating life and the fact that the power and energy rating can be independently varied to meet the requirements of different applications. Additionally, they have the potential to offer very low capital and operating costs compared with other energy storage technologies for applications requiring more than 4 hours of storage.

The Vanadium Redox Battery (VRB), pioneered at the University of New South Wales (Australia) in the early 80's, employs V(II)/V(III) and V(IV)/V(V) redox couples in sulphuric acid as the negative and positive half-cell electrolytes respectively.¹⁻⁵ In contrast to other redox flow batteries, the VRB makes use of the same elements in both half-cell solutions, eliminating cross contamination problems. The VRB also shows high energy efficiency of over 80%, very low maintenance costs and an indefinite electrolyte life.³

Apart from the simplified set of half-cell reactions displayed below

Positive half-cell:



Negative half-cell:



Other relevant side reactions take place within the cell which lead to imbalance and loss of capacity. Firstly, the differential rates of diffusion of vanadium ions across the cell membrane will lead to a build-up of vanadium ions in one half-cell and a depletion in the other,⁶ leading to capacity loss. This is further exacerbated by water and solution transfer from one half-cell to the other, the direction and magnitude of which depends on the type of membrane used. While these processes can be reversed and capacity restored by simply remixing the two half-cell solutions periodically, other side reactions can occur that cannot be reversed by remixing. These include hydrogen evolution at the negative electrode and to a lesser extent, the evolution of oxygen at the positive electrode during charging.⁷

The higher rate of hydrogen evolution at the negative electrode will inevitably lead to an imbalance between the oxidation states of the two solutions since a portion of the current is consumed by hydrogen ion reduction rather than the V(III) oxidation reaction. Furthermore, when the system is not perfectly sealed, the oxidation of V(II) to V(III) in the negative half-cell solution will also reduce the V(II):V(V) ratio in the two electrolytes, causing a further loss in capacity that requires chemical or electrochemical rebalancing for capacity restoration.

Taking into account the effect of these side reactions, it becomes essential to provide a method for accurately determining the state of charge (SOC) of each individual half-cell solution of a redox flow cell during charge-discharge operation. Different alternatives have been considered including the use of the variation in solution absorbance as a function of state-of-charge.² The non-linearity in absorbance versus state-of-charge observed however, precludes the application of this technique, so alternative, simpler state-of-charge sensors still need to be developed and evaluated.

A very common method for measuring the SOC of a redox flow cell is the installation of open-circuit cell at the entry or exit ports of the electrolytes in the cell stack. By using the Nernst equation, the SOC can be readily obtained from the measured open circuit voltage (OCV). However, as the OCV gives an overall value of the two half-cells, it is assumed that the two half-cells are balanced. Thus, whenever the system becomes unbalanced, this procedure would not accurately indicate the SOC, since it is not possible to determine the imbalance from the cell open circuit potential. Ideally, a method that allows independent monitoring of each half-cell electrolyte should be employed so as to achieve both the determination of the system balance and the state of charge.

In this study, different alternatives have been evaluated for this purpose. Earlier studies showed that the conductivity of both the positive and negative half-cell electrolytes varies in a linear manner as a function of state-of-charge.² Conductivity measurement was thus selected as a possible technique for use in the development of a SOC monitoring system for the VRB. In addition, the use of an indicator and reference electrode to measure the potential of each of the half-cell electrolytes was also evaluated to determine the suitability of this approach for SOC monitoring during charge-discharge cycling.

Initial experiments were conducted to first calibrate both conductivities and solution potentials as a function of SOC for commonly used VRB electrolyte compositions. The potentiometric method was further evaluated during a series of charge-discharge experiments to monitor any imbalance arising between the two half-cell solutions during continuous cycling. Once imbalances in the system can be determined, both chemical and electrochemical rebalancing measures can be introduced to ensure the optimum performance of the whole battery. In the present study, a chemical reductant was added to the positive half-cell electrolyte in order to balance the oxidation states of the two half-cell solutions and thereby restore capacity. Such a technique could be readily integrated into a battery management and control system along with other sensors, in order to instigate appropriate actions such as automated electrolyte remixing and rebalancing procedures that would be able to maintain optimal condition of the VRB during extended operation with minimal human interaction.⁹

Experimental

Two solutions were first prepared with compositions of 1.6 M vanadium in sulphuric acid supporting electrolytes with total sulphate levels of 4 M and 4.2 M. These solutions were prepared by mixing V_2O_3 and V_2O_5 powders in the required ratio in order to produce a 50:50 mixture of V(III) and V(IV), referred to as V(3.5+). Inductively Coupled Plasma (ICP) analysis was performed to verify the concentrations of both V and S in the final solutions and adjustments were made as required.

The V(3.5+) solution was subsequently placed in a flow cell and fully charged to 2.4 V so as to obtain a yellow V(V) solution in the positive half-cell and a violet V(II) solution in the negative half-cell, corresponding to the desired 100% SOC catholyte and anolyte solutions respectively. The V(V) and V(II) solutions were then mixed

in the appropriate ratios to obtain the V(III) and V(IV) oxidation states. The four solutions were subsequently used to produce a series of solutions with different oxidation states corresponding to states-of-charge of 0%, 5%, 10%, 25%, 50%, 75%, 90%, 95% and 100% for both the positive and negative half-cells. Argon was used for sealing the containers to ensure that no air oxidation occurred during storage. Conductivity measurements were taken at three different temperatures: room temperature (25°C), 10°C and 40°C. The sample solutions were allowed to equilibrate in a water bath set at 10 and 40°C with a temperature deviation of $\pm 1^\circ C$. In the case of the room temperature measurements, since the tests took place over a few different days, some variation in room temperature contributed to a discrepancy in the temperature ranges for the negative and positive half-cell electrolytes samples. The equipment used for the conductivity measures was a SCHOTT Conductivity Meter CG-856 with SCHOTT Instruments Electrode LF-613T. It has to be noted that a previous calibration was done using a KCl 0.01M solution to fix the cell constant and the temperature compensation, activated by default, was defused.

For the potentiometric measurements, a carbon rod (indicator electrode) and a saturated calomel electrode (SCE) were immersed in each of the two half-cell electrolyte reservoirs of a flow cell containing the vanadium electrolyte to be used in the calibration. The electrodes were then connected to two separate digital multimeters and the measured solution potential values were automatically recorded in two separate text files. Around 70ml of the 1.6M V solution was placed in each half-cell reservoir and the cell was fully charged at a constant current of 1 A to an upper voltage limit of 2.4V until the distinctive violet (V(II)) and yellow (V(V)) colours were observed in the negative and positive half-cell solution reservoirs respectively. The cell was then cycled between 0.8 and 1.8 V. In order to magnify the effects of air oxidation of V(II) on capacity loss, no effort was made to seal the negative half-cell reservoir, nor was any inert gas used to blanket the V(II) solution during cycling.

During charge-discharge cycling of the cell, half-cell potential values were monitored and the values converted to half-cell solution SOC values using the Nernst Equation. Once a substantial capacity loss was observed, different measures were employed to try to rebalance the electrolytes and restore capacity. These involved (i) remixing the two half-cell solutions and (ii) adding a fixed volume of a proprietary chemical reductant to the positive half-cell solution to determine the cause of the capacity loss and to restore capacity as appropriate.

Results and discussion

Electrolyte conductivity as a function of state of charge

Previous studies with 2 M vanadium electrolytes⁸ have confirmed that both the negative and positive half-cell electrolyte conductivities vary linearly with state of charge. Since conductivity varies considerably with solution composition and temperature, the conductivity values for the 2 M vanadium solution cannot be employed if the solution composition differs.

In this study, the total concentration of vanadium was fixed at 1.6M (being a commonly used composition for VRB systems) while the SOC and temperature were varied in order to reproduce an empirical model which could be employed in a VRB control system for SOC monitoring and electrolyte maintenance.

Tables 1 and 2 summarise the conductivity values obtained at the three different temperatures for the positive and negative half-cell solutions respectively at different SOC's.

Table 1. Conductivities of 1.6 M V solutions in 4.2 M total sulphate corresponding to different states-of-charge of the VRB positive half-cell electrolyte

SOC	Positive half cell					
	room temp.		hot bath		ice bath	
	T,°C	k, mS cm ⁻¹	T,°C	k, mS cm ⁻¹	T,°C	k, mS cm ⁻¹
100%	22.3	410			11	338
95%	22.3	401			10.8	328
90%	22.5	401			10.6	321
75%	22.3	375			10.6	302
50%	22.2	345	42.7	465	10.5	277
25%	22.2	308	42.8	411	10.5	248
10%	22.2	293	43.5	403	10.5	234
5%						
0%	22.4	275	43.6	374	10.7	222

Table 2. Conductivities of 1.6 M V solutions in 4.2 M total sulphate corresponding to different states-of-charge of the VRB negative half-cell electrolyte

SOC	Negative half cell					
	room temp.		hot bath		ice bath	
	T,°C	k, mS cm ⁻¹	T,°C	k, mS cm ⁻¹	T,°C	k, mS cm ⁻¹
100%						
95%	22.2	250	44	321	10	197
90%	22.3	241	44.6	321	10	190
75%	22.3	237	44.8	311	9.7	186
50%	22.4	215	44.5	282	9.5	169
25%	22.3	190	44.7	264	9.6	149
10%	22.3	181	44.8	252	9.5	142
5%	22.3	181	44.5	254	9.2	141
0%	22.3	183	44	238	9.1	146

The above data was used to develop an empirical model based on the linearity of the electrolyte conductivity (k) with the state of charge of both the negative and positive half-cell electrolytes. In addition to SOC, temperature (T) is also introduced as a variable.

Briefly, the following equations are the basis of the model:

$$\kappa = a(T) * SOC + b(T) \quad (3)$$

where

$$a(T) = a_1 * T + a_2 \quad (4)$$

$$b(T) = b_1 * T + b_2 \quad (5)$$

$$\kappa = (A * T + B) * SOC + (C * T + D) \quad (6)$$

where k is the solution conductivity in mS cm⁻¹, T is the temperature and A , B , C and D are empirical coefficients that are determined by fitting the experimental data to the model. Table 3 presents the model coefficients for both the positive and negative half-cell solution conductivities.

Table 3. Conductivity model coefficients

	Positive half-cell electrolyte	Negative half-cell electrolyte
A	1.8000	0.7050
B	93.5030	55.0420
C	4.6713	2.6176
D	172.07	122.37

In order to test the accuracy of the empirical model, calculated conductivity values were compared with experimental values as illustrated in Figures 1 and 2. The good correlation shows that the empirical model should provide an accurate prediction of the conductivities of the vanadium electrolytes over the SOC range 0 to 100 % and temperature range 10 to 40 °C for the solution composition used in this study.

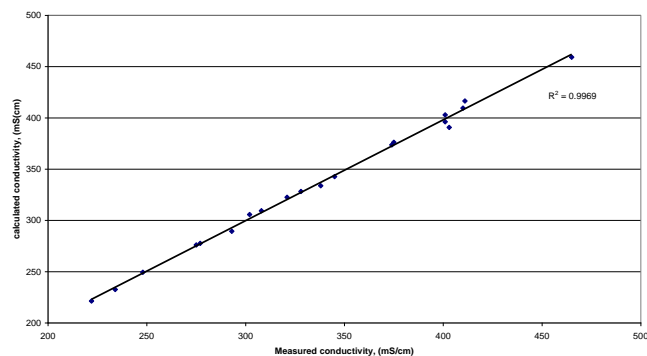


Figure 1. Correlation measure vs. calculated positive half-cell electrolytes conductivity

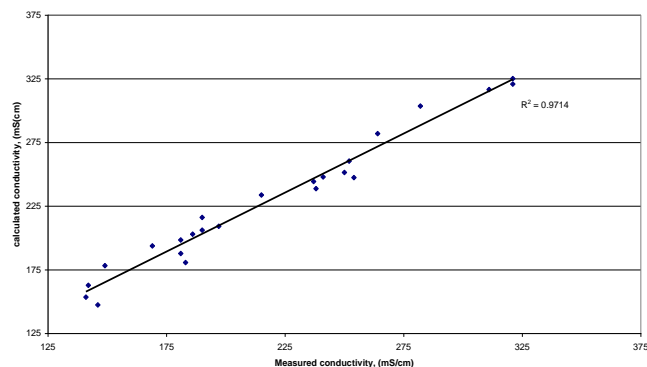


Figure 2. Correlation measure vs. calculated negative half-cell electrolytes conductivity

The above results thus suggest that the solution state of charge for each half-cell electrolyte could be directly indicated by simply measuring the conductivity of each solution provided that no changes in the total vanadium and total sulphate concentrations occur during battery operation. It has previously been shown however, that diffusion processes across the cell membrane will give rise to a transfer of each of these ions from one half-cell to the other, leading to a build-up in one half-cell and a dilution in the other.⁸ These processes will have a significant effect on solution conductivity that will not be predicted by the empirical model and will give an erroneous value of SOC. By regularly remixing the two half-cell solutions however, solution composition could be restored, so that recalibration of the SOC monitor would be possible. A second independent monitoring method would therefore be needed for calibration purposes in order to provide the most accurate measure of SOC.

Half-cell solution potentials as a function of state of charge

As previously mentioned, the continuous independent measurement of the potential of each half-cell solution could provide a relatively accurate quantitative measure of the state-of-charge of each half-cell and give an additional indication of any imbalance arising as a result of side reactions during operation of the VRB.

The Nernst potentials for the two reduction reactions (Equations 1 and 2) that take place in each half-cell of the VRB can be represented as follows:

Positive half-cell:

$$E^+ = E^{o+} - \frac{RT}{F} \ln \left[\frac{[VO^{2+}]}{[VO_2^+][H^+]^2} \right] \quad (7)$$

Negative half-cell:

$$E^- = E^{o-} - \frac{RT}{F} \ln \left[\frac{[V^{2+}]}{[V^{3+}]} \right] \quad (8)$$

where

R (the Universal Gas Constant) = 8.314472
J K⁻¹mol⁻¹

F (Faraday's constant) = 96485.3399 C mol⁻¹

T temperature, K

[V] are the concentrations of the different vanadium species in solution

[H⁺] is the hydrogen-ion concentration in the positive half-cell electrolyte

E^{o+} and E^{o-} are the standard half-cell potentials for the positive and negative half-cell reactions, respectively.

The concentration of the ions that take part in the reactions is directly proportional to the state of charge and the total vanadium concentration of the electrolyte. In the case of the proton or H⁺ concentration in the catholyte

however, this is more difficult to calculate accurately. A large number of ion pairing equilibria between vanadium ions, sulphate and bisulphate ions in the solutions will also affect the equilibrium proton concentrations and since their equilibrium constants are not accurately known, the true H⁺ ion concentration cannot be accurately calculated.

Commonly, the hydrogen ion concentration in the catholyte is considered as 1M so as to eliminate its influence on the Nernst potential. Alternately, many researchers assume that the hydrogen ion concentration remains constant during cell cycling, so that its value can be incorporated into the formal potential that can be experimentally determined for a particular solution composition. In fact, the standard cell potential E^o is often replaced in the Nernst Equation by the formal potential, which includes corrections to incorporate activity coefficients of the ions and is the potential that is more readily measured in an electrochemical cell. In this study, both possibilities will be considered in order to develop an empirical relationship between solution potential and SOC.

In order to estimate the formal potential of the positive half-cell electrolyte, the vanadium solution was placed into a flow cell and charged to 100% SOC as evidenced by the distinct yellow colour of the resultant V(V) solution. Assuming that the potential at this point represented a state of charge of 99% (since 100% would correspond to a V(IV) concentration of zero that cannot be used into the Nernst equation), the formal potential, E^{o'}, was determined from the Nernst Equation as -0.207 V and 1.182 V for the negative and the positive half-cell, respectively. This value was then used as the calibration constant to calculate the SOC values at different times during cycling. In our case, this parameter was defined for the positive half-cell as follows:

$$E^+ = E^{o+} - \frac{RT}{F} \ln \left[\frac{[VO^{2+}] \cdot \gamma_{VO^{2+}}}{[VO_2^+] \cdot c_{H^+}^2 \cdot \gamma_{VO_2^+} \cdot \gamma_{H^+}^2} \right] \quad (9)$$

$$E^+ = E^{o+} - \frac{RT}{F} \left(\ln \left[\frac{[VO^{2+}]}{[VO_2^+]} \right] - \ln \left([H^+]^2 \right) + \ln \left[\frac{\gamma_{VO^{2+}}}{\gamma_{VO_2^+} \cdot \gamma_{H^+}^2} \right] \right) \quad (10)$$

where

E^{o+} standard reduction potential for the positive half-cell

γ_x activity coefficient for species x

Assuming that the hydrogen-ion concentrations and the activity coefficients remain constant, it is possible to incorporate these terms into the new formal potential term as follow:

$$E^+ = E^{o+} - \frac{RT}{F} \left(\ln \left[\frac{[VO^{2+}]}{[VO_2^+]} \right] \right) \quad (11)$$

and since

$$[VO^{2+}] = (1 - SOC) \cdot [V] \quad (12)$$

$$[VO_2^+] = SOC \cdot [V] \quad (13)$$

$$E^+ = E^{\circ+} - \frac{RT}{F} \left(\ln \left[\frac{1 - SOC}{SOC} \right] \right) \quad (14)$$

where

E^{0+} formal potential for the positive half-cell
SOC state of charge (%)

Equation 14 above thus shows that with the use of the formal potential, in which value the hydrogen ion is included, a simple relationship between solution potential and state of charge can be obtained for the positive half-cell.

In a similar way the negative half-cell formal potential was also defined as follows.

$$E^- = E^{\circ-} - \frac{RT}{F} \ln \left[\frac{\gamma_{V^{2+}}}{\gamma_{V^{3+}}} \right] - \frac{RT}{F} \ln \left[\frac{[V^{2+}]}{[V^{3+}]} \right] \quad (15)$$

$$E^- = E^{\circ-} - \frac{RT}{F} \ln \left[\frac{[V^{2+}]}{[V^{3+}]} \right] \quad (16)$$

Since

$$[V^{2+}] = SOC \cdot [V] \quad (17)$$

$$[V^{3+}] = (1 - SOC) \cdot [V] \quad (18)$$

$$E^- = E^{\circ-} - \frac{RT}{F} \left(\ln \left[\frac{SOC}{1 - SOC} \right] \right) \quad (19)$$

where,

E^{0-} standard reduction potential for the negative half-cell
 E^{0+} formal potential for the negative half-cell

The formal cell potential for the VRB can also be calculated using the formal half-cell potentials measured above. Using values of $E^{\circ+}=1.182V$ and $E^{\circ-}=-0.207$ for the positive and negative half-cells respectively, a formal cell potential of 1.39 V was calculated for the vanadium cell under the current electrolyte composition. This agrees well with formal cell potential values of 1.4 V (measured from

the open circuit potential at 50% SOC) previously determined in the laboratory with operating cells at 50% SOC.¹⁰

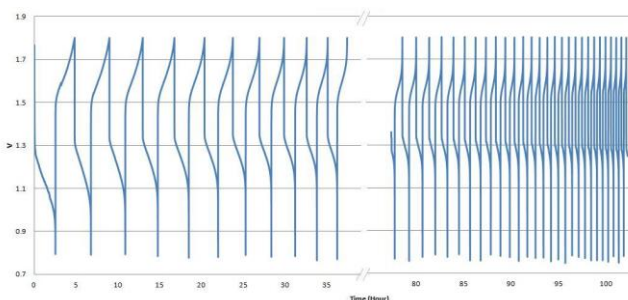


Figure 3. Vanadium redox flow cell voltage vs time over 100 hours cycling (1.8-0.8V) at constant current (1Amp)

Having calibrated potential as a function of SOC for each half-cell, a small flow cell was subjected to continuous charge-discharge cycling while monitoring the potential of two carbon indicator electrodes vs and SCE reference electrode immersed in each electrolyte reservoir. Figures 3 and 4 depict the cell voltage and charge/discharge current capacity variation during the 100 hour cycling period. A significant drop in capacity is observed and its cause can be understood from Figures 5 and 6 that show the potential values vs. SCE (standard calomel electrode) and SOC for the positive and negative half-cells respectively during the duration of the experiment, around 100 hours and 40 cycles.

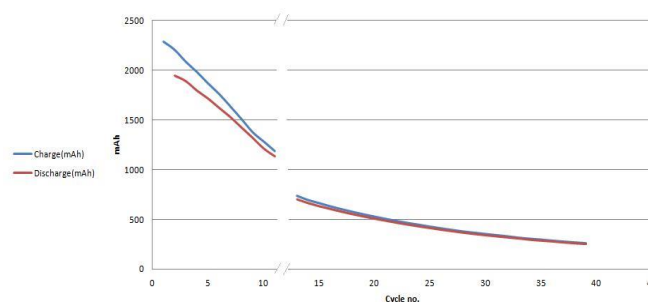


Figure 4. Charge (blue)/discharge (red) capacity (mAh) vs. cycle number for vanadium cell cycling of Figure 3.

The presented results show very interesting phenomena. Firstly, the SOC limits in the positive half-cell are steadily increasing with each cycle so that after 80 hours, the positive side of the cell is only cycling between 50 and 100% SOC. The reverse is seen in the negative half-cell where the solution is only cycling between 50 and 100% after 80 hours of operation. The SOC imbalance continues further over the next 2 hours until the capacity eventually falls to 250 mAh from the initial 1900 mAh.

State-of-Charge Rebalancing

In order to understand the cause of the above capacity loss and to demonstrate the practical value of the SOC monitor, a series of additional experiments were performed. In the first instance, the solutions from the above cell were remixed to

see whether the capacity could be restored. In the second instance, chemical rebalance was performed using a proprietary reducing additive and the half-cell potential monitoring was used to observe any changes in the half-cell solution balance.

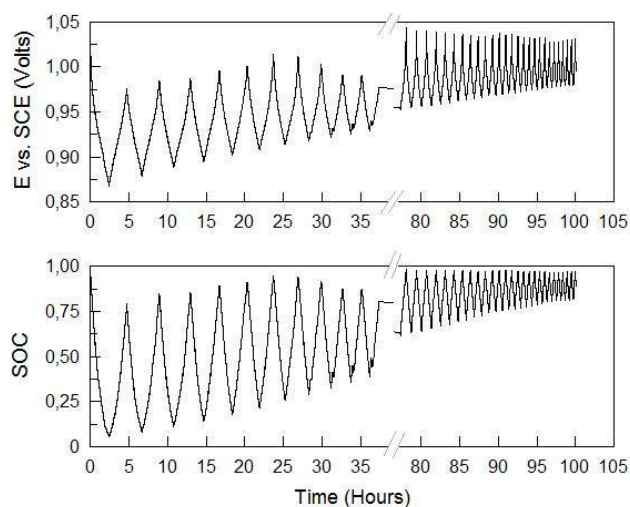


Figure 5. Positive half-cell potential vs. SCE (V)/SOC vs. time(hour) for vanadium cell cycling of Figure 3

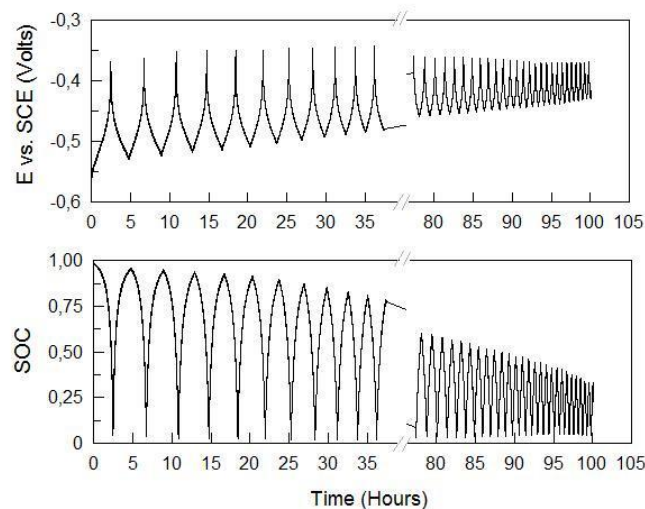


Figure 6. Negative half-cell potential vs. SCE (V)/SOC vs. time(hour) for vanadium cell cycling of Figure 3

As mentioned previously, capacity loss in all flow batteries will arise as a result of side reactions and the differential transfer of active ions and solution from one half-cell to the other during charge-discharge cycling, this leading to a limiting active material concentration in one half-cell. Capacity losses from solution and ion transfer can be readily restored by simple periodic electrolyte remixing, but this is not the case for losses due to side reactions such as hydrogen evolution and air oxidation in the negative half-cell that requires chemical restoration of the V(II);V(V) ratio in the cell.

Skyllas-Kazacos and co-workers reported **0** that rebalance in the VRB cells can be obtained by adding certain organic compounds to the positive electrolyte that allow the partial reduction of the V(V). Particularly, oxalic acid, methanol

and ethanol have been suggested to be good rebalancing agents since carbon dioxide and water are the products of the reactions, introducing no impurities in the electrolyte.

This part of the study focusses on the use of the half-cell potential SOC monitoring as part of an electrolyte maintenance regime that would involve a simple electrolyte remixing followed by chemical rebalancing to restore capacity in a redox flow battery. In this study, a proprietary chemical reductant was added to the positive electrolyte of a vanadium redox flow cell in order to equalise the states of charge of both half-cell electrolytes. The electrolyte used in the cell comprised 1.6M vanadium in 4M sulphuric acid, while other parameters were as follows:

Voltage limits: 0.7-1.9V

Current: 1A

As in the earlier experiment, the negative electrolyte reservoir was exposed to atmosphere in order to speed up the air oxidation of the V(II) ions, while a higher voltage limit was used for charging to permit some hydrogen evolution at the negative electrode. The cell was initially subjected to a 100 hour charge-discharge cycling regime during which the capacity decreased from above 2,000 mAh after the first charge cycle to 300 mAh after 50 cycles, representing a loss of 70%. The 2 half-cell electrolytes were then remixed and the cell cycling resumed.

Figure 7 shows the charge-discharge curves obtained after the remix, while the variation in capacity is illustrated in Figure 8.

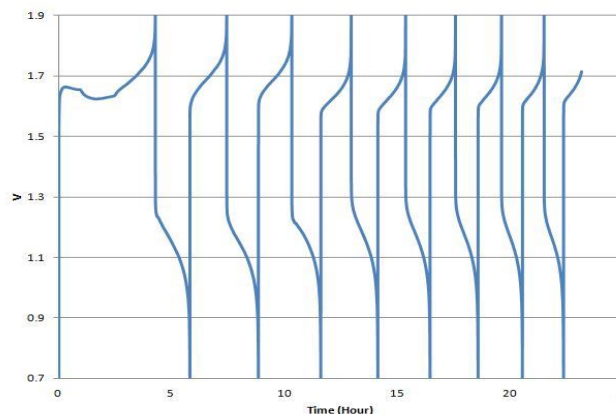


Figure 7. Charge-discharge curves for cell of Figure 3 after electrolyte remixing

By remixing the 2 half-cell solutions, the capacity is seen to be restored to around 1500 mAh, slightly lower than the original capacity of the cell, but considerably higher than the 300 mAh capacity observed after the first 100 hours of cycling. After only 8 cycles, however, the capacity dropped once again to around 700 mAh at which point a second remix was conducted, followed by further cycling that dropped capacity to less than 400 mAh. A third remix failed to restore cell capacity, indicating that the cell imbalance was now dominated by side reaction processes that do not respond to remixing.

A chemical rebalancing procedure was therefore conducted, this involving the addition of 2 ml of a proprietary chemical reductant to the fully charge positive half-cell electrolyte. The electrolyte was allowed to circulate through the cell stack overnight to allow reaction to occur and cell cycling was resumed using the same conditions as before.

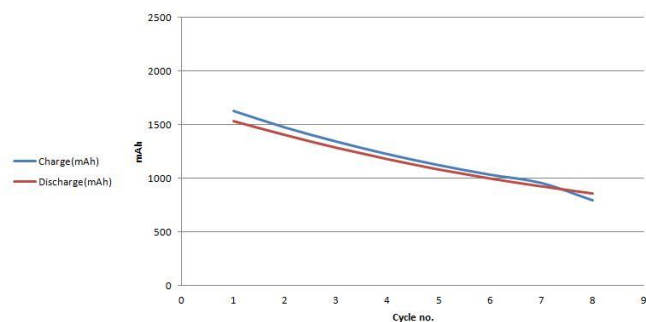


Figure 8. Capacity versus cycle number for cell of Figure 7 after electrolyte remixing.

As seen in Figures 9 and 10, the chemical rebalance had the effect of almost completely restoring the cell capacity to its original value. The slight increase observed during the first few cycles in Figure 10 is due to the on-going chemical reaction by the reductant and the V(V) ions in the positive half-cell electrolyte, this being due to the relatively slow kinetics of the reduction reaction in the solution.

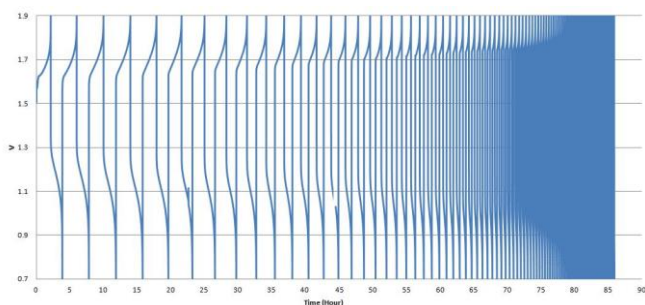


Figure 9. Cell potential vs. time/hour for cell of figure 7 after chemical rebalance.

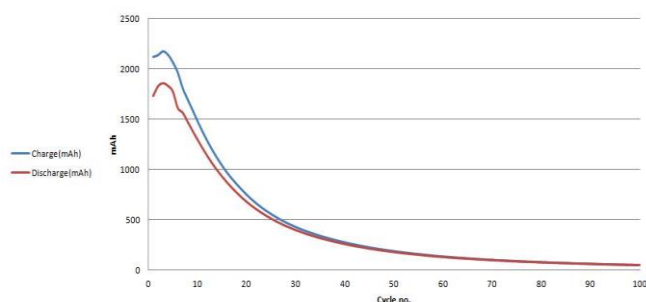


Figure 10. Charge (blue)/discharge (red) capacity (mAh) vs. cycle number for cell of Figure 9 after chemical rebalance.

As with the previous cycling experiments however, the cell capacity steadily declines as the solutions continue to get out of balance, as illustrated in Figures 11 and 12 that show the changes in state-of-charge ranges for the positive and negative half-cell electrolytes during cycling respectively.

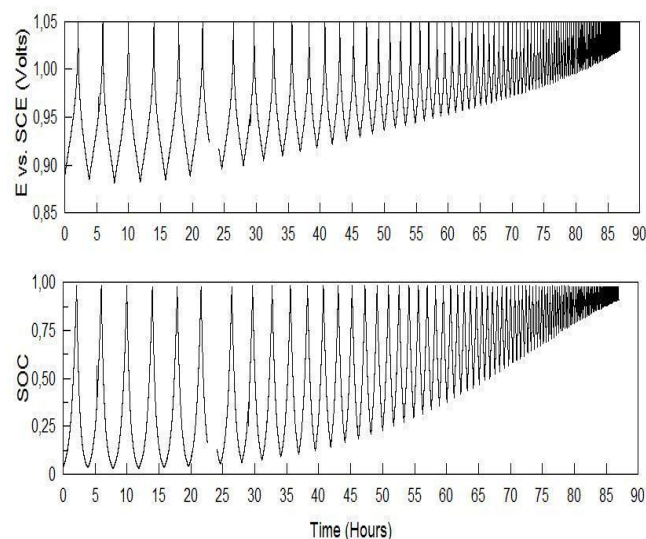


Figure 11. Positive half-cell potential vs. SCE (V)/SOC vs. time for cell of Figure 9.

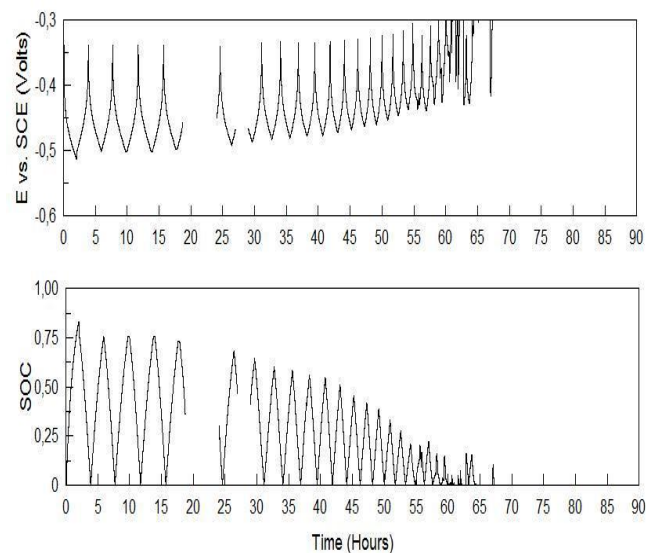


Figure 12. Negative half-cell potential/SOC vs. time for cell of Figure 9 (irregularities due to equipment connection errors)

Simple electrolyte remixing could not this time restore capacity, but on addition of a further 2ml of reducing agent to the fully charged positive solution, the cell capacity was once again restored to its original value as shown in Figure 13.

The above experiments have clearly demonstrated the value of independent monitoring of the individual half-cell potentials in order to identify imbalances in the state-of-charge of the two half-cells that lead to capacity losses. Although the loss in capacity may be clearly seen from the length of the discharge curves during the continuous charge-discharge cycling experiments conducted here, the same would not apply in practical situations where the battery would not necessarily undergo full charge and discharge cycles during operation, nor would scheduled full discharges be desirable from an operational perspective. The availability of an accurate capacity monitor is therefore of great value for commercial battery systems. Capacity monitors using open circuit cell potential for redox flow cells have been shown to be unreliable where an imbalance

exists between the oxidation states of the two half-cells, so independent SOC monitoring is desirable.

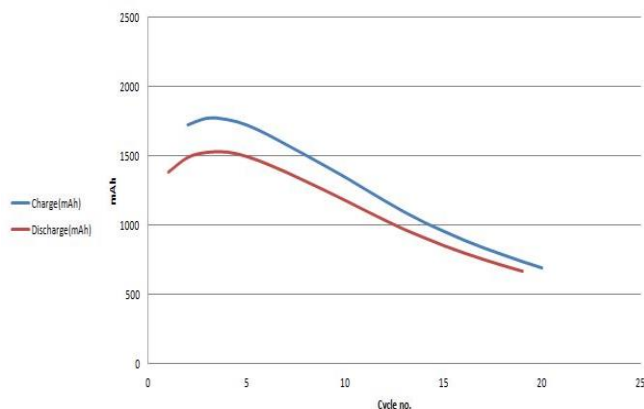


Figure 13. Cell capacity versus cycle number after second addition of ethanol. Charge (blue)/discharge (red) capacity (mAh).

In this study the potentials of the two half-cell electrolytes have been applied to the Nernst Equation in order to calculate the SOC of each half-cell. While a distinct trend in SOC is seen as a function of time, this relationship is not linear as would be expected if there were no interferences in the application of the Nernst Equation in the determination of SOC.

Considering separately the displayed SOC vs time plots of Figures 5 and 6 and focusing on the negative half-cell values, a considerably large curvature is observed. This would suggest that two things may be happening during the charge cycle: air oxidation of the V(II) and hydrogen evolution during charging, which gets larger at higher states of charge. Additionally, also at higher SOC a higher rate of self-discharge would be expected since the rate of self discharge is a function of the concentration gradient of the V(II) and V(V) ions across the membrane, which increase at higher SOC. The above processes do not however explain the curvature observed during the discharge cycle.

Some unusual characteristics are also observed in relation to the curvature in the positive half-cell SOC plots; the curvature is surprising in the lower SOC region. Although the curves in the discharge part are understandable since the rate of self-discharge would be higher at higher SOC, this would not explain the observed curvature during the charging cycle. One possible explanation for the curvature in the positive half-cell potentials vs. time plots may be associated with the assumption that the proton concentration remains constant over the entire SOC range. This would affect the theoretical potential calculated from the Nernst Equation and the SOC value thereby determined. Further modelling of the solution potentials was therefore conducted in order to determine any errors introduced by the assumption of constant proton concentration in the Nernst Equation.

Effect of varying hydrogen ion concentration on SOC determination

It is readily seen from the positive half-cell reaction, that protons are produced and consumed during the charge-discharge processes. Protons also cross the membrane to

balance the charge. While the complex ion equilibria in the electrolyte makes it difficult to determine the precise hydrogen-ion concentration, it is known, it should be possible to estimate changes in the hydrogen-ion concentration with time during charge-discharge cycling of the VRB. It is known that the H^+ quantity in the positive half-cell electrolyte will increase by 1M when 1M of vanadium V(V) is produced during charging. A direct relationship should therefore exist between the H^+ and V(V) concentrations in the solution, from which changes in the hydrogen-ion concentration can be obtained. Therefore, at any state of charge the hydrogen-ion concentration in the catholyte becomes:

$$[H^+]_x = [H_2SO_4]_0 + [VO_2^+] \quad (20)$$

where

$[H_2SO_4]_0$ is the acid concentration at 0% SOC and $[VO_2^+]$ is the concentration of V(V) in the positive half-cell solution at any time.

But since $[VO_2^+]$ is directly proportional to SOC,

$$[H^+]_x = [H_2SO_4]_0 + [V_T] \cdot SOC \quad (21)$$

where

$[V_T]$ is the total V electrolyte in the solution

Substituting this into the Nernst Equation (Equations 11 and 14) for the reduction potential equation for the positive half-cell,

$$E^+ = E^{o+} - \frac{RT}{F} \ln \left[\frac{1-SOC}{SOC} \times \frac{1}{\left[[H_2SO_4]_0 + [V_T] SOC \right]^2} \right] \quad (22)$$

Assuming values of $[H_2SO_4]_0 = 4 \text{ mol L}^{-1}$ and $[V_T] = 1.6 \text{ mol L}^{-1}$, the cell potential vs. SOC plot of Figure 14 is obtained.

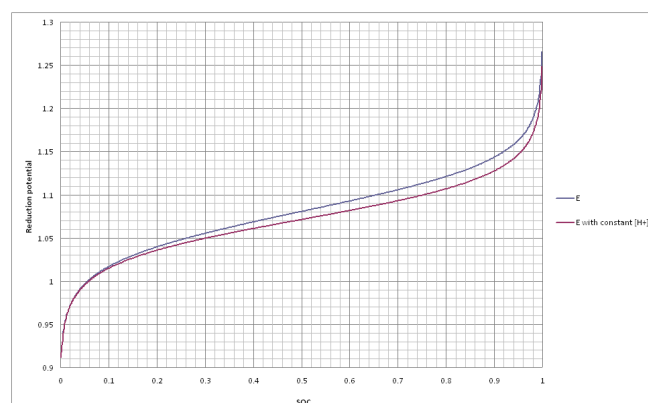


Figure 14. Positive half-cell potential (V) vs. SOC with constant and variable $[H^+]$.

As can be seen the difference between both scenarios for the 1.6M V in 4M sulphuric acid solution is considerable, specially, from states-of-charge values above 20%, reaching for the same positive half-cell potential values a SOC difference up to 8%. This would explain some of the curvature observed in the SOC vs time plots presented previously. Despite this curvature however, the independent plots of SOC vs time for each of the two half-cell solutions provides an excellent indication of the imbalance between the two half-cells that gives rise to a loss of capacity with each cycle.

Conclusions

Different methodologies have been discussed on small laboratory scale for obtaining an accurate technique for state-of-charge monitoring. A first method focused on the linear variability of the conductivity of each electrolyte with state of charge that allowed the derivation of an empirical model that could be employed for SOC monitoring and rebalancing in a VRB control system.

Moreover, in order to solve inaccurate predictions of the open circuit voltage, each of the half-cell electrolyte potentials were also monitored and system imbalance was readily detected, allowing the introduction of cell rebalancing measures such as electrolyte remixing or chemical reduction to equalize the state-of-charge levels on both half-cells and thereby restore capacity in an operating VRB system.

References

- ¹Skyllas-Kazacos, M. Robins, R., *US* 4,786,567; **1986**.
- ²Skyllas-Kazacos, M., Kasherman, D., Hong, R., M. Kazacos, *J. Power Sources*, **1991**, 35, 399–404.
- ³Skyllas-Kazacos, M., Chakrabarti, M. H., Hajimolana, S. A., Mjalli, F. S., and Saleem, M., *Crit. Rev. Electrochem. Solid-State Sci. Technol. J. Electrochem. Soc.*, **2011**, 158(8) R55-R79.
- ⁴Skyllas-Kazacos, M. Chapter on “Secondary Batteries: Redox Flow Battery – Vanadium Redox” in: *Encyclopedia of Electrochemical Power Sources*, Ed.: J. Garche, P. Moseley, Z. Ogumi, D. Rand & B. Scrosati, Elsevier, **2009**, 444-453, 2009.
- ⁵Skyllas-Kazacos, M., Chapter on “Energy storage for stand-alone/hybrid systems: Electro-chemical Energy Storage Technologies”, in: *Stand-alone and Hybrid Wind Systems: Technology, Energy Storage and Applications*, Ed Kaldellis, J. K., Woodhead Publishing, **2010**.
- ⁶Skyllas-Kazacos, M., Goh, L., *J. Membrane Sci.*, **2012**, 399– 400, 43– 48.
- ⁷Tang, A., Skyllas-Kazacos, M., Bao, J., *J. Power Sources*, 2011, 196, 10737– 10747.
- ⁸Skyllas-Kazacos, M. Kazacos, M., *J. Power Sources*, 2011, 196, 8822– 8827
- ⁹Kazacos, C., Kazacos, M., *WO 2006/135958 A1*.
- ¹⁰Skyllas-Kazacos, M. Kazacos, M. Wegner, R. Burford, R. Lin, G., Final Report NSW., Dept. of Minerals & Energy, **1991**, pp. 200.

Received: 07.11.2012.

Accepted: 24.11.2012.



TESTING OF SELENIUM INHIBITION EFFECT ON SELECTED CHARACTERISTICS OF GARDEN PEA

Alžbeta Hegedúsová^{[a]*}, Silvia Jakobová^[b], Ondrej Hegedús^[c], Magdaléna Valšíková^[a], Anton Uher^[a]

Paper was presented at the 4th International Symposium on Trace Elements in the Food Chain, Friends or Foes, 15-17 November, 2012, Visegrád, Hungary

Keywords: Garden pea, Selenium phytotoxicity, Half maximal inhibitory concentration, Probit analysis.

Phytotoxicity effect of sodium selenite Se(IV) and selenate Se(VI) was followed on selected characteristics of garden pea (*Pisum sativum*), such as germination, growth, chlorophyll production, content of dry material and water in the seedlings. Laboratory experiments were established in the Petri dishes, which were treated with sodium selenate (Na₂SeO₄) and sodium selenite pentahydrate (Na₂SeO₃·5 H₂O) on the selenium concentration levels 5.0; 20.0; 100.0; 300.0 and 500.0 mg Se/l. Phytotoxicity was tested by the tests of chronic phytotoxicity and the results obtained were evaluated as IC₅₀ values (half maximal inhibitory concentration) by probit analysis. Treatment of seedlings with the solutions of Se(IV) and Se(VI) on the concentration levels 5 mg and 20 mg/l resulted in enhanced growth of shoots and roots, especially after application of Se(IV), where the growth exceeded control for about 70 %. The IC₅₀ value was higher for the growth of shoots as well as for roots after application of Se(VI), the growth inhibition in early growth stages of garden pea can be observed only in the high selenium concentrations (over 200 mg Se/l). Se(IV) showed more significant inhibition of chlorophyll production in the shoots of peas seedlings than Se(VI). Lower concentrations of Se(IV) and Se(VI) (below 100 mg Se/l) did not show significant differences between the water contents, but the higher concentrations (300 mg Se(IV)/l and 500 mg Se(VI)/l) resulted in significant differences, more than 9-times higher in roots.

* Corresponding Authors

E-Mail: alzbeta.hegedusova@uniag.sk

[a] Slovak University of Agriculture, Horticulture and Landscape Engineering Faculty, Department of Vegetables-Production, Tr. A. Hlinku 2, SK-949 76 Nitra, Slovakia, Magdalena.valsikova@uniag.sk, anton.uher@uniag.sk

[b] Constantine the Philosopher University, Department of Chemistry, Faculty of Natural Sciences, Tr. A. Hlinku 1, SK-949 74 Nitra, Slovakia, sjakabova@ukf.sk

[c] Regional Authority of Public Health Nitra, Štefániková 58, SK-949 63 Nitra, Slovakia, hegeduso@gmail.com

Therefore, it is important to increase selenium content in the areas with low selenium levels, what helps to increase selenium intake in humans³.

Average selenium intake in Slovakia is only 38 µg per person per day what presents an insufficient intake. This low intake is a result of low selenium content in soil and food chain. Selenium content in food chain is a function of its total quantity and chemical forms in the soil-plant system. Selenite selenium presents its dominant form in the soil. Selenites are strongly bounded in soil and less available for plants. Plants have a unique role in selenium transformation and allow its transfer into food chain. Selenium is absorbed by plants from soil and transferred through the xylem to above ground parts, especially to shoots and leaves. Transfer of selenium ions inside the plant and their distribution in different organs is influenced by the movement in floem, xylem followed by the transformation into selenomethionine and selenocysteine⁴.

Selenium distribution in plants is dependent on a concrete plant species. Plants are able to absorb inorganic selenium from soil (selenates and selenites) and transform its portion or total amount into organic compounds⁵. Toxic effect of selenium on plants is affected by its total concentration, chemical form, growth phase of plant, physiologic state and other factors^{6,7}. Toxicity of selenium compounds is affected by the production of selenium analogues of aminoacids and other compounds, in which selenium replaces sulphur, and by the oxidation of compounds containing –SH group (e.g. enzymes). Phytotoxicity can be tested by two categories of tests: tests of acute toxicity and tests of chronic toxicity. The results obtained are evaluated as the IC₅₀ values on the corresponding level of reliability.

Introduction

Selenium as an essential element is the object of scientific interest from the middle 50's, when its importance for living organisms was proven. Selenium is a part of several enzymes and some of them have also antioxidative function¹. The most important role of selenium is in formation of glutathionperoxidase. The enzyme reduces hydrogen peroxide and organic peroxides, which were created from unsaturated fatty acids, to water or to alcohols and water, respectively. Selenium is also a part of other enzymes like acid phosphatase in leukocytes and glucuronidase. It is also essential for production of hormones in thyroic gland, for health skin, hair and eyes. Selenium helps in prevention of cancer and cardiovascular disease together with vitamin E. Selenium is approximately thousand times more efficient than the vitamin E, which, as a vitamin soluble in oils, is more slowly absorbed in organism².

Adequate daily intake of selenium in humans is necessary for the optimal function of immunity, cardiovascular and reproduction system, it presents an important defense against infections and carcinoma and prevention from inflammatory and allergic diseases.

The aim of the work was to follow the phytotoxicity effect of sodium selenite Se(IV) and sodium selenate Se(VI) on the selected characteristics (germination, growth, chlorophyll production, content of dry matter and water) of garden pea (*Pisum sativum*).

Material and methods

Inhibition effect of Se(VI) and Se(IV) on germination and growth of roots and shoots of garden pea

Effect of different concentrations of selenium salts on germination was followed in laboratory conditions. Germination was performed in sodium selenate (Na_2SeO_4) and sodium selenite pentahydrate ($\text{Na}_2\text{SeO}_3 \cdot 5\text{H}_2\text{O}$) solutions with selenium concentrations 5.0; 20.0; 100.0; 300.0 and 500.0 mg dm^{-3} . Germination experiments were established in four replications on the Petri dishes in the thermostat adjusted to 25°C. Seeds of garden pea (*Pisum sativum*), variety 'Oskar' were used. Dynamics of germination was realized by counting of germinated seeds in regular time intervals. After seven days of germination, the lengths of roots and shoots were measured and IC_{50} values were calculated.

Inhibition effect of Se(VI) and Se(IV) on the content of chlorophyll *a* and *b*

After measuring the root lengths seedlings were put on Petri dishes and grew in laboratory condition with daily light at the temperature 25–27°C during 7 days. The contents of photosynthetic pigments were measured by UV-VIS spectrophotometer (Varian Cary 50, Australia) 14 days after germination. IC_{50} values were calculated by the probit analysis⁸.

Inhibition effect of Se(VI) and Se(IV) on the content of dry matter and water in the roots and shoots of garden pea

Fresh samples of roots and shoots were cut into pieces and dry matter was prepared at 105°C (ED115 Binder GmbH, Germany). Contents of water in shoots and roots were calculated.

Results and Discussion

Inhibition effect of Se(VI) and Se(IV) on the germination and growth of roots and shoots of garden pea

The results of germination of garden pea showed that the IC_{50} achieved value 586.8 mg Se dm^{-3} after application of Se(IV), and IC_{50} was 876.0 $\text{mg} \cdot \text{dm}^{-3}$ after application of Se(VI). Higher value of IC_{50} after application of Se(VI) means that inhibition of germination of pea seeds is observed in higher selenium concentration (over 876.0 mg Se dm^{-3}). Application of Se(VI) in concentrations below 20 mg Se dm^{-3} increased germination intensity in first days, but the reduced form Se(IV) in the concentrations below the value did not have visible effect on germination. Slight decrease of germination (from 13.4%) was observed in the variants

with application of concentrations over 100 $\text{mg Se(VI)} \cdot \text{dm}^{-3}$ to 35% decrease after germination in solution with 500 mg Se dm^{-3} as Se(IV) (Fig.1).

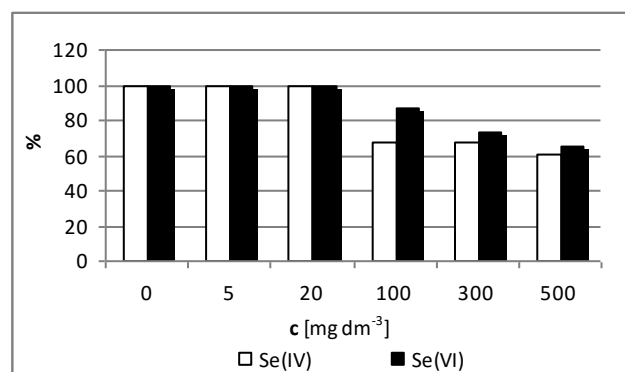
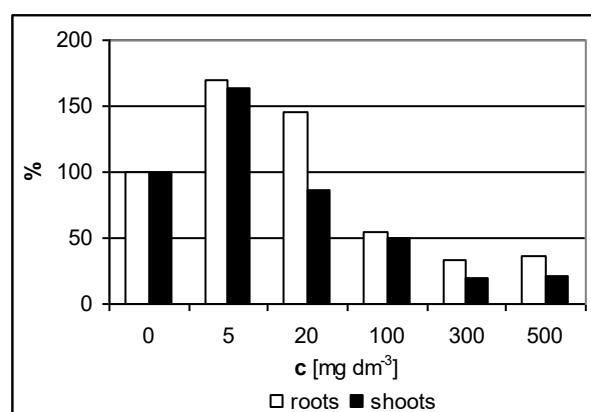
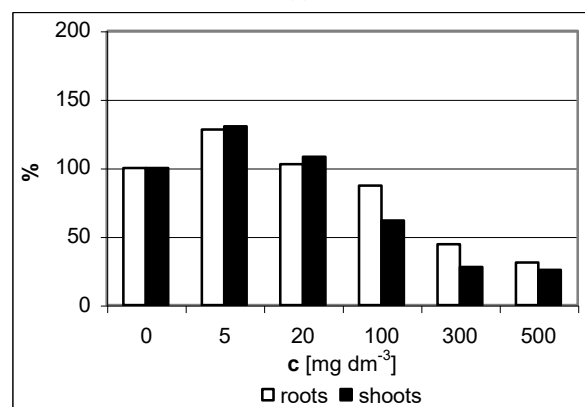


Figure 1. Inhibition of garden peas germination in the presence of Se(IV) and Se(VI)

Standard approach in toxicity determination presents monitoring of growth inhibition of roots and shoots. As a normal growth (100%) is considered a growth of shoots and roots in the control samples. After application of Se(IV) were the IC_{50} values for the roots and shoots 228.7 mg dm^{-3} and 124.1 mg dm^{-3} , respectively. Application of Se(VI) resulted in the higher IC_{50} with the values 331 $\text{mg} \cdot \text{dm}^{-3}$ and 213 mg dm^{-3} for the roots and shoots, respectively (Fig.2).



(a)



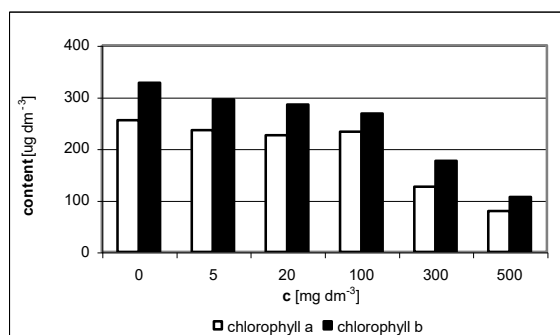
(b)

Figure 2. Inhibition of the roots and shoots growth in the presence of Se(IV) (a) and Se(VI) (bg).

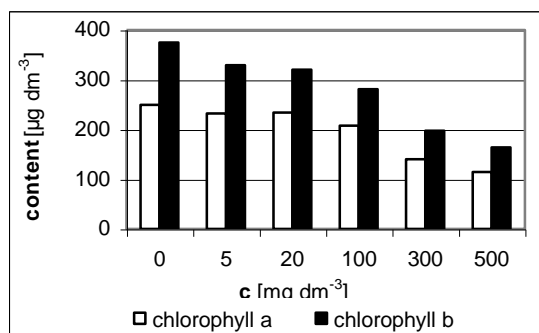
Treatment of seedlings with the solutions of Se(IV) and Se(VI) on the concentration levels 5 mg and 20 mg dm⁻³ resulted in enhanced growth of shoots and roots, especially after application of Se(IV), where the growth exceeded control for about 70%. Our observation is in agreement with the results of Yao et al.⁹, who observed enhanced growth of Chinese cabbage (*Brassica chinensis* L.) after application of 5 mg Se(VI) dm⁻³. The IC₅₀ value was higher for the growth of shoots as well as for roots after application of Se(VI), what means that the growth inhibition in early growth stages of garden pea can be observed only in the high selenium concentrations (over 200 mg Se dm⁻³). Negative effect of the both forms of selenium was more visible on the growth of shoots than roots. It is supposed that the actively growing plant parts, such as young leaves, accumulate higher selenium amounts.^{10,11}

Inhibition effect of Se (VI) and Se(IV) on the content of chlorophyll *a* and *b*

Inhibition effect of Se(IV) and Se(VI) was evaluated on photosynthetic pigments. Concentrations of chlorophyll *a* and chlorophyll *b* in the control variants are considered as a 100% content of chlorophyll *a* and chlorophyll *b*. In the presence of Se(IV) the IC₅₀ values for the chlorophyll *a* and *b* were 417.3 mg.dm⁻³ and 372.0 mg dm⁻³ for the shoots. Application of Se(VI) resulted in IC₅₀ values 604.0 mg dm⁻³ for the chlorophyll *a* and 444.0 mg dm⁻³ for the chlorophyll *b* (Fig.3). Se(IV) showed more significant inhibition of chlorophyll production in the shoots of peas seedlings than Se(VI). Inhibition effect of selenium on the production of chlorophyll *b* was observed also on the lower concentration levels in the presence of the both examined selenium forms.



(a)



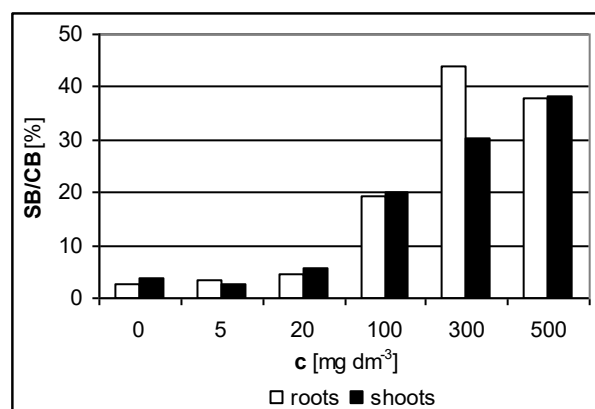
(b)

Figure 3. Content of photosynthetic pigments in the shoots of garden peas in the presence of Se(IV) (a) and Se(VI) (b).

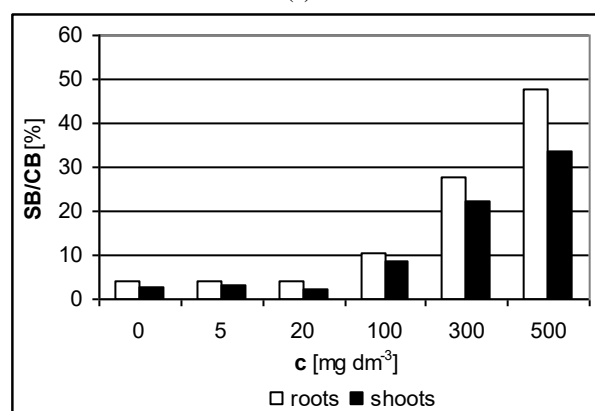
Decreasing trend of chlorophyll *b* content in the presence of metal salts (including selenium) was followed also in other similar studies with white mustard (*Sinapis alba*).¹²

Inhibition effect of Se(VI) and Se(IV) on the content of dry matter and water in the roots and shoots of garden pea

Water uptake by plants can be affected by several factors, including the presence of metals. Contents of dry matter and water in the roots and shoots of young seedlings treated by Se(IV) and Se(VI) solutions are shown in Fig.4. Application of Se(IV) in the concentration range 100 – 500 mg Se dm⁻³ significantly decreased weight of fresh shoots and roots.



(a)

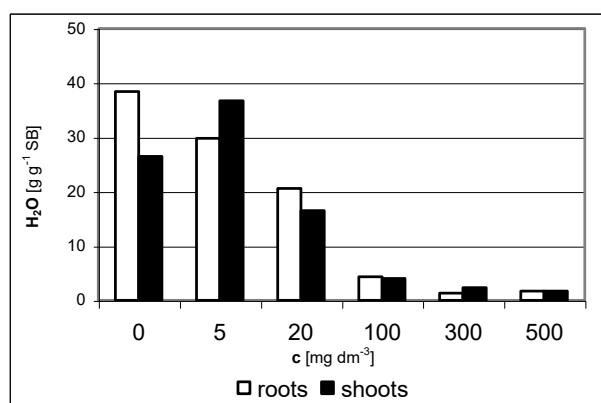


(b)

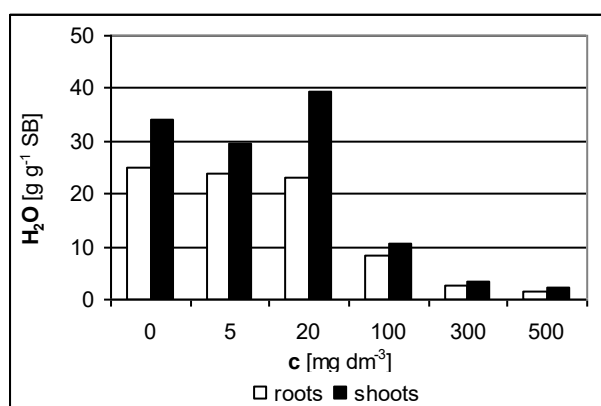
Figure 4. Relation between dry matter (SB) and fresh matter (CB) (in %) in garden pea in the presence of Se(IV) (a) and Se(VI) (b).

Lower concentrations of Se(IV) and Se(VI) (below 100 mg Se.dm⁻³) did not show significant differences between the water contents, but the higher concentrations resulted in significant differences, more than 9-times higher in roots (300 mg Se(IV) dm⁻³ and 500 mg Se(VI) dm⁻³).

The water content in shoots and roots had decreasing trend after application of 20 mg Se(IV) dm⁻³ (double decrease), and after application of Se(VI) solution with 100 mg Se(VI) dm⁻³ (triple decrease) (Fig.5). Application of Se(VI) solution in the concentration of 20 mg dm⁻³ increase the content of water in shoots of 18%.



(a)



(b)

Figure 5. Water content in roots and shoots of garden pea in the presence of Se(IV) and Se(VI).

References

- ¹Burk, R. F. *Nutr. Clinic. Care*, **2002**, *5* (2), 75 – 79.
- ²Sharma, M. C. - Joshi, C. - Kumar, M. *Indian J. Anim. Sci.*, **2005**, *75* (2), 246-257.
- ³Ferenčík, M., Ebringer, L. *Clin. Immunol. Allergy.*, **2000**, *2* (2), 9–16.
- ⁴Clarkson, T. W., Fishbein, L., Mallinckrodt, M. G. *Metals and their compounds in the environment*. **1991**.
- ⁵Hegedús, O., Hegedúsová, A., Jakobová, S., Vargová, A., Pavlík, V. *Acta fyto. zoot.*, **2009**, *12*, 206 – 215.
- ⁶Terry, N., Zayed, A. M., Souza, M. P., Tarun, A. S. *Annu. Rev. Plant. Phys.*, **2000**, *51*, 401-432.
- ⁷Hegedús, O., Hegedúsová, A., Šimková, S. *Selén ako biogénny prvok*. UKF, Nitra, **2007**, 76.
- ⁸Stephan, C.E. *Aquat. Toxicol. and Hazard Eval.*, F.L. Mayer and J.L. Hamelink, Eds., ASTM, Philadelphia, **1977**, PA, 65-84.
- ⁹Yao, X. - Chu, J. - Wang, G. *Biol. Trace Elem. Res.*, **2009**, *130* (3).
- ¹⁰Kahakachchi, C., Boakye, H. T., Uden, P.C., Tyson, J. F. *J. Chromatogr. A*, **2004**, *1054*, 303-312.
- ¹¹Smrkolj, P., Germ, M., Kreft, I., Stibilj, V. *J. Exp. Bot.*, **2006**, *57*, 3595-3600.
- ¹²Fargašová, A., Pastierová, J., Svetková, K. *Soil Environ.*, **2006**, *52*, 8 – 15.

Received: 22.10.2012.
Accepted: 26.11.2012.



EFFECTS OF VARIOUS GRAPE ROOTSTOCKS ON MACRO AND MICROELEMENT UPTAKE OF 'CSERSZEGI FÜSZERES' GRAPE CULTIVAR

István Fekete^{[a]*}, Nándor Rakonczás^[b], Dávid András^[a], Éva Bódi^[a], Béla Kovács^[a]

Paper was presented at the 4th International Symposium on Trace Elements in the Food Chain, Friends or Foes, 15-17 November, 2012, Visegrád, Hungary

Keywords: grape rootstock, microelements intake, Cserszegi fűszeres, grape variety

Data on mineral uptake of various scion-cultivar combinations demonstrated in the paper represent preliminary findings of a long term field experiment. The variety collection was established on immune sand soil in 2003. In the experimental field leaf samples were collected from 9 different rootstock and 'Cserszegi fűszeres' scion cultivars (the same stocks) before vintage of 2011, along with that of own rooted stocks as control. In the samples 9 elements were analysed (K, Ca, Mg, Cu, P, B, Mn, Fe and Zn). Differences were found between mineral composition of leaf samples of rootstocks and 'Cserszegi fűszeres' scion grafted on them. A consequently higher content of K, Mg, Mn, and Zn was found in scion, and P, Ca, B, Cu, Fe in rootstock leaf samples.

* Corresponding Authors

Fax: 36-52-417572

E-Mail: feketei@agr.unideb.hu

[a] University of Debrecen,
Centre for Agricultural and Applied Economic Sciences,
Institute of Food Science, Quality Assurance and
Microbiology, H-4032 Debrecen, Böszörményi str. 138.

[b] University of Debrecen,
Centre for Agricultural and Applied Economic Sciences
Institute of Horticulture, H-4032 Debrecen, Böszörményi str.
138.

scion combination at the establishment has determinative role in the life of a plantation. An ideal rootstock-scion combination according to the aim of the production (wine- or table grape) has beneficial effects on the quality parameters of the grape, must and wine, and it can even result higher yields together with better quality.^{2, 11} In this context, an important result was highlighted by Hegedűs and I'só (1965)⁶, that showed, that not the same rootstock result the best data on the range of scion cultivars.

Rootstocks have direct and indirect effects on scion.^{4, 13} Rootstock varieties differently affect fruiting, rate of growth, yield and fruit quality. In the process of these effects a highly crucial role has both the rootstock and the scion.³ It is important from the point of growth and evolution of the stocks, that grafts fruit earlier than own rooted plants.¹⁶

Accumulation of inorganic mineral elements change in grafts compared to that of own rooted stocks⁹. However rootstock-scion interaction has a crucial effect on mineral uptake of the grape⁷, this effect might alter or decrease to a great extent due to ecological factors and geographical characteristics.⁴

Materials and methods

Grape variety collecting point of the University of Debrecen was established in 2003 on immune sand soil in Pallag (10 km north from Debrecen) having 3 m between row and 1 m between stock spacing.

The Table 1. shows the properties of soil of model farm at 0-30 cm and 30-60 cm sampling depths. Table 2. shows the plant available K, Mg, P, Ca, Mn, B, Cu, Fe and Zn content of soil of model farm in 0-30 cm and 30-60 cm sampling depths. The soil samples were prepared for chemical analyses by extraction with 0.5 M ammonium acetate + 0.5 M acetic acid + 0.02 M EDTA solution (pH 4.65) according to Lakanen-Erviö.¹⁰ Analyses of 9 elements in soil extract were performed with an iCAP 6300 Dual type ICP-OES.

Introduction

After devastative invasion of phylloxera (*Dactulosphaira vitifoliae* Fitch.) to Europe the common biological preventive technology of graft making is used to eliminate the risk of infection. Since then, plantations on not immune sandy soils (with quartz content lower than 75%¹⁵) can only be established with the use of grafts.

According to summary of Angeli et al. (1959)¹ some characteristics of rootstock varieties are the following: mineral take up, soil demand, tolerance to lime and salt content of the soil, affinity and effects on biological cycle of the scion. Characteristics of rootstock varieties were studied by many researchers, since at their selection this crucial information give basic guideline to find the one, which mostly suits conditions of the planed vineyard. These characteristics of commonly used rootstock varieties show good correlation with corresponding data on their parent species of different geographical origin. The most common parental species used in ennobling of rootstocks are the following: *Vitis Riparia* Scheel., *Vitis Rupestris* Mich., *Vitis Berlandieri* Plan. and *Vitis Vinifera* L..⁸

Lately there are 19 rootstock varieties listed in National Variety Register of Hungary, however only a few is used.²

Range of commonly propagated rootstock varieties is larger in the neighbouring countries. Choice of ideal rootstock-

Table 1. Properties of soil of model farm

PARAMETERS	AVERAGE	
Sampling depth (cm)	0-30	30-60
pH (KCl)	5.93	5.91
pH (distilled water)	6.85	6.87
Soil texture	sand	sand
All water soluble salt (m/m)	0.005	0.006
CaCO ₃ % (m/m)	0.5	0.5
Humic % (m/m)	1.12	1.08

Table 2. Plant available elements content of soil of model farm

PARAMETERS	AVERAGE (mg kg ⁻¹)	
Sampling depth (cm)	0-30	30-60
Potassium (K)	337	288
Magnesium (Mg)	171	191
Phosphorus (P)	144	105
Calcium (Ca)	1790	1891
Boron (B)	0.63	0.60
Manganese (Mn)	329	382
Copper (Cu)	9.95	7.02
Iron (Fe)	239	213
Zinc (Zn)	6.93	4.65

The 28 rootstock variety of the collection was trained with bald-head training leaving no buds at regular pruning on the heads. Green grafting of 'Cserszegi fűszeres' on 14 rootstock varieties out of 28 was started in 2010. Further on grafts were trained according to single curtain training system, together with leaving one sampling shoot growing each year from the rootstock.

Leaf samples were collected about 2-3 weeks before vintage, from 'Cserszegi fűszeres' standing on 9 rootstocks and from sample shoots of the rootstocks in the cropping year 2011. Thus leaf samples of the scion and rootstock originate from the same stocks.

Rootstocks of the 1st year of the experiment were: 'Vitis Berlandieri', 'Berlandieri x Riparia S.O.4', 'Berlandieri x Riparia T.G. 5.A.5.', 'Berlandieri x Riparia T.8.B.', 'Berlandieri x Riparia T.K. 5.BB', 'Berlandieri x Riparia K.125 AA', 'Riparia Sauvage', 'Riparia Selecta' 'Riparia Tomentosa'.

The scion, 'Cserszegi fűszeres' ('Traminer' x 'Irsai Olivér'), also called 'Woodcutters white' is a tolerant, middle time ripening white grape cultivar.

In 2011 and 2012 grafting of the 28 rootstocks was continued with changing success, since the range of the rootstocks represent a broad range of different compatibility.

Sample preparation was conducted in laboratory of University of Debrecen, Centre for Agricultural and Applied Economic Sciences, Institute of Food Sciences, Quality Assurance and Microbiology. Nine elements were analysed

(K, Ca, Mg, P, B, Mn, Cu, Fe, Zn), which could be informative from the point of plant physiology. Digestion of the leaf samples was done open with HNO₃-H₂O₂. Prepared samples were measured by iCAP 6300 Dual type ICP-OES.

Data shown in our paper represented first year results of a provisional long term experiment. Counting with the great impact of ecological factors, we would not draw conclusion. Vintage of 2011 could be characterised with rainy July and extremely arid August.

Results and discussion

The aim of our experiment was to show how different rootstocks affect mineral composition of the scion. The Table 3.- 4. represents data on mineral composition of leaf samples of 'Cserszegi fűszeres' standing on 9 rootstocks and leaf samples of the rootstocks correspondingly, collected 2-3 weeks before vintage from the same stocks.

Results show, that potassium content of rootstock leaf samples were below optimum values given by reference data¹⁴, withstanding that potassium contents of scion leaf samples show optimum status concerning this element. Data of 2011 show a higher potassium concentration in leaf samples of the scion independent to the rootstock cultivar.

It is obvious, that magnesium contents of leaf samples both of rootstocks and of the scion show lower values compared to previous data. The reason could be the period of extreme drought during August 2011. It is also visible, that magnesium content of scion leaves was somewhat higher than measured in the case of rootstocks. Exceptions were *Vitis Berlandieri*, *Berlandieri x Riparia T.G. 5A5* and *Berlandieri x Riparia S.O.4*. with higher values in the rootstock leaf samples.

Results show, that average phosphorus content of leaf samples both in the case of rootstock and scion was over the reference optimum level given by Szűcs et al. (1981)¹⁴. Data of 2011 also show, that average phosphorus content of rootstock leaves was higher than that of scion leaves. For two exceptions, *Vitis Berlandieri* and *Berlandieri x Riparia T.G. 5A5* stands the opposite.

Average calcium content of the leaf samples of rootstock and scion grafted on them is well according to reference optimum value given by Szűcs et al. (1981)¹⁴. According to data of 2011, higher average calcium content was experienced in rootstock leaves. In the case of three exceptions, *Berlandieri x Riparia T. 8B*, *Riparia Tomentosa*, and *Riparia Selecta* the higher calcium level was measured in scion leaf samples.

Average boron content both of rootstock and scion leaf samples was in accordance with reference optimum values. Data of 2011 showed, that boron content of rootstock leaves was somewhat higher compared to scion samples.

In respect to manganese content it is clear to see, that a much higher level was experienced in both cases compared to the reference data (Szűcs et al., 1981)¹⁴. More over a toxic manganese level was measured in the case of own rooted control 'Cserszegi fűszeres' leaf samples. Data of 2011 showed, that manganese level of scion leaves was higher than in the case of rootstock samples.

Table 3. Element content of leaf samples of 9 rootstocks and 'Cserszegi fűszeres' grafted on them (Pallag, 2011)

Variety/ Element	K %	Mg %	P %	Ca %
Optimum values of leaf analysis*	1.01-1.40	0.30-0.40	0.16-0.23	2.50-3.20
Cserszegi fűszeres own rooted	1.25	<u>0.295</u>	0.257	<u>3.48</u>
V. Berlandieri rootstock	0.950	0.184	<u>0.269</u>	2.83
V. Berlandieri scion	1.32	0.176	0.277	2.78
BxR T.G. 5 A 5 rootstock	0.739	<u>0.216</u>	0.337	3.37
BxR T.G. 5 A 5 scion	1.05	0.205	<u>0.372</u>	2.95
BxR S.O.4 rootstock	<u>0.727</u>	0.152	0.365	3.01
BxR S.O.4 scion	1.19	<u>0.143</u>	<u>0.188</u>	<u>1.95</u>
Riparia Sauvage rootstock	0.786	0.178	<u>0.509</u>	<u>3.83</u>
Riparia Sauvage scion	1.27	0.208	0.289	2.86
BxR T. 8B rootstock	0.843	0.169	0.350	2.39
BxR T. 8B scion	1.29	0.203	0.248	3.11
Riparia Tomentosa rootstock	<u>0.999</u>	<u>0.124</u>	0.300	<u>1.45</u>
Riparia Tomentosa scion	1.14	0.172	0.266	3.05
BxR K 125 AA rootstock	0.997	0.160	0.318	3.14
BxR K 125 AA scion	1.09	0.205	0.313	3.06
BxR T.K. 5BB rootstock	0.825	0.163	0.321	3.75
BxR T.K. 5BB scion	<u>1.022</u>	0.168	0.220	3.11
Riparia Selecta rootstock	0.900	0.150	0.330	2.23
Riparia Selecta scion	<u>1.46</u>	0.161	0.253	2.55
Average rootstock	0.863	0.166	0.344	2.89
Average scion	1.208	0.194	0.268	2.89
Deviation rootstock	0.100	0.030	0.070	0.76
Deviation scion	0.140	0.040	0.050	0.41
RSD% rootstock	12.1	15.4	19.7	26.5
RSD% scion	11.3	21.7	18.8	14.3

Comments: K-, Mg-, P- and Ca: %, B-, Mn-, Cu, Fe- and Zn: ppm (in dry matter) **Data in boldface type** represent the lowest values of the element, whereas **Underlined and bolded data** represent the highest values, in respect to rootstock varieties and scion grafted on them.^{5,14}

Data show, that average copper content both in the case of rootstock and scion leaf samples was much lower, than the reference data. A reason for this effect could be the extremely dry vintage of 2011, and the well-known antagonism of manganese and copper.¹² Data of 2011 showed, that average copper concentration of rootstock leaves was higher than in the case of leaf samples collected from the scion parts of the stocks.

One exception was experienced in this comparison. In the case of *Berlandieri x Riparia K 125 AA* rootstock, leaf sample from the scion showed higher copper content.

Table 4. Element content of leaf samples of 9 rootstocks and 'Cserszegi fűszeres' grafted on them (Pallag, 2011)

Variety/ Element	B ppm	Mn ppm	Cu ppm	Fe ppm	Zn ppm
Optimum values of leaf analysis*	20-40	80-120	20-25	80-120	25-40
Cserszegi fűszeres own rooted	<u>28.2</u>	<u>336</u>	<u>6.28</u>	137	<u>122</u>
V. Berlandieri rootstock	23.7	<u>224</u>	4.87	181	<u>16.1</u>
V. Berlandieri scion	19.5	247	2.96	193	16.0
BxR T.G. 5 A 5 rootstock	28.1	171	<u>5.52</u>	<u>310</u>	<u>21.0</u>
BxR T.G. 5 A 5 scion	27.0	217	5.28	<u>257</u>	23.3
BxR S.O.4 rootstock	<u>14.7</u>	140	4.86	166	20.7
BxR S.O.4 scion	11.7	<u>143</u>	3.30	115	13.6
Riparia Sauvage rootstock	25.5	181	4.31	203	20.5
Riparia Sauvage scion	24.3	247	2.81	211	17.1
BxR T. 8B rootstock	<u>28.2</u>	148	5.14	302	20.3
BxR T. 8B scion	22.1	219	2.82	184	16.4
Riparia Tomentosa rootstock	19.1	<u>122</u>	<u>3.18</u>	172	17.2
Riparia Tomentosa scion	18.0	155	2.81	<u>105</u>	15.1
BxR K 125 AA rootstock	26.1	171	4.75	161	16.4
BxR K 125 AA scion	19.9	233	6.11	181	17.5
BxR T.K. 5BB rootstock	16.7	211	4.10	164	16.6
BxR T.K. 5BB scion	<u>10.8</u>	211	2.80	149	<u>12.8</u>
Riparia Selecta rootstock	21.9	157	5.16	<u>113</u>	19.8
Riparia Selecta scion	18.6	261	<u>2.32</u>	109	26.2
Average rootstock	22.7	169	4.65	197	18.7
Average scion	20.0	227	3.75	164	28.0
Deviation rootstock	4.93	32.7	0.70	66.1	2.09
Deviation scion	5.75	54.3	1.52	49.7	33.4
RSD% rootstock	21.8	19.3	15.1	33.6	11.1
RSD% scion	28.7	23.9	40.5	30.3	119.1

Comments: K-, Mg-, P- and Ca: %, B-, Mn-, Cu, Fe- and Zn: ppm (in dry matter) **Data in boldface type** represent the lowest values of the element, whereas **Underlined and bolded data** represent the highest values, in respect to rootstock varieties and scion grafted on them.^{5,14}

In respect to both leaf samples average iron content was higher, zinc content was lower, than the reference data.¹⁴ In the case of own rooted 'Cserszegi fűszeres' an extremely high zinc level (110%) was measured.

Conclusion

In our experiment leaf samples of 9 different rootstock varieties and 'Cserszegi fűszeres' grafted on the same stocks were analysed. Results of 2011 support the statement, that rootstock variety affect mineral take up of the scion. Experienced differences between rootstocks can be due to genetic background, environmental factors of the vintage and differences in compatibility of the scion-rootstock combination, since the range of examined rootstocks represent a broad range of compatibility and affinity. A comprehensive examination of this question needs a long term experiment to define the range of rootstocks, that facilitate best quality potential and stability in mineral take up and resistance to climatic extremities.

Acknowledgements

The publication is supported by the TÁMOP-4.2.2/B-10/1-2010-0024 and TÁMOP-4.2.1/B-09/1/KONV-2010-0007 projects. The projects are co-financed by the European Union and the European Social Fund.

References

- ¹Angeli L. – Horváth J. – Hullai L. *Kertészeti Ismeretek*, Mezőgazdasági kiadó, Budapest, **1959**, 322-323.
- ²Bánszki E. *A különböző alanyfajták hatása a Cabernet sauvignon és a Chardonnay fajták mennyiségi és minőségi teljesítményére a mátrai borvidéken*. Diplomadolgozat, Debreceni Egyetem, Debrecen, **2009**, 4.
- ³Bényei F. – Lőrincz A. *Szőlőfajtáink* [In: Bényei F., Lőrincz A., Sz. Nagy L. (szerk.) *Szőlőtermesztés*], Mezőgazda kiadó, Budapest, **1999**, 196-199.
- ⁴Csikászné K. A. *A termés mennyiség, a termés minőség és a levelek tápelem tartalmának összefüggése különféle alanyokra oltott Cabernet sauvignon szőlőfajtán*, Doktori Értekezés, Pannon Egyetem Georgikon Mezőgazdaságtudományi Kar, Keszthely, **2008**, 18-28.
- ⁵Fregoni, M. *Nutrizione e fertilizzazione della vite*. Edagricole, Bologna, **1980**
- ⁶Hegedüs Á. – I'só, A. *Kísérleti Közl.*, **1965**, 3, 61-77.
- ⁷Kocsis L. – Lehoczky É. – Keresztes Z. – Angyal M. – Walker, M.A. *ASEV 52nd Annual Meeting*, San Diego, California, **2001**, 21.
- ⁸Kocsis L. *Szőlőalanyok egyes fiziológiai jellemzőinek és biotikus tényezőinek értékelése*, MTA doktori értekezés, Pannon Egyetem Georgikon Mezőgazdaságtudományi Kar, Keszthely, **2010**, 4-8.
- ⁹Kozma P. *A szőlő és termesztése II.*, Akadémiai Kiadó, Budapest, **1993**, 403.
- ¹⁰Lakanen, E. - Erviö, R., *Acta Agr. Fenn.*, **1971**, 123, 223-232.
- ¹¹Lőrincz A. – Barócsi Z. *A szőlő metszése és zöldmunkái*, Mezőgazda kiadó, Budapest, **2010**, 306.
- ¹²Oláh L. *Szőlészek Zsebkönyve*, Mezőgazdasági kiadó, Budapest, **1979**, 131.
- ¹³Striegler, R.K. – Howell, G.S., *Vitis*, **1991**, 30, 1-10.
- ¹⁴Szűcs E. – Horák E. – Kovácsné M. Zs. *Az álló kultúrák fenntartó műtrágyázási irányelvei*, MÉM NAK, Budapest, **1981**
- ¹⁵Vanek, G. *A szőlő védelme* [In: Szőke L. (szerk.) *A szőlő növényvédelme*], Mezőgazda kiadó, Budapest, **1996**, 158-159.
- ¹⁶Zsukov, A.I. – Szododova, N.P. – Komarov, M., *Szadov. Vино. Vinod. Moldavii*, **1973**(3), 41-43.

Received: 26.10.2012.

Accepted: 26.11.2012.



QUADRUPLE IMMUNE RESPONSE OF PLANTS TO PATHOGENS AFTER PRETREATMENT WITH DIFFERENT DOSES OF TRACE ELEMENTS

Ernő Tyihák^{a*}, Ágnes M. Móricz^a, Mihály Szilágyi^b, Ferenc Billes^c

Paper was presented at the 4th International Symposium on Trace Elements on the Food Chain, Friends or Foes, 15-17 November, 2012, Visegrád, Hungary

Keywords: formaldehyde, hormesis, inducer, pretreatment, quadruple immune response, trace elements.

The enzymatic and/or non-enzymatic methylation / hydroxymethylation of main trace elements renders a special, indispensable bridge between biological (organic) and inorganic world. These modified trace elements are potential formaldehyde (HCHO) generators and HCHO formed from them can participate in different characteristic interactions. On the basis of up-to-date biochemical results with HCHO it is supposed that trace elements as HCHO carriers transport HCHO molecules in dose-dependent level to different points of a given biological unit. On the basis of experiences with the time- and dose-dependent double immune response of plants to pathogens, a logical step was to extend it to the total Avogadro number range (in vivo conditions) in the case of trace elements as potential inducers as well. These new findings support that HCHO and its reaction products (mainly O₃) as drastic molecules are responsible for the immunostimulating activity of trace elements as inducers. It is especially important that there are always four bioequivalent immunostimulating activity ranges in plants for the pretreatment with different doses of trace elements similar to organic compounds. It has to be noted that the trace elements as inducers actually don't participate directly in the induction of the immunostimulating effect similar to organic inducers.

* Corresponding Authors

Fax: 00-36-1-48-77-555

E-Mail: tyihak.erno@agrar.mta.hu

- [a] Centre for Agricultural Research, Plant Protection Institute, Hungarian Academy of Sciences, H-1525 Budapest, POB 102, Hungary
- [b] Research Institute for Animal Breeding and Nutrition, H-2053 Herceghalom, Hungary
- [c] Department of Physical Chemistry, Budapest University of Technology and Economics, H-1521 Budapest, Budafoki út 8, Hungary

new horizons in this field: antibodies can catalyze the generation of very reactive biological oxidants including ozone (O₃) – through H₂O₃ -from the interaction of singlet oxygen (¹O₂) with H₂O.⁷⁻⁹ It is obvious that the formation of ¹O₂ is crucial step in this complicated system. Both HCHO and H₂O₂ can be formed continuously and are present (HCHO mainly in hydroxymethyl groups) intracellular and extra-cellular by almost all cells^{10,11}. These two reactive molecules can interact (also endogenously) and the very reactive ¹O₂ and excited HCHO can be formed^{10,12}, that is, the formation of ¹O₂ may be continuous in all cells at different levels. According to preliminary experiments these very reactive molecules (from HCHO to O₃) can be formed in plant tissues and biological world in general.^{13,14}

Introduction

The recent increase in the number of studies concerning the defence mechanisms of plants reflects the interest in a better understanding of plant immunity as pre-formed (constitutive, innate) defence systems and adaptive immunity as induced resistance mechanisms.¹⁻⁴

Plant immunity is composed of several layers including robust pre- and post-invasion defences⁵. It is fact that plants successfully use pre-formed physical and chemical innate defence systems as well as inducible adaptive immune strategies to pathogens, although, circulating cells, immunoglobulin molecules and phagocytic processes lack in plant tissues⁶.

Until recently, the mechanisms of antibody-mediated immunity in humans and animals against microorganisms are not well known and it is fact that until now immunoglobulin-like proteins have not been found in plants. Therefore, it is high time to find a common point (e.g. biochemical pathway) that is valid for innate and adaptive immunity in animals and plants similar. Recent studies open

Resistance phase of stress syndrome can be activated by biotic (e.g. avirulent forms of pathogens, incompatible races of pathogens)¹⁵⁻¹⁸ and by abiotic (inorganic and organic compounds, UV-ray, high temperature, etc.) inducers.¹⁹⁻²² Induced resistance means an improvement of the natural (innate) resistance of plants without alteration of their genome. Induced resistance is generally systemic, because the defensive capacity is increased not only in the primary infected plant tissues, but also in distant parts of the plant.

Among the abiotic inducers the trace elements with double effect²³ and as HCHO carriers²⁴ play a determining role. The aim of this work is to demonstrate the basic elements of the time- and dose-dependent quadruple, non-linear, however, specific immune response of plants to pathogens regarding interactions and function of formaldehyde (HCHO) and its reaction products in it using different doses of trace elements for pretreatment of plants.

Experimental

Chemicals

All chemicals were obtained from Merck Hungary (Budapest, Hungary) and Sigma Co (St Louis, USA) as well as Reanal Chemical Co (Budapest, Hungary).

Plant and pathogens

Bean (*Phaseolus vulgaris* cv. Debreceni tarka, Békési fehér) plants were cultivated in commercial compost in the greenhouse held at 24°C with 4 hours supplementary light (6000 lux) in the morning and evening to give a light period of at least 16 hours per day. The investigations were limited to primary leaves. Bean rust (*Uromyces phaseoli*) was maintained on bean in the greenhouse.

Biochemical immunization (pretreatment) and inoculation

Aqueous solutions of potential inducers (decimal dilution) were used. The solutions were sprayed onto the abaxial leaf surface in case of bean plants. Plants treated with water were used as controls.

Bean plants were inoculated with an aqueous spore suspension of bean rust 4 days after pre-treatment with inducer and then incubated at 20-22°C for 24 hours at high relative humidity.

Capture of HCHO in bean plants (in vivo) with dimedone

To aqueous solution of inducers dimedone (a HCHO capturing molecule) was given for the elimination of this reactive molecule. The decimal dilution was carried out similar to biochemical immunization process for all inducers and capturer.

Evaluation of data

Pustule densities were assessed 9-10 days after inoculation and disease severity (infection rate, infectivity) was expressed as the number of pustules cm⁻² (by means of a homemade pattern) in the case of bean plants. The mathematical evaluation of the data was carried out by moving average calculations using an appropriate software.

Results and Discussion

On the basis of earlier experiences with the time- and dose-dependent double immune response of plants to pathogens¹³ a logical step was to extend it to the total Avogadro number range for example from 10⁻¹ to 10⁻²³ mol/L. Figure 1 supports the original conception. As it can be seen at the 4 day interval between pre-treatment and inoculation in bean-*Uromyces* sp. relationship there is a characteristic time- and dose-dependent quadruple immune response of plants to pathogens using in this case N-methyl-L-methionine as special natural amino acid derivative (organic compound) with N- and S-methyl groups as potential formaldehyde generators.²⁵

It seems that Cu(II) might be an especially important and suitable agent (inducer) for such a pretreatment of plants because this molecule does not contain methyl group (HCHO precursor) but it can mobilize and transport a relatively high amount of HCHO (four molecules) in hydroxymethyl groups from plant tissues and/or pathogen cells according to recent observations²⁴ and there are preliminary immunization results with this trace element.²³

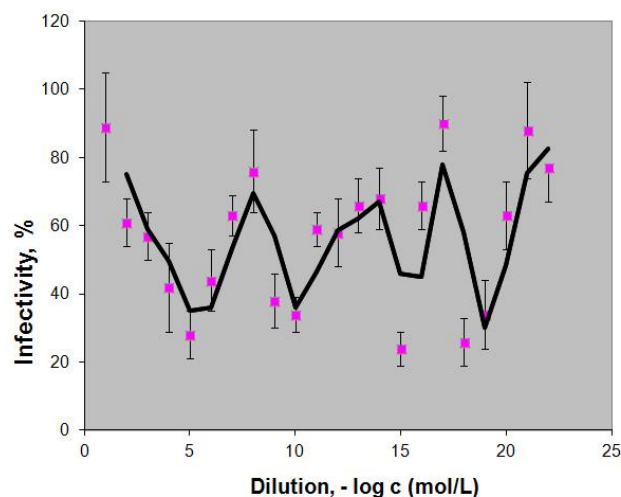


Figure 1. Quadruple immune response of bean plants to *Uromyces phaseoli* using N-methyl-L-methionine as inducer for pretreatment (with permission, from Ref. ²⁵).

It is obvious that there is a non-linearity for the Avogadro number range and it follows from these results that there is a molecular order in the induced resistance of plants (e.g. there is a similar or same inactive range between two active ranges and there is receptor-directed exact dose-effect etc.). The Figure 1 illustrates clearly that methyl-methionine generated 4 immunostimulating ranges with practically same activity intensity, that is, for example 10⁻⁵ mol/L (at allopathic dose-range) and 10⁻²⁰ or 10⁻¹⁹ mol/L (homeopathic dose-range yet within Avogadro range) generate practically same immunostimulating activity.²⁵ These results with a non-toxic, endogenous molecule show – among others – that in the immunostimulating activity the given inducer doesn't participate directly in the inducing effect. These results with different doses of some trace elements support also the preliminary results with HCHO reactions of trace elements²⁶ including the quantumchemical calculations.²⁷ It has to be noted down now to this figure that the activity of the last, very low dose will be especially interesting for understanding and answering the unique phenomena after Avogadro range.

Our present results illustrate clearly that the trace elements can also generate hormesis effect (Figure 2 and 3) as the organic compounds in which HCHO and its special reaction products (e.g. O₃) play a crucial role (Figure 4). These results with trace elements eliminate also the idea on the two-phase hormesis.^{28,29} Our results show that hormesis and its phases are in the resistance phase. On the basis of quadruple immune response of plants to pathogens the resistance phase of stress syndrome can be divided into four equivalent (?) parts. The further study of trace elements in vitro (BioArena¹⁴) and in vivo (e.g. greenhouse²⁵) conditions regarding to HCHO/O₃ idea assures further revelation.

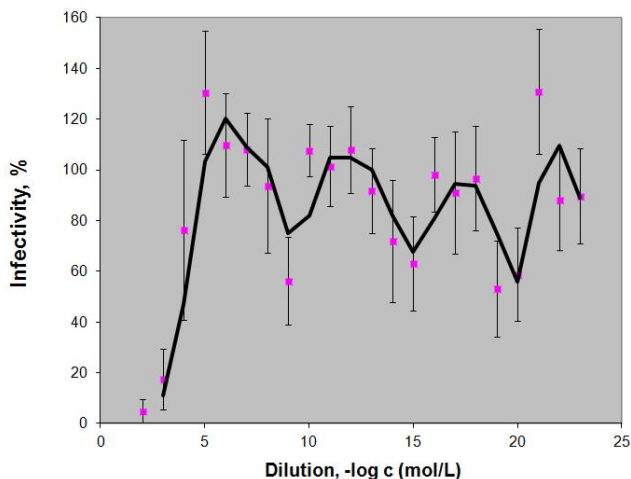


Figure 2. Effect of Cu(II) ion pretreatment on the resistance potential of bean plants to *Uromyces phaseoli*

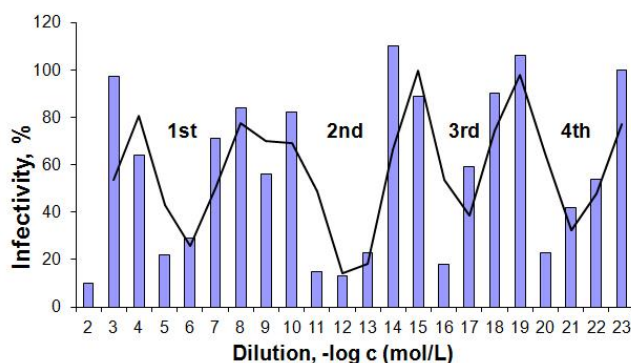


Figure 3. Effect of Ni(II) ion on the resistance potential of bean plants to *Uromyces phaseoli*

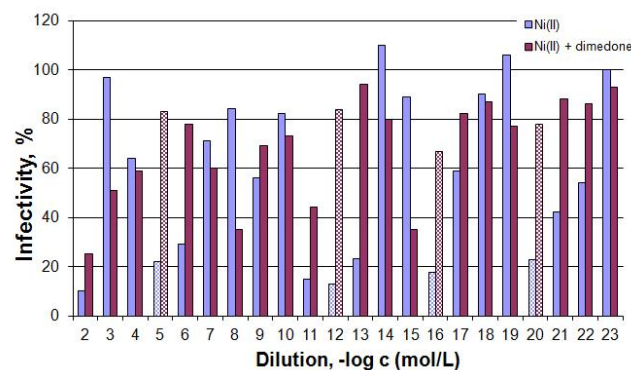


Figure 4. Effect of dimedone on the immunostimulating activity of Ni (II) ion in bean-*Uromyces phaseoli* relationship. The checked columns mean the four active ranges and their elimination with dimedone as a HCHO capturer.

References

¹ Cohn, J., Sessa, G., Martin, G. B., *Curr. Opin. Immunol.*, **2001**,13, 55.
² Bostock,R. M., *Annu. Rev. Phytopathol.*, **2005**, 43, 545.
³ Zhai, Z., Liu ,Y., Wu, L., Senchina, D.S., Wurtele, E. S., Murphy., P. A., Kohut, M. L., Cunnick, J. E., *J. Med. Food*, **2007**, 10, 423.
⁴ Jung, H. W., Tschaplinski, T. J., Wang, L., Glazebrook, J., Greenberg, J.T., *Science*, **2009**,324, , 89.
⁵ Da Cunha, L., McFall, A. J., Mackey, D., *Microbes Infect.*, **2006**, 8, 1372.

⁶ Menezes, H., Jased, C., *Comp. Biochem. Phys. C.*, **2002**, 132, 1.
⁷ Wentworth, A. D., Jones, L. H., Wentworth, P. Jr., Janda, K. D., Lerner, R. A., *P. Natl. Acad. Sci. USA.*, **2000**, 97, 10930.
⁸ Wentworth, P., Jr., Janda, K. D., *Cell Biochem. Biophys.*, **2001**, 35, 63.
⁹ Babior, B. M., Takeuchi, C., Ruedi, J., Gutierrez, A., Wentworth, P, Jr., *P. Natl. Acad. Sci. USA.*, **2003**, 100, 3031.
¹⁰ Tyihák, E., Rozsnyay, S., Sárdi, E., Gullner, G., Trézl, L., Gáborjányi. R., *Acta Biol. Acad. Sci. H.*, **1994**, 45, 3.
¹¹ Tyihák, E., Trézl, L., Szende, B., *Ann. N. Y. Acad. Sci.*, **1998**, 851, 259.
¹² Trézl, L., Pipek, J., *J. Mol. Struc. – Theochem.*, **1988**, 170, 213.
¹³ Tyihák, E., In: Teixeira da Silva, J.A., (editor), *Floriculture, Ornamental and Plant Biotechnology, Advances and Topical Issues*. Vol. III, London (UK), Global Science Books, **2006**, 380.
¹⁴ Tyihák, E., Móricz, Á. M., Ott, P. G., *J. Planar Chromat.*, **2008**, 21, 77.
¹⁵ Hostetter, M. K., *Curr. Opin. Microbiol.*, **2000**, 3, 344.
¹⁶ Klement, Z., Bozsó, Z., Keckés, M. L., Besenyei, E., Celleng, A., Ott, P. G., *Pest Manag. Sci.*, **2003**, 59, 465.
¹⁷ Kothari, I. L., Patel, M., *Indian J. Exp. Biol.*, **2004**, 42, 244.
¹⁸ Xia, Y., Gao, O. M., Yu, K., Lapchyk, L., Navarre, D., Hildebrand, D., Kachroo, A., Kachroo, P., *Cell Host Microbe*. **2009**, 5, 151.
¹⁹ Alvarez, M. E., Pennell, R. I., Meijer, P. J., Ishikawa, A., Dixon, R. A., Lamb, C., *Cell*, **1998**, 192, 773.
²⁰ Zhao, H., Wang, B-Ch., Zhao, H.-Ch., Wang, J. B., *Colloid Surface B.*, **2005**, 44, 36.
²¹ Park, S. W., Kaimovo, E., Kumar, D., Mosher, S., Klessig, D. F., *Science*, **2007**, 318, 31.
²² Endo, J-i, Takahashi, W., Ikegami, T., Beppu, T., Tanaka, O., *Biochem.*, **2009**; 73, 183.
²³ Tyihák, E., Móricz, Á. M., Ott, P. G., Király-Véghely, Zs., Kátay, Gy., In: *Procs Intern. Symp. On Trace Elements in the Food Chain*, Budapest, May 25-27, (Eds.: Szilágyi, M., Szentmihályi, K.), **2006**, 394.
²⁴ Tyihák, E., Takátsy, A., Móricz, Á. M., Ott, P. G., Ohmacht, R., In: *Trace Elements in the Food Chain, Vol.3. Deficiency or Excess of Trace Elements in the Environment as a Risk of Health*. Budapest, Hungary, (Eds.: Szilágyi, M., Szentmihályi, K.), **2009**, 392.
²⁵ Tyihák, E., Mincsovcics, E., *J. Planar Chromat.*, **2010**, 23, 382.
²⁶ Móricz, Á. M., Ott, P. G., Szilágyi, M., Otta, K., Tyihák, E., *Acta Biol. Acad. Sci. H.*, **2007**, 58, 301.
²⁷ Billes, F., Mohammed-Ziegler, I., Mikosch, H., Tyihák, E., *Spectrochim. Acta A.*, **2007**, 68, 669.
²⁸ Calabrese, E. J., *Mutat. Res.*, **2002**, 511, 181.
²⁹ Calabrese, E. J., Mattson, M.P., Calabrese, V., *Human. Exp. Toxicol.*, **2010**, 29, 1034.

Received: 18.10.2012.
 Accepted: 14.11.2012.



BIOCHAR PROPERTIES FROM DIFFERENT MATERIALS OF PLANT ORIGIN

Kateřina Břendová^{a*}, Pavel Tlustoř^a, Jiřina Száková^a, Jan Habart^a

Paper was presented at the 4th International Symposium on Trace Elements in the Food Chain, Friends or Foes, 15-17 November, 2012, Visegrád, Hungary

Keywords: biochar, soil, heavy metals, slow pyrolysis, biomass.

Biochar is a highly porous solid substance, made of different biomass by pyrolysis. Conditions of pyrolysis as well materials used in it can substantially affect biochar properties. Samples with sufficient amount of stable carbon can be added into soil to be sequestered; high sorption surface of biochar could characterize it as a soil additive, able to immobilize risk elements in soil. Soil contamination by risk elements is a serious problem needs to be solved. There are available remediation methods, using plants to remove these elements from soil. Biomass produced during remediation has limited application and biochar production could be one option. Plants for our experiments were grown on contaminated soil of Příbram area. For the experiment they were used: meadow grass, wood mixture of poplar and willows twigs and finally maize. Biomass of these plants was used to prepare biochar. The effect of the type of biomass and the final temperature of pyrolysis on specific surface area and yield of biochar was studied in our experiments. Both temperature and plant material affected properties of biochar. While the final temperature increased, the specific surface area increased and the yield of biochar decreased. The highest surface area was found at biochar from wood mixture and the lowest one from meadow grass.

*Corresponding Author

E-Mail: brendova@af.czu.cz

[a] Department of Agro-Environmental Chemistry and Plant Nutrition, Faculty of Agrobiolgy, Food and Natural Resources, Czech University of Life Sciences Prague, Prague-Suchdol, 165 21, Czech Republic

Introduction

The reuse of harvested plant biomass previously used for remediation of contaminated soils by risk elements is under detailed investigation by several authors.^{1,2} One possibility how to process harvested material is to pyrolyse it to get energy fuels (oil, gas) and char- biochar, which could be use as a soil amendment for phytostabilisation of highly contaminated soils³.

Generally, biochar is a carbon-rich, highly porous material, which can be prepared from various types of biomass (wood, agriculture residues, leaves etc.). The biochar production is based on thermal decomposition of raw materials under limited or no supply of oxygen. The process is called pyrolysis.⁴ The products of the pyrolysis are bio - oil and bio - gas and finally char. These products could be used as fuels.⁵ Here we should describe the terminology: the differences between the words char, charcoal and biochar. Char is the most general term and expresses the product of pyrolysis or natural fires, whether from biomass or other materials. Charcoal is prepared by pyrolysis of animal manure or plant biomass and the product is primarily used for heating.⁶ Another author reported that charcoal is surprisingly used in French cuisine.⁷ Its use in health care is well known. The production of biochar corresponds to charcoal one though the purpose of using is the soil application.⁴

The biochar application to soil is known since long. In 1929 John Morley in *The National Greenkeeper* notes the positives of charcoal application into soil and described the

improvement of soil porosity.⁸ There were also described soils in Amazonia, where burnt biomass and other organic matters led to creation of very fertile soil.⁹

The interest of biochar research has been widely spread recently primarily due to its ability to sequester carbon to soil.⁴ Its ability to improve the soil properties causing improvement of crop production was observed.¹⁰ It was also found, that biochar is stable because of aromatic arrangement structure supports slow decomposition in soil, because microorganisms can use such compounds only with difficulty.¹¹ Finally many interests in biochar are due to its ability to sorb undesirable contaminants of organic and inorganic origin, as pesticides¹² or even heavy metals.^{13,14} Various authors support the hypothesis restriction of mobility of risk elements. It was observed significant reduction of acceptable cadmium and copper and increasing pH values after biochar application within 1-2 months in the incubation experiment.¹⁵ The properties of biochar affect its retention ability^{13,16,17} as well as the characteristic of retained element. The higher specific surface area of diary - manure derived biochar can positively increased the cadmium retention¹⁶, but it was also observed greater heavy metal retention capacity of the lower pyrolysis temperature at cottonseed hull biochar. So it was suggested that the biochar for specific soil amendment should be selected on the bases of the biochar characteristics, soil property, and the requested function.¹³

It is known that pyrolytic condition and the feedstock biomass can influence the final products of this process.⁷ On the basis of pyrolytic condition; there are several types of pyrolysis processes. These are namely fast pyrolysis, slow pyrolysis (also called carbonization) and gasification. The three already meant final products (char, gas and liquid – oil) arise in different ratio according to chosen type of pyrolysis. Reaction mechanisms of biomass pyrolysis are complex processes, but can be defined in three main steps. In the first step, there is a loss of moisture and some volatile

substances. In the second step the primary char is formed. Fast reaction is followed by a slower and involves other chemical reactions to form secondary char.¹⁸ Thus the highest yields of char are produced during slow pyrolysis. Lower temperatures, slow heating rate and long residence time favor the formation of char.⁵ During the slow pyrolysis the portion of products is: 35% of the char, 35% gas and 30% pyrolysis liquid. The final temperature is around 500° C. The retention time of the vapor in the reactor at a slow pyrolysis is of the order of minutes (5-30 minutes). Vapors don't leak as quickly as during fast pyrolysis, and thus components of the gas phase may further react to form char and liquid.¹⁹

In recent studies authors reported that the study of biochar properties is very important to understand its ability to sequester heavy metals into soil¹³ and as Lehmann and Joseph (2009) reported, further research of changes of availability of heavy metals in biochars is not available.⁴ But as Trakal et al. (2011) found, the contaminated biochar has similar effect on sorption risk elements in soil as uncontaminated one.³ Up to our knowledge studies describing sorption biochar capacity with relation to source material and temperature of pyrolyses are missing for contaminated feedstock biomass.

The aim of our work was to prepare biochar from different types of plant materials harvested at contaminated sites under different pyrolysis temperatures and to determine main characteristic of biochar mainly element composition and sorption capacity to get immobilization agent for further studies of heavily damaged contaminated sites.

Experimental

Plants that grew on the contaminated soil were used as raw materials for the biochar preparation. Specifically, it was whole plants of maize (*Zea mays*), a mixture of fast-growing trees of the family *Salicaceae* of the genera *Salix* and *Populus* and meadow grass harvested in the area of long-term contaminated with cadmium, lead and zinc. This area belongs to the most polluted in the Czech Republic.²⁰ The contamination of this area is caused primarily by anthropogenic activity, but also because of original subsoil. Natural contamination is the result of the composition of parent rock, where it is found in high contents of heavy metals: like cadmium, lead and zinc. Anthropogenic contamination of this area was caused by two major sources: atmospheric fallouts of metal works and flood water contaminated by waste from the mills in nearby areas.²¹

The plant material was first dried to the optimum moisture content of 15%. Biomass was ground and homogenized. It was subsequently made into pellets with a diameter of 6 mm.

Pyrolytic process was carried out in a muffle furnace under flow of inert gas (nitrogen) 1 m³ h⁻¹, at atmospheric pressure and retention time of 30 minutes. The process followed under three different temperatures of 450, 500 and 550 °C.

Surface areas were measured by nitrogen adsorption isotherms at 77 K using ASAP 2050 (Micrometrics Instrument Corporation, USA) surface area analyzer.

Specific surface areas were detected by layered adsorption isotherm BET model.²²

For each raw feedstock and biochar sample, a single estimate analysis was carried out using FlashEA 1112th from Thermo Scientific Company. The principle of the determination of these elements is based on the momentary combustion of the sample in a stream of oxygen at high temperatures. Gas products of combustion (nitrogen, carbon dioxide, sulfur dioxide and water) are then separated on chromatographic packed column and analyzed by thermal conductivity detector. The oxygen content is determined by difference. These results were used to calculate atomic H/C, O/C and N/C ratios.

Results and Discussion

The elemental composition of feedstock biomass and biochar

Table 1. describes the elemental composition of feedstock biomass. It was found that grass biomass had higher ash content, it is because the grass takes up higher amount of nutrients during their growing period.²³ The lowest content of nitrogen was found at wood biomass that was compared by Vassilev et al.'s review,²⁴ where it is reported that the nitrogen content is higher at wood biomass in general. The content of nitrogen corresponds to the content of sulfur, the lower values of sulfur were found in wood biomass too. The hydrogen content in biomass was ranging about to 6% according to earlier work and similar values were found at our plant materials also.²⁴

Table 1. Elemental composition of feedstock biomass

Type of plant material	Elemental composition (% w/w)*				
	C	H	O	N	S
Wood mixture**	50.43	6.16	42.68	0.70	0.03
Maize	48.15	6.37	43.83	1.57	0.08
Meadow grass	48.99	6.14	43.49	1.33	0.06

*moisture and ash free values, **wood mixture of poplar and willow

Table 2. Trace elements and ash content in feedstock biomass

Type of plant material	The content of trace elements (ppm)			Ash (% w/w)
	Cd	Zn	Pb	
Wood mixture*	14,77±2,58	176,9±39,4	26,73±12,21	3.71
Maize	1,74±0,17	35,8±4,70	13,14±4,35	6.69
Meadow grass	0,76±0,31	33,1±11,2	11,01±4,28	6.54

*wood mixture of poplar and willow

The evaluation of all three types of feedstock biomass showed that the highest content of all observed risk elements showed a mixture of willow and poplar wood. However the uptake of risk elements into tissues of maize plants and meadow grass is similar, maize tissues contained significantly more cadmium compared to meadow grass. The zinc content was lower in the meadow grass, but statistically insignificant, as well as the content of lead (Table 2).

The elemental analysis was done at all type of biochars. The content of carbon was lower at biomass of maize and meadow grass. It was found that the carbon content in biochar prepared from woody biomass at lower temperatures (450 °C) is higher than biochar prepared from maize straw at a higher temperature (600 °C).²⁵ So the carbon yield from herbaceous materials occurs lower than from wood materials.^{7,13,26} It was also reported similar results of ash content of feedstock biomass, as was shown in Table 1., the herbaceous materials have higher ash contents resulted in lower carbon yield.²⁷

In general in the studies of various authors,^{13,18,28} it was reported that the content of carbon increased with increasing temperature. Our results showed the opposite trend (Table 3). This is most probably caused by imperfect pyrolysis condition. It seems that only limited oxygen conditions are insufficient and the strict controlled conditions are required for biochar preparation.

The nitrogen is conserved by 41% in wood biochar and by 80% in biochar from maize, prepared at 500 °C. Gaskin et al. (2008) reported 3.4% of N in biochar from poultry litter and the higher conservation of nitrogen in biochar from pine (89%) than in poultry litre (24%) at temperature ranged from 400–500 °C, and on the basis of these values suggest biochars as fertilizers.²⁹ No sulphur was found in prepared biochar, most probably it was escaped during pyrolysis.

Table 3. The elemental composition of biochars from different plant materials, prepared at three different temperatures

Type of biochar	Temperature, °C	Elemental composition (% w/w)*				Ash (% w/w)
		C	H	O	N	
Wood mixture**	450	63.58	2.35	20.16	1.17	12.74
	500	63.84	2.21	19.04	1.11	13.80
	550	62.83	1.97	19.27	1.01	14.92
Maize	450	58.82	2.15	14.17	1.88	22.98
	500	54.97	2.05	13.75	1.95	27.28
	550	44.19	1.56	22.73	1.79	29.73
Meadow grass	450	59.38	2.44	16.67	1.78	19.73
	500	57.93	2.21	17.34	1.72	20.80
	550	55.24	1.83	17.63	1.66	23.64

*moisture and ash free values, **wood mixture of poplar and willow

Table 4. Atomic ratios of prepared biochars

Type of biochar	Temperature, °C	Atomic ratios		
		C:N	O:C	H:C
Wood mixture*	450	54.34	0.32	0.04
	500	57.51	0.30	0.03
	550	62.21	0.31	0.03
Maize	450	31.29	0.24	0.04
	500	28.19	0.25	0.04
	550	24.69	0.51	0.04
Meadow grass	450	33.36	0.28	0.04
	500	33.68	0.30	0.04
	550	33.28	0.32	0.03

*wood mixture of poplar and willow

The highest C/N ratio was detected in biochar from wood mixture at 550 °C on contrary the lowest was observed at maize biochar. We cannot conclude that the pyrolysis

temperature affects the molar ratios (Table 4). In the literature, there was also described that the possibility to use molar ratio of C and H organic compounds to determine the bonding arrangement. Authors suggested when H/C is 1.3, the C is directly bonded to a proton or connected through an OH group.³⁰ It was already reported that a biochar possessing higher H/C, O/C and (O+N)/C ratios to be more interactive with polar compounds.³¹ At good chars the molar ratio decrease with increasing temperature, because of O and H losses and the biochars are most polar (high O/C and O+N/C ratios) at the lower pyrolysis temperatures²⁶. Here the authors claim that the biochar prepared at lower temperature could react with water well. The H/C ratios show the aromaticity of biochar.^{26, 30} It was concluded that an H/C ratio between 0.4 to 0.6 of the aromatic portion of chars can determine that every second to third C is connected to a proton, unlike soot and lignite, which often have H/C ratio < 0.1, that indicates a more like graphite structure.²⁵ The molar H/C ratios of biochars are lower in our experiment in comparison to other studies.²⁷ The polarity is more or less similar at each type of biochar.

It has already been reported that the ash content increased with increasing temperature.^{13, 26} These results correspond to our experiment, the values of ash content are higher in biochar from grasses (around 20 %), and the ash content of wood biochar is higher than the other studies reported. Our results ranging between 12-15%, but Uchymia et al. reported 2-4% of ash in biochar prepared from grass biomass under temperature of 700 °C.¹³

The specific surface area and yield of biochars

Although some of the previous results of biochars analyses were different from literature the results of specific surface area and yields of prepared biochars corresponded well with literature. It was found that feedstock biomass influences the physical properties of prepared biochar. The biochar from wood mixture showed the highest values of specific surface area (to 369 m² g⁻¹), while the lowest values were observed at biochar from meadow grass (Figure 1). These results correspond to the other authors who showed the specific surface biochar prepared from wood which was higher than biochar from grass biomass.³³ The strong positive correlation was observed between pyrolysis temperature and specific surface area of prepared biochars from all types of biomass

The final temperature also affects the physical properties of biochar. For all types of biomass with increasing pyrolysis temperature, the values of specific surface area increased as in other studies also.^{13,33}

Lignin compared to cellulose dehydrated more difficult and created more of residual char: up to 45%.¹⁹ which implies that the yield of char depends on the amount of lignin in biomass - a higher content of lignin leads to the higher yield of char, which is confirmed by various studies.^{13,33} Raverdeen et al. reported that the cellulose/lignin ratio influences the yield of char, the highest char yields was achieved within ratio 1:3.²⁸ The lowest yield was observed at biochar biomass of maize. The highest values of yield showed a biochar from meadow grass: up to 28% (w/w) (Figure 2). This may be due to results of higher ash content of feedstock and also higher presence of SiO₂ at

grasses as Vassilev et al. reported.²⁴ Other authors claim that the char yield of a lignocellulosic material cannot be predicted by a simple model that sums the yields of the substrate's cellulose, hemicellulose, and lignin components, because the char yield is strongly dependent on the vapor-phase conditions presented in the pyrolytic reactor.³⁴

Authors indicate with increasing final temperature, the yield decreases, while increased biochar bio-oil and gas production. In their study there was an assumption that the yields of char are high at low temperatures, because the input biomass doesn't completely transform into char.³⁵ In our experiment, the yield biochar generally decreased with increasing temperature for all types of biomass. The positive linear correlation was detected between pyrolysis temperature and biochar yields.

Basically, at low temperatures of 200-300 °C under slow heating rate (<50 °C / min), the thermal process is called torrifaction. Gas portion escapes from biomass primarily and up to 90% of solids remains. The balance of torrifaction products of willow biomass is: 87% of solid product and 8% of water, 3% of gases (CO, CO₂) and 3% of organic matter escaped.³⁶

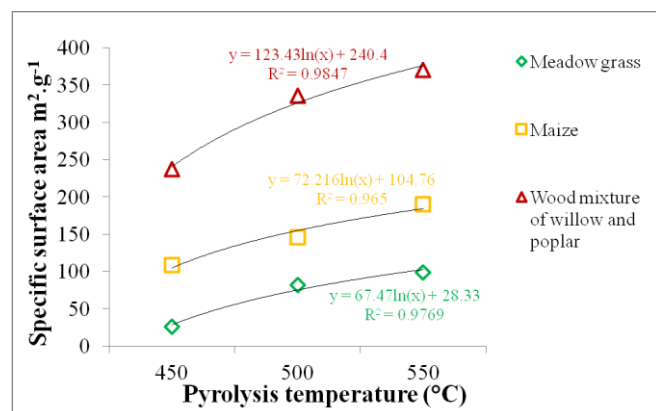


Figure 1. The influence of pyrolysis temperature of prepared biochar on specific surface area

Biomass losses can happen through depolymerisation of hemicelluloses folder. Final product of torrifaction is completely dried out and the air moisture is not received into the material as in raw one. Thanks to these properties, the torrifaction is considered as a preparatory process for subsequent use of biomass for energy purposes.³⁶ It was said, grass biomass has higher content of ash. There can be higher contents of silicates in contrast to wood biomass, thus the yield of biochar from grass biomass was shown higher than that of wood one.²⁵

Conclusion

This study reported, that the composition of feedstock material and pyrolysis condition highly influence the final product, in our case it is biochar.

The production of the char - biochar, which will be used as a soil additive, has to fulfil certain parameters. It is necessary to prepare a material with sufficient specific surface area, allowing sufficient adsorption of undesirable ions or molecules.

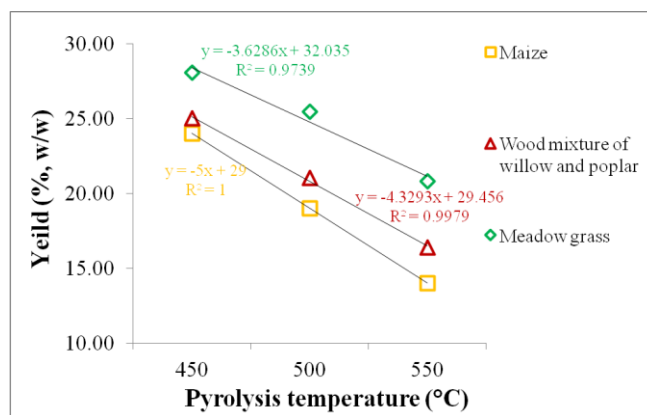


Figure 2. The influence of pyrolysis temperature on biochar yields

From a practical point of view, the biomass mixtures of willow and poplar, pyrolyzed at temperatures from 500 °C appears as suitable to prepare char, which shows high specific surface area. Presence of heavy metals in feedstock has not affected parameters of biochar, but the content of ash played more important role in it.

Next step of our experiments is to analyse the produced biochar and found out the amount of risk elements there. Then the research will continue with batch sorption and desorption experiment, where the availability of risk elements in biochars will be observed as well as its sorption ability of prepared biochar at contaminated and uncontaminated soils.

Acknowledgement

This work was financially supported by the project of Technology Agency of the Czech Republic BROZEN No. TA01020366.

References

- Sas-Nowosielska, A.; Kucharski, R.; Malkowski, E.; Pogrzeba, M.; Kuperberg, J. M.; Krynski, K. *Environ. Pollut.*, **2004**, 128, 373.
- Šyc, M.; Pohořelý, M.; Kameníková, P.; Habart, J.; Svoboda, K.; Puncochar M. *Biomass Bioenergy*, **2012**, 37, 106.
- Trakal, L.; Komárek, M.; Száková, J.; Zemanová, V.; Tlustoš, P. *Plant, Soil Environ.*, **2011**, 57, 372.
- Lehmann, J.; Joseph, J. *Biochar for Environmental Management: Science and Technology*. Earthscan, London, **2009**.
- Bridgwater, A. V.; Peacocke, G. V. C. *Renewable Sustainable Energy Rev.*, **2000**, 4, 1.
- Brown, R. In Lehmann J.; Joseph, J. *Biochar for Environmental Management: Science and Technology*. Earthscan, London, **2009**.
- Antal, M.J.; Gronli M. *Ind. Eng. Chem. Res.*, **2003**, 42, 1619.
- Morley, J. *The National Greenkeeper*, **1929**, 3, 10, 26.
- Sombroek, W. *Amazon Soils*. Centre for Agricultural Publications and Documentation, **1966**.
- Laird, D.; Fleming, P.; Wang, B.; Horton, R.; Karlen, D. *Geoderma*, **2010**, 158, 436.

- ¹¹Rosa, J. M.; Knicker, H.; Capel, E.; Manning, D. A. C.; González-Perez, J. A.; González-Vila, F. J. *Soil Sci. Soc. Am. J.*, **2007**, *72*, 258.
- ¹²Jones, D. L.; Edwards-Jones, G.; Murphy, D. V. *Soil Biol. Biochem.*, **2011**, *43*, 804.
- ¹³Uchimiya, M.; Wartelle, L.H.; Klasson, K.T.; Fortier, C.A.; Lima, I.M. *J. Agri. Food Chem.*, **2011**, *59*, 2501.
- ¹⁴Zhang, Z.; Solaiman, Z. M.; Meney, K.; Murphy, D. V.; Rengel, Z. J. *Soils Sediments* 2012, DOI: 10.1007/s11368-012-0571-4.
- ¹⁵Gomez - Eyles, J. L.; Sizmur, T.; Collins, C. D.; Hodson, M. E. *Environ. Pollut., Ser. B*, **2011**, *159*, 616.
- ¹⁶Uchimiya, M.; Lima, I. M.; Klasson, K. T.; Chang, S.; Wartelle, L. H.; Rodgers, J. E. *J. Agric. Food Chem.*, **2010**, *58*, 5538.
- ¹⁷Cao, X.; Harris, W. *Bioresour. Technol.*, **2010**, *101*, 5222.
- ¹⁸Demirbas, A. *J. Anal. Appl. Pyrolysis*, **2004**, *72*, 243.
- ¹⁹Mohan, D.; Pittman, C. U.; Steele, P. H. *Energy Fuels*, **2006**, *20*, 848.
- ²⁰Šichorová, K.; Tlustoš, P.; Száková, J.; Kořínek, K.; Balík, J. *Plant, Soil Environ.*, **2004**, *50*, 525.
- ²¹Borůvka, L.; Huan – Wei, Ch.; Kozák, J.; Křišťoufková, S. *Rostl. Vyroba*, **1996**, *42*, 543.
- ²²Brunauer S.; Emmett, P. H.; Teller, E. *J. Am. Chem. Soc.*, **1938**, *60*, 309.
- ²³Van Loo, S.; Koppejan, J. *Handbook of biomass combustion and cofiring*. The Netherlands: Twente University Press. **2002**.
- ²⁴Vassilev, V. S.; Baxter, D.; Andersen, L. K.; Vassileva, C. G. *Fuel*, **2010**, *89*, 913.
- ²⁵Chen, X.; Chen, G.; Chen, L.; Chen, Y.; Lehmann, J.; McBride, M. B.; Hay, A. G. *Bioresour. Technol.*, **2011**, *102*, 8877.
- ²⁶Novak, J. M.; Lima, I.; Xing, B.; Gaskin, J. W.; Steiner, C.; Das, K. C.; Ahmedna, M.; Rehrh, D.; Watts D. W.; Busscher, W. J.; Schomberg, H. *Ann. Environ. Sci.*, **2009**, *3*, 195.
- ²⁷Hammes, K.; Smernik, R. J.; Skjemstad, J. O.; Herzog, A.; Vogt, U. F.; Schmidt, M. W. I. *Eur. J. Org. Chem.*, **2006**, *37*, 1629.
- ²⁸Raverdeen, K.; Ganesh, A.; Khilar K. C.; *Fuel*, **1996**, *75*, 987.
- ²⁹Gaskin, J. W.; Steiner C.; Harris K.; Das, K. C.; Bibens, B. *Trans. ASABE*, **2008**, *51*, 2061.
- ³⁰Knicker, H.; Totsche, K.U.; Almendros, G., *Org. Geochem.*, **2005**, *36*, 1359.
- ³¹Wang, X. R.; Cook, S.; Tao, S.; Xing, B. *Chemosphere*, **2007**, *66*, 1476.
- ³²Chen, B. L.; Zhou, D. D.; Zhu, L. Z. *Environ. Sci. Technol.*, **2008**, *42*, 5137.
- ³³Keiluweit, M.; Nico, P. S.; Johnson M. G.; Kleber M. *Environ. Sci. Technol* **2010**, *44*, 1247.
- ³⁴MacKay, D. M.; Roberts, P. V. *Carbon*, **1982**, *20*, 87.
- ³⁵Williams, P. T.; Besler, S. *Renewable Energy*, **1999**, *7*, 233.
- ³⁶Bergman, P. C. A; Kiel, J. H. A. *Torrefaction for biomass upgrading, 14th European Biomass Conference & Exhibition*, Paris, France. **2005**.

Received: 25.10.2012.

Accepted: 25.11.2012.



SEDIMENT STUDIES IN HUNGARIAN SURFACE WATERS

Erzsébet Krausz^{[a]*}, Judit Vallner^[b], Judit L. Halász^[a]

Paper was presented at the 4th International Symposium on Trace Elements in the Food Chain, Friends or Foes, 15-17 November, 2012, Visegrád, Hungary

Keywords: sediment, epipelon, ETS-activity, water, trophity

The role of sediment and epipelon (organisms living on the surface of or in the fine-sized sediments) is significant in the life of aquatic ecosystems. The sediment is the place where the change of ion-transport occurs between the aquatic and solid phases, there are dynamic balance and buffer system between the sediment particles and the particles in the surrounding medium. As a result of the activity of the epipelon and the sediment organisms the metabolism pathways exist in the aquatic ecological systems that can indicate or influence on the habitat characteristics. Changes in the quality or quantity of epipelon indicate changes in water quality. From the point of view of nature conservation it can characterize a natural status or indicate the degree of disturbance (degradation). We measured the ETS (Electron Transport System) activity of the epipelon which gives the maximal intensity of the respiration metabolism. In the analysis of the epipelon the measuring of the ETS-activity can be used of the returns of taxonomic effects such as sublethal or physiologic damage caused by toxic poisons which cannot be discovered immediately and directly by taxonomic parameters, but the changing breath-activity can mark a changing state. ETS tests are suitable for indicating environmental stress.

* Corresponding Author

e-mail: krausz.erszebet@nyf.hu

[a] Institute of Environmental Sciences, College of Nyíregyháza, H-4400 Nyíregyháza, Sóstói út 31/b., Hungary,

[b] Institute of Teacher Training, College of Nyíregyháza, H-4400 Nyíregyháza, Sóstói út 31/b., Hungary.

Introduction and Theory

Sediment and epipelon play a significant role in wetlands and aquatic ecosystems. Sediment consists of three primary components: organic matter in various stages of decomposition, particulate mineral matter (including clays, carbonates and no clay silicates) and an inorganic component of biogenic origin¹. Total organic carbon within ecosystems results from autochthonous production augmented by imported allochthonous organic carbon from wetland and terrestrial sources. All of the organic carbon is not mineralized because much is deposited within low redox conditions within sediment. Most of the intense microbial respiration and fermentation is associated with the sediment².

The organic sediments of lakes are considerably similar to the upper most A0 horizon in terrestrial soils³. The upper layer of the sediment has a great influence on the water quality. Exchange of ions takes place on the sediment-water interface and particles of the sediment and those of the surrounding medium are constantly in a physical contact and form a dynamic equilibrium. In this process living organisms, including bacteria, play a key-role. "A conspicuous feature of microbial populations in lakes is the great increase in numbers in the transition from the overlying water to the diffuse, uncompact zone of the surficial sediment. Bacteria increase about 3-5 orders of magnitude from the water to the surface sediments and decrease rapidly with increasing depth in the sediments. Expressed in numbers per gram dry weight of sediment, bacterial populations in the surficial sediments can reach 6-7 orders of magnitude greater than in an equivalent weight

of overlying water. Saprophytic bacteria decrease much more rapidly than do total bacteria with increasing depth below the sediment interface, which suggests a reduction of readily assimilable organic substrates below the interface."²

The autotrophic organisms of the epipelon produce oxygen and synthesize organic compounds by taking up inorganic plant nutrients from the soil and absorbing light energy. The organic matter produced this way is an essential food source for heterotrophic organisms of the epipelon just like for higher heterotrophic organisms such as fish⁴. The activity of organisms of epipelon in aquatic ecosystems leads to activation of metabolic pathways, which can determine or greatly influence the features of a given habitat.

Electron Transport System (ETS) in organisms functions as a link between molecular oxygen and biological oxidation of organic compounds. The occurrence of ETS in aerobic organisms is universal, this way 90 % of biological oxidation in biosphere is the result of the activity of ETS⁵.

According to the Water Framework Directives (WFD) of EU, common principals are needed in order to coordinate Member States' efforts to improve the protection of waters in terms of quantity and quality. Standardisation of monitoring, sampling and analysis methods is required. Common definitions of the status of water in terms of quality should be established and common water quality standards should be laid down. Aquatic ecosystems should be monitored on a systemic and comparable basis throughout the Community. It is necessary to reveal the principals lying behind the evaluation of present classification systems of water quality and there is a need for optimizing monitoring systems through developing the monitoring methods of ecological indicators and seeking for new indicators or new indicative parameters.

Already in 1962 was stated, that the relationship of increased bacterial populations and metabolic activity to

greater organic matter in sediments might appear obvious. A significant correlation between dehydrogenase activity and organic content of surface sediment has been found in eutrophic reservoirs. However, these correlations cannot be expected in organic-rich sediments, in which certain conditions depress the activity of microorganisms; or in sediments where much of the organic matter is chemically recalcitrant.²

From the ETS-activity value the maximal intensity of respiration can be calculated. ETS tests are used widely for measuring the metabolic activity of various prokaryotic and eukaryotic aquatic organisms. With the help of an empiric factor, the value of maximal oxygen consumption can be estimated from the ETS-activity, during field studies. Originally, ETS tests were worked out for sea-plankton⁶⁻⁸.

In the analysis of epipelon, measuring ETS-activity can be more informative than taxonomic studies, because taxonomic parameters cannot indicate immediately and directly sublethal physiological damage. Decreased respiration activity, in contrast, is suitable for revealing such changes. ETS tests can detect the presence of every compound that stimulates or inhibits the cytochrom system. If an ETS inhibitor is present in the surrounding water body, it can possibly get into the cytosol, and as a response to the inhibition of the specific activity of ETS multienzyme complex, the synthesis of enzymes is enhanced. Thus ETS tests are suitable for indicating environmental stress. Several studies confirmed that there is a direct connection between ETS-activity and the intensity of respiration in bacteria, phyto- and zooplankton, and sediment^{5, 9-15}.

The ETS-activity of microbial community in sediment was affected by temperature and/or the amount and origin of the organic matter¹⁶. The negative correlations that were found between EHI (ecosystem health index) and ETS-activity indicated a higher ETS activity at higher trophic status¹⁷. At the meantime a positive correlation between the ETS-activity of the sediment and that of *M.sppicatum* and *R.circinatus* was also measured, while negative correlations or no correlation were observed for mosses and macroalgae¹⁶.

Looking through the literature we can agree with Simcic when saying sediment ETS-activity is a valuable source of information on the lake ecosystem, its functioning and its health, in combination with other indicators of information about the system¹⁷. However there are no data on how exactly ETS-activity indicate environmental stress - see the (apparent) contradiction between: the higher ETS activity indicate higher trophic status¹⁷ and: ETS-activity is notably higher in the eutrophic lake than in the hypertrophic lake¹⁸.

Investigating the structure and function of epipelon is of a great importance, since its structure and complexity characterises the conditions of different habitats. The aim of our study was to investigate the effect of a possible environmental stress on ETS-activity of a surface waters.

Experimental

Natural (a) and constructed (b) still waters and running waters (c) from Hungary were chosen as sampling sites (in

each year are given the number of samples, varying on sampling possibilities):

(a) lakes: Lake Velencei (2003 $n=24$, 2004 $n=27$, 2005 $n=24$), Balaton (2003 $n=73$, 2004 $n=51$, 2005 $n=48$);

(b) two reservoirs: Kis-Balaton (2003 $n=45$, 2004 $n=51$, 2005 $n=51$), Kisköre Reservoir (2003 $n=30$, 2004 $n=24$, 2005 $n=24$), wastewater pond: Nyírbogdány (2003 $n=9$, 2004 $n=18$, 2005 $n=18$);

(c) running waters: Kerka (2003 $n=15$, 2004 $n=15$, 2005 $n=18$), Tisza (2003 $n=42$, 2004 $n=39$, 2005 $n=42$).

Samples were taken in the summer of 2003, 2004 and 2005, due to the fact that ETS-activities are temperature-dependent¹⁶. Epipelon samples were taken with a Hargrave-sampler from underwater, the 2-3 cm upper layer of the sediment was analysed¹⁵.

Commonly used characteristic, as dry weight content, organic matter content and chlorophyll-a concentration of the sediment samples were measured¹⁹, and ETS-activity characteristic of biological oxidation capacity of the sediment was determined. Till measurements of ETS-activity samples were stored in a $-30\text{ }^{\circ}\text{C}$ deep-freeze. This way the ETS-activity of the samples remains unchanged for two or three weeks²⁰.

First we optimized the reaction circumstances (technique and time of homogenisation, separation of ETS fractions). Then we determined the saturation level of substrates (NAD, NADP and succinate) and reagent iodo-nitro-phenyl tetrazolium chloride (INT). The effect of pH, incubation time and homogenisation on formazane production was determined as well and the rate of breakdown of formazane was measured. All examinations were carried out in the laboratory, at 20 to 24°C room temperature. Frozen epipelon samples weighed 20-80 mg (wet weight) was used for the analysis. Results were expressed in terms of absorbance or as $\mu\text{l}/\text{O}_2/\text{g}$ wet weight/h⁶.

The primary biomass production plays a central role in the algae population. Simplest approach of its determination is the measurement of chlorophyll-a in sediment per dry weight. The pigments were dissolved in boiling ethanol and quantified spectrophotometrically²¹.

The two main components of the sediment are water and dry matter. Drying on 105 °C till constant mass gives the amount of dry matter. Dry matter is composed by two basic ingredients: organic matter and inorganic ash constituents. Mass of organic matter was determined as the difference between sediment dry weight of the residue (ash) after combustion on 600 °C.

Results and discussion

The measured parameters characterize the sampling sites. Mean and SD for each year and variable are given in Table 1. Factor-analyzes (using Kaiser normalization) and hierarchical cluster analyzes were carried out on the measured variables (organic matter, dry weight, klorofill-a and ETS-activity). Although some overlapping occurred, the sampling sites were grouped on a level of 5 Euclidean Distance.

Table 1. Summary table of means and standard deviations for measured variables in studied years.

Studied variable_year	Min	Max	Mean	Std. Dev.
dry_matter_2003	3.99	77.17	40.3681	22.27995
organic_matter_2003	0.00	82.32	15.6381	18.31068
chlorophyll_a_2003	0.00	0.10	0.0057	0.01469
ETS_a_2003	0.26	24.32	5.8937	4.79339
dry_matter_2004	5.40	85.78	47.9518	23.45787
organic_matter_2004	0.53	53.97	11.1320	12.23302
chlorophyll_a_2004	0.00	0.04	0.0048	0.00906
ETS_a_2004	0.95	18.13	5.5809	4.02681
dry_matter_2005	5.70	96.40	46.9560	25.58895
organic_matter_2005	0.34	71.64	15.4490	18.43211
chlorophyll_a_2005	0.00	0.20	0.0162	0.03672
ETS_a_2005	0.72	62.20	8.9582	10.16995

The result of an Analyze of Variance (ANOVA) (Bonferroni Post Hoc Multiple Comparison) on the sampling sites shows that regarding each variable the sites differ significantly ($p < 0.05$, except chlorophyll-a which was found not in each year significantly different between sites). So, these commonly measured variables and ETS-activity do not duplicate each-other.

We have also tested whether running waters (Kerka, Tisza) and still waters (Lake Velencei, Balaton, Kis-Balaton, Kisköre Reservoir, wastewater pond Nyírbogdány) do differ significantly. We found that neither considering all investigated years, nor analyzing individual years there is no grouping tendency by water-type (hierarchical cluster on 3 principal components, cumulative variance above 93 %). We were given the same results testing the grouping tendency between “small” (Kerka) and “big” (Tisza) rivers: no evident differences between them were shown by the investigated variables.

We have carried out the hierarchical cluster analyzes on artificial vs. natural waters too. (Artificial: Kis-Balaton, Kisköre, Nyírbogdány; natural: Kerka, Tisza, Lake Velencei, Balaton.) Although Lake Balaton and Kisköre are forming separate groups (on 2 Eukleides Distance), the other waters do not show similar pattern, not even on 5 Eukleides Distance. This results from other present differences between waters, not the artificial vs. natural factor is crucial.

However when testing one after the other the parameters, different patterns occur. Altering sites show significant differences by measured variables and the studied year. As an example see Table 2.

These data are in strong correlation with our observations in both years about vision wastewater pollution prior to sampling (due to a foul-up of sewage-work) of Kis-Balaton (data not published). Although there is no any evidence about the mentioned pollutions, must be pay attention to this result. Calculated linear correlations (Pearson) are in concordance with our hypothesis; the changes in ETS-activity indicate disturbance in the water-life. When organic pollution appears, ETS-activity raises together with trophity (we found the same result as Muri et al.²²).

Table 2. Result of an Analyze of Variance (ANOVA) (Bonferroni Post Hoc Multiple Comparison) for dry weight, 2003. Sampling sites: Tisza (1), Lake Velencei (2), Kis-Balaton (3), Kisköre (4), Kereka (5), Balaton (6), Nyírbogdány (7).

Dry weight/2003	1	2	3	4	5	6	7
1		**	***	-	-	-	-
2		**	-	-	*	-	-
3		***	-	-	***	**	-
4		-	-	-	-	-	-
5		-	*	***	-	-	-
6		-	-	**	-	-	-
7		-	-	-	-	-	-

Contrary in the case of ETS-activity Kis-Balaton (site 3) differed significantly from all the other sites (Table 3).

Table 3. Result of an Analyze of Variance (ANOVA) (Bonferroni Post Hoc Multiple Comparison) for ETS-activity, 2003. (Sampling sites coded as in Table 2.)

Ets/2003	1	2	3	4	5	6	7
1		-	***	-	-	-	-
2		-	***	-	-	-	-
3		***	***	***	***	***	**
4		-	***	-	-	-	-
5		-	***	-	-	-	-
6		-	***	-	-	-	-
7		-	**	-	-	-	-

The same ETS-activity significance occurred in 2005 too. The amount and origin of organic matter affects the ETS-activity of the microbial community in sediment. This is a relatively short period, and is more sensitive than taxonomic parameters would indicate an external organic matter excess (environmental stress) within a few days or weeks after pollution occurred. During the next period the living organisms are growing, preparing the conditions to the next step, when anaerobic processes start. In this period ETS-activity and chlorophyll-a are negatively correlated, because autotrophic living organisms are hindered ($R = -0.22$ N.S). The recovery of a still water takes time (months or years). Year 2004 shows positive correlation between ETS-activity and chlorophyll-a, but not significant ($R = +0.80$). By 2005 the $R = +0.76$ and $p < 0.05$ indicate the beginning of a new health period in lake's life.

These are questioning the statement of Simcic et al.¹⁷, whether on the whole trophity-scale is valid that higher ETS-activity belongs to a higher trophic status? The scientific literature also mentions similarly apparent contradictions. According to our results, such contradictions arises from the fact that time is not distinguished from proper organic stress which occurred in the water.

Our result may be a solution for this problem, since it describes ETS-activity as a kind of maximum curve in function of time. Our suggestion is presented on Figure 1.

For determining the ETS-activity of undisturbed water we excluded Kis-Balaton (site 3) from our calculations (mean: 5.63 $\mu\text{l}/\text{O}_2/\text{g}$ wet weight/h, SD: 4.66) – although there is no proof neither for its pollution nor for other water's unpolluted status. Compared to different data found in the literature, this is not extreme data. Strong spatial differences were observed in ETS-activities in different sites (in Guanabara Bay, Brazil, mean: 0,13, range 0,004-0,620²³; in

Spain range: 24.99-34.91¹⁸). Therefore, we concluded that determination of the so-called normal ETS-activity-range on a given site need long term (i.e. a few year long) monitoring of the given water, on a finer map scale.

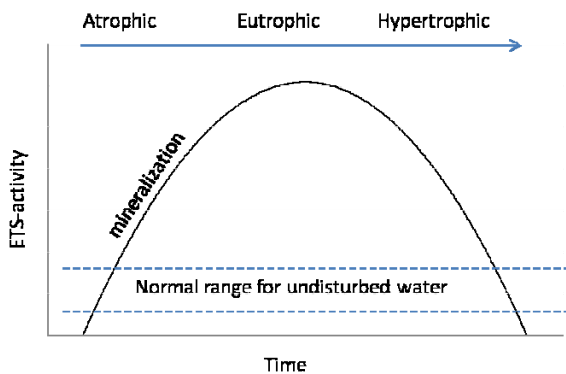


Figure 1. Predicted ETS-activity in function of time after an organic stress occurred in a natural water being in different trophity-stages.

Due to the fact that we could not find significant difference between artificial vs. natural waters, but the raised ETS-activity can be in correlation with organic influence of water, it is supposable that ETS-activity measurement could be used as a quick indicator of organic pollution occurrence. This preliminary study needs further investigations using published and proofed organic pollutions on different waters and well known undisturbed areas' ETS-activity measurement, as well as the proper normal ETS-range determination (by monitoring) for Hungarian waters. After these steps we could possess a special, easy to carry and quickly signing method to find out illegal or hidden water-pollutions, earlier than taxonomic parameters would show, making possible an earlier action of environmental protection.

1. References

¹Lerman, A., Lakes, E., *Chemistry, Geology, Physics*, Springer-Verlag, New York, **1978**.

- ²Wetzel, R., *Limnology Lake and River Ecosystems*, Academic Press, San Diego, **2001**, ISBN-10: 0-12-744760-1
- ³Hansen, K. J., *Sediment. Petrol.*, **1959** 29, 38.
- ⁴Lakatos, G., Kozák, L., Bíró, P., *Verh. Internat. Verein. Limnol.* **2001** 27, 3893.
- ⁵Packard, T. T., *J. Marine Res.* **1971**(29), 235.
- ⁶Kenner, R. A., Ahmed, S. I., *Marine Biol.* **1975**(33), 119.
- ⁷Owens, T. G., King, F. D., *Marine Biol.* **1975**(30), 27.
- ⁸Christensen, J. P., Pacard, T. T., *Limnol. Ocenogr.* **1979**(24), 576.
- ⁹Packard, T. T., *Adv. Aquat. Mikrobiol.* **1985**(3), 207.
- ¹⁰Packard, T. T., Denis, M., Rodier, M., Garfield, P., *Deep-Sea Res.* **1988**(35), 371.
- ¹¹Vosjan, J. H., Nieuwland, G., *Limnol. Oceanogr.* **1987**(32), 767.
- ¹²Vosjan, J. H., Tijssen, S. B., Nieuwland, G., Wetsteyn, F. J., *Neth. J. Sea Res.* **1990**, 25, 89.
- ¹³Span, A. S. W., *Water Res.* **1986**(20) 1497.
- ¹⁴Span, A. S. W., *Arch. Hydrobiol.* **1988**, 31, 141.
- ¹⁵Tóth G., Driks, A. V., *Verh. Internat. Verein. Limnol.* **1991** 24, 993.
- ¹⁶Germ, M., Simcic, T. *J. Limnol.*, **2011** 70, 305.
- ¹⁷Simcic, T., Brancelj, A., *Fundam. Appl. Limnol.*, **2009** 175 (4), 317.
- ¹⁸Vicente, I., Amores, V., Guerrero, F., Cruz-Pizarro, L. *Biomed. Life Sci. Naturwissenschaften*, **2010**, 97 (7) 627.
- ¹⁹Lakatos, G., Kiss, M., Mészáros, I., *Hydrobiologia* **1999**, 415, 47.
- ²⁰Yamashita, Y., Bailey, K. M., *Theragra chalcogramma*, **1990**, 56, 1059.
- ²¹Felföldy, L., *Vízügyi hidrobiológia*, 4th Edition, VGI, Budapest, **1987**.
- ²²Muri, G., Simcic, T., *Aquat. Microb. Ecol.* **2004**, 34(3), 291.
- ²³Fontana, F. L., da Silva, F. S., de Figueiredo, N. G., Brum, D. M., Pereira Netto, A. D., de Gigueiredo Junior, A. G., Crapez, M. *A. C An. Acad. Bras. Cienc*, **2010**, 82(4), 1013.

Received: 15.10.2012.
Accepted: 27.11.2012.



PRELIMINARY STUDIES ON THE REACTION OF Ca^{II}, Sr^{II} AND Ba^{II} CHLORIDES WITH EPHEDRINE HYDROCHLORIDE

Moamen S. Refat^{[a,b]*} and Abeer A. El-Habeeb^[c]

Keywords: Ephedrine HCl, infrared spectra, Raman spectra, ¹H-NMR.

Ephedrine hydrochloride complexes of Ca(II), Sr(II) and Ba(II) non-transition metal ions were prepared. The compounds formed contains various amount of crystalline water (6, 8 and 4 for Ca, Sr and Ba, respectively) and were studied by IR, Raman and NMR methods. Electrolytic conductivity measurements showed that the complexes decompose into ionic particles in DMSO. The compounds show unusual high thermal stability.

* Corresponding Authors

E-Mail: Email: msrefat@yahoo.com

[a] ^a Department of Chemistry, Faculty of Science, Port Said, Port Said University, Egypt

[b] Department of Chemistry, Faculty of Science, Taif University, 888 Taif, Kingdom Saudi Arabia

[c] Department of Chemistry, Faculty of Science, Princess Nora Bint Abdul Rahman University, Riyadh, Kingdom Saudi Arabia

Introduction

Ephedra is a Phanerogame-Gymnosperme from the family of Gnetaceen. Specially ephedra vulgaris, ephedra equisetina and ephedra sinica contain ephedrin with its other isomers. A certain ephedra species has been used in ancient Chinese medicine since ages. The pharmacological studies have indicated that ephedrine is a sympathomimetic agonist at both α and β -adrenergic receptors, which determine an increase of cardiac rate and contractility, peripheral vasoconstriction, broncho-dilatation and central nervous system (CNS) stimulation.^{1,2} However, severe contraindications have been given for individuals with hypertension or other cardiovascular diseases, glaucoma, diabetes and hyperthyroidism. Products containing *E. sinica* (or another botanical source of ephedrine) were among the most popular dietary supplements on the market, until their sale was banned by the U.S. Food and Drug Administration (FDA) in April 2004. After the ban of *Ephedra* products, “*Ephedra*-free” dietary supplements for weight loss were introduced. However, *Ephedra*-free is not necessarily danger-free.³ *Citrus aurantium* is an ingredient in many of these *Ephedra*-free dietary supplements. The main active constituent of *C. aurantium* fruit extracts is (-)-synephrine,³ a phenethylamine alkaloid similar in structure to ephedrine. Depending on the oxidation state of metal, the coordination number and the kind of coordinated ligand, there are many structures, which show different biological and physico – chemical properties.^{4,5} The literature shows that there is a direct relationship between chemical structure and the antimicrobial properties of chemical compounds.^{6,7} Previously, the relationship between the chemical structure characterized by spectral parameters and antimicrobial activity was studied.^{5,8,9} In this work, we prefer to throw a light on an essential compound as ephedrine to evaluate the probability of its interaction

with some metals presented in the body like calcium ions. Also, the preparation of its complexes may leads to the preparation of new compounds having the similar role. Sometimes these complexes are preferable than the original ligand especially with the blocking of active sites which may aggregated the essential metals from the body. This research is considered the initial point for the specialists in the medicinal field for condensed investigation.

Experimental

Reagents

Ephedrine (2-(methylamino)-1-phenylpropan-1-ol hydrochloride) (Eph) used in this study was obtained from the Egyptian International Pharmaceutical Industrial Company (EIPICO). All other chemicals used in the preparations were of analytical reagent grade, commercially available from different sources (Fluka Co. and Aldrich Co.). All the metal salts hydrated calcium, strontium and barium used as chloride. All solvents are used as it is without further purification.

Synthesis of ephedrine HCl complexes

All the complexes were prepared by molar ratio 1:1 (1 mmol M^{II}: 1 mmol Eph) in water/ethanol (50/50%) solution. The resulting mixtures were heated under reflux for 2 hr. and filtered suddenly after precipitation. The complexes were separated from the reaction mixture and washed with boiling ethanol and dried in vacuo over CaCl₂

Equipment and measurements

Carbon and hydrogen content was determined at the Microanalytical Unit of Cairo University. The analysis of metal ions and their conjugated anion (chloride) were carried out according to standard methods.¹⁰ IR spectra were recorded on a Genesis II FT-IR spectrophotometer (KBr – discs) in the $\nu = 400 - 4000 \text{ cm}^{-1}$ range. Raman spectra of samples were measured on the Bruker FT-Raman with laser 50mW at Taif University, Saudi Arabia. ¹H-NMR spectra were recorded on a Varian Gemini 200 MHz spectrometer using d⁶-DMSO as solvent and TMS

as internal standard. The molar conductivities of freshly prepared 1.0×10^{-3} mol cm^{-3} DMSO solutions were measured for the soluble complexes using Jenway 4010 conductivity meter. The number of crystalline water molecules was estimated upon thermogravimetric analysis.

Results and Discussion

The analytical data of all the white color isolated complexes were displayed on Table 1. All the complexes are stable in air. The higher melting point of all isolated anhydrous complexes (> 300 °C) than the integral ligand (190 °C) may reflect their relative stability. All the complexes are insoluble in water, soluble to very limited extent in common organic solvents but considerable extent in dimethylformamide (DMF) and DMSO. The metal chelates solutions in DMSO showed slightly low conductance ($49\text{--}63 \Lambda_{\text{m}} \text{ ohm}^{-1}\text{cm}^2\text{mol}^{-1}$) supporting the non-electrolyte nature of the complexes. The ephedrine compounds formed contains various amount of crystalline water (6, 8 and 4 for Ca, Sr and Ba, respectively) upon thermogravimetric analysis.

Infrared spectra and chelation mode

A comparison of the most intense band positions in the free ligand (ephedrine hydrochloride) and the formed precipitates are listed in Table 2. The spectrum of free ligand displays a series of significant bands as: 3330 , 2972 , 1591 and 1395 cm^{-1} which may assign to $\nu(\text{OH})$, $\nu(\text{NH})$, $\delta(\text{NH})$ and $\delta(\text{OH})$ in plane. The lower appearance shinned on bands of $-\text{OH}$ and $-\text{NH}$ groups supports of the presence of intraligand H-bonding (Fig. 1) between the two neighboring groups. This is expected due to the distribution of $-\text{OH}$ and $-\text{NH}$ groups, which primates this behavior as appeared from Molecular Modeling for the minimum internal energy structure (3.385 kcal/mol) by the use of MM^+ force field as implemented in hyperchem 5.1. According to elemental analysis and thermogravimetric studies, all the complexes obtained contain coordinated and crystalline water as well. The bands observed at $900 - 950$ and $810 - 850 \text{ cm}^{-1}$ can be assigned to coordinated water molecules.¹³

The new bands assigned for $\nu(\text{M-N})$ and $\nu(\text{M-O})$ are easily characterized in the low frequency field except $\nu(\text{M-Cl})$ which cannot be detected in the scanning range but detectable in Raman spectra.

Resonance Raman spectra

Figure 2 displays the Raman spectra of investigated complexes in solid state as Ca(II) , Sr(II) and Ba(II) complexes. As can be seen, all the complexes show a very similar pattern. The significant spectral similarity among the bivalent metal complexes reflects the same nature of the ligand in coordination with all metal ions. Table 2 summarizes the observed vibrational

wavenumbers aggregated with infrared spectral data. The resonance Raman spectra of Ca(II) , Sr(II) and Ba(II) complexes show band profile characteristic of compounds.

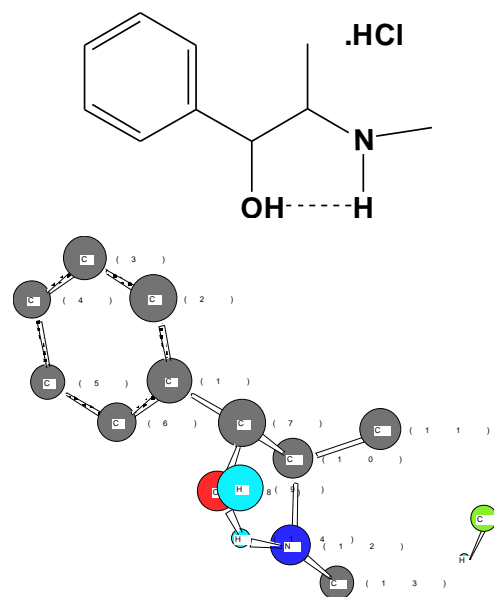


Figure 1: The Modeling and 3D structures of ephedrine hydrochloride

The bands at 3008 cm^{-1} in the three ephedrine hydrochloride complexes belong to the N-H stretching, $\nu(\text{NH})$.^{14,15} One of the most intense band observed at 1598 (Ca^{II}), 1458 (Sr^{II}) and 1551 (Ba^{II}) cm^{-1} , respectively is a very characteristic for N-H deformation, $\delta(\text{NH})$. The other intense band at 1304 cm^{-1} is characteristic for O-H deformation, $\delta(\text{OH})$ in plane. The band observed at 1045 and 1038 cm^{-1} for Ca(II)+Sr(II) and Ba(II) complexes, respectively, assigned to $\delta(\text{CH})$ with a strong contribution of $\nu(\text{C-O})$.¹⁶ This band is shifted towards lower wavenumbers in comparing with ephedrine hydrochloride and its intensity slightly decreases. The bands derived from the aromatic ring out-of-plane bending modes are located at $694 - 631 \text{ cm}^{-1}$ in the spectrum of ephedrine hydrochloride. These bands are shifted towards lower wavenumbers in the spectra of complexes. The absence or shifting the aromatic Raman bands toward a lower wavenumbers is an evidence of an increase in the perturbation of the aromatic system of the studied compounds. The disturbance of the aromatic system takes place by deforming the uniform distribution of π -electron charges in the ring.¹⁷ All the metal ions influence the electronic charge distribution to a small extent, on the basis of the magnitude of bands shifts from spectra. The spectral regions around 1000 cm^{-1} show a very similar pattern for all the Eph complexes. The most intense band is assigned tentatively to the in-plane bonding $\delta(\text{CH})$.¹⁸ The low frequency spectral region gives important information about the nature of the metal-ligand bonds. We observed bands around $\sim 600 \text{ cm}^{-1}$ in all complexes spectra are assigned to $\nu(\text{M-O})$,¹⁵ and some bands were observed around $400\text{--}500 \text{ cm}^{-1}$. Other significant low intense band at $200\text{--}300 \text{ cm}^{-1}$ may be assigned to $\nu(\text{M-Cl})$ which doesn't detect from IR spectra at all.

Table 1: Analytical and Physical data for the Ephedrine complexes and its metal complexes

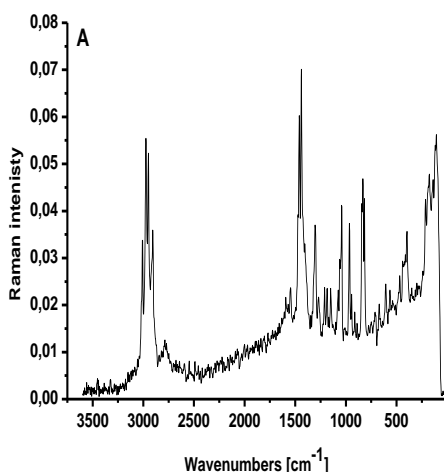
Compound/Empirical formula (M. Wt.)	Color	Elemental analysis (%) Calcd. (Found)			
		C	H	M	Cl
CaCl ₂ .Eph. HCl.6H ₂ O (420.77)	White	28.54(28.43)	6.71(6.63)	9.52(9.45)	25.28(25.11)
SrCl ₂ .Eph. HCl.8H ₂ O (504.34)	White	23.81(23.64)	6.40(6.21)	17.37(17.25)	21.09(20.98)
BaCl ₂ .Eph. HCl.4H ₂ O (481.99)	White	24.92(24.87)	5.02(4.97)	28.49(28.31)	22.07(21.89)

Table 2: Assignments of the IR (Raman) Essential Spectral bands (cm⁻¹) of ephedrine HCl and its metal complexes

Compound	ν _{OH}	ν _{NH}	δ _{OH}	ν _{C-O}	δ _{OH}	δ _{NH}	ν _{M-Cl}	ν _{M-N}	ν _{M-O}
			(out of plane)		(in plane)				
Ephedrine (Eph.HCl)	3330 (3500)	2972 (3064)	751 (725)	1051 (1044)	1395 (1303)	1591 (1654)	--	---	---
CaCl ₂ .Eph. HCl.6H ₂ O	3245 (--)	3013 (3008)	741 (672)	1017 (1045)	1385 (1304)	1569 (1598)	-- (213)	409 (466)	540 (566)
SrCl ₂ .Eph. HCl.8H ₂ O	3246 (--)	3012 (3008)	740 (658)	1014 (1045)	1324 (1304)	1566 (--)	-- (273)	444 (472)	533 (546)
BaCl ₂ .Eph. HCl.4H ₂ O	3242 (--)	3013 (3008)	740 (672)	1017 (1038)	1262 (1304)	1569 (1551)	-- (279)	-- (466)	576 (526)

¹H-NMR of SrCl₂.Eph. HCl.8H₂O complex

¹H-NMR spectrum of the strontium(II) complex was recorded in DMSO and compared with the ligand one¹⁹ to confirm the binding of active sites towards the metal ion. The spectrum showed a multiplet in the region δ = 0.77 – 0.78 ppm, which has been assigned for methyl protons (CH₃–CH-). A singlet peak in the region δ = 2.46 – 2.49 ppm for the other methyl protons (CH₃–NH). Singlet peaks appeared at region δ = 3.12 – 3.13 and 4.93 – 4.92 pp were assigned for CH proton of MeCH–NH and PhCH(OH) groups, respectively. In the region δ = 7.25 – 7.27 ppm were assigned chemical shifts for hydrogen of symmetrical aromatic ring of the ligand.

**Figure 2:** Raman spectrum of the calcium(II) chloride – ephedrine hydrochloride complex

The position of the OH and NH peaks in the SrCl₂.Eph. HCl.8H₂O complex are relatively unaffected in comparing with that in free ligand, this is suggesting their participation after the removal of intraligand hydrogen

bonding between the two groups causing their appearance as more or less unshifted. Although, the usual behavior is the downfield appearance for the peaks assigned for the coordinating groups due to the deshielding caused coherently with the movement of unchained paired of electrons towards the metal ion to form a coordinate bonds. Due to flexibility of the structural variations in these type of compounds formed, the studies on the nature of chemical bond, coordination mode and number of the ligands and other structural features are in progress.

References

- Schaneberg, N. T., Crockett, S., Badir, E., Khan, I. A., *Phytochemistry*, **2003**, 62, 911–918.
- Roman, M.C., *J. AOAC Int.*, **2004**, 87, 1–14.
- Pellati, F., Benvenuti, S., *J. Chromatogr. A*, **2007**, 1161, 71–88.
- Lieberman, R. L., Bino, A., Mirsky, N., Summers, D. A., Thompson, R. C., *Inorg. Chim. Acta*, **2000**, 297, 1.
- Koczoń, P., Piekut, J., Borawska, M., Lewandowski, W., *J. Mol. Struct.*, **2003**, 651, 67.
- Cui, X., Joannou, C., Hughes, M., Cammack, R., *FEMS Microbiol. Lett.*, **1998**, 98, 67.
- Hueso-Urena, F., Moreno-carretero, M., Romero-Molina, M., Salas-Peregrin, J., Sanchez-Sanchez, M., Alvarez de Cienfuegos-Lopez, G., Faure, R., *J. Inorg. Biochem.*, **1993**, 51, 613.
- Koczoń, P., Piekut, J., Borawska, M., Świsłocka, R., Lewandowski, W., *Spectrochim Acta, A*, **2005**, 61, 1917.
- Koczoń, P., Piekut, J., Borawska, M., Świsłocka, R., Lewandowski, W., *Anal. Biochem.*, **2005**, 384, 302.
- Vogel, A. I., *A Text Book of Quantitative Inorganic Analysis*, Longman, London, (1994).
- Allinger, N. L., *J. Am. Chem. Soc.*, **1977**, 99, 8127.
- Hyper chem. Version 7.51 Hyper cube, INC
- Zaki, Z. M., Mohamed, G.G., *Spectrochim. Acta, A*, **2000**, 56, 1245.

- ¹⁴ Hartl, F., Barbaro, P., Bell, I. M., Clark, R. J. H., Snoeck, T. L., Vlcek, A., *Inorg. Chim. Acta*, **1996**, 252, 157.
- ¹⁵ Karpshin, T. B., Gehard, M. S., Solomon, E. I., Raymond, K. N., *J. Am. Chem. Soc.*, **1991**, 113(8), 2977.
- ¹⁶ Michaud-Soret, I., Andersson, K.K., Que, L., *J. Biochemistry*, **1995**, 34(16), 5504.
- ¹⁷ Lewandowski, W., Kalinowska, M., Lewandowska. H., *J. Inorg. Biochem.*, **2005**, 99, 1407.
- ¹⁸ Ohrstrom, L., Michaud-Soret, I., *J. Phys. Chem., A*, **1999**, 103, 256.
- ¹⁹ Kim, H. K., Choi, Y. H., Erkelens, C., Lefeber, A. W. M., Verpoorte, R., *Chem. Pharm. Bull.*, **2005**, 53(1), 105.

Received: 01.11.2012.

Accepted: 30.11.2012.